uOttawa

L'Université canadienne
Canada's university

FACULTÉ DES ÉTUDES SUPÉRIEURES ET POSTOCTORALES

uOttawa

L'Université canadienne
Canada's university

FACULTY OF GRADUATE AND POSDOCTORAL STUDIES

Chris Bestfather
AUTEUR DE LA THÈSE / AUTHOR OF THESIS

M.A.Sc. (Environmental Engineering)
GRADE / DEGREE

Ottawa-Carleton Institute for Environmental Engineering
FACULTÉ, ÉCOLE, DÉPARTEMENT / FACULTY, SCHOOL, DEPARTMENT

Upgrading Landfill Gas to Natural Gas Quality: Bulk Separation by Pressure Swing Adsorption
TITRE DE LA THÈSE / TITLE OF THESIS

Dr. H. Tezel
DIRECTEUR (DIRECTRICE) DE LA THÈSE / THESIS SUPERVISOR

CO-DIRECTEUR (CO-DIRECTRICE) DE LA THÈSE / THESIS CO-SUPERVISOR

EXAMINATEURS (EXAMINATRICES) DE LA THÈSE / THESIS EXAMINERS

Dr. M. Warith

Dr. J. Zhang

Dr. C. Lan

Dr. O. Basu

Gary W. Slater
Le Doyen de la Faculté des études supérieures et postdoctorales / Dean of the Faculty of Graduate and Postdoctoral Studies

Upgrading Landfill Gas to Natural Gas Quality:

Bulk Separation by Pressure Swing Adsorption

Chris Bestfather

Thesis submitted to the

Faculty of Graduate and Postdoctoral Studies

In Partial Fulfillment of the Requirements for the Degree of

Masters of Applied Science

in

Environmental Engineering

Department of Chemical and Biological Engineering

University of Ottawa

Your file Votre référence
ISBN: 978-0-494-61310-8
Our file Notre référence
ISBN: 978-0-494-61310-8

SHORTENED ABSTRACT

Equilibrium adsorption properties are studied on zeolites for the application of upgrading biogas from landfills. Pure adsorption isotherms of carbon dioxide (CO_2) and methane (CH_4) measured with a constant volume apparatus. The Henry's Law constant and the heat of adsorption for NaLSX is also determined. The adiabatic working capacity and selectivity of four adsorbents is compared. NaLSX showed the highest capacity for CO_2 at elevated temperatures.

The binary equilibrium of CO_2/CH_4 on NaLSX is measured in a modified gas chromatograph at total mixture pressures of 1 and 3.3 atmospheres. The adsorbed phase is dominated by CO_2 with a selectivity of 20 to 100 for the separation of CO_2 and CH_4. The increase in total pressure resulted in an increase in adsorbent capacity and a decrease in selectivity. Finally, an economic analysis relates landfill size to PSA operational costs and returns.

ABSTRACT

Equilibrium adsorption properties are studied on various adsorbents for the application of upgrading biogas from landfills. The study begins with an examination of the pure adsorption isotherms of carbon dioxide (CO_2) and methane (CH_4) on various adsorbents. These measurements are performed with a constant volume apparatus. The differences in capacity at various temperatures are studied. In addition to isotherms, the Henry's Law constants and the heat of adsorption for the zeolite NaLSX is determined by employing the concentration pulse chromatographic technique. This experimental information is combined with a temperature dependant equilibrium model to evaluate the selectivity of various adsorbents based on the adiabatic working capacity of a vacuum pressure swing adsorber (VPSA) cycle. The conclusions of these analyses indicate that the adsorbents NaLSX, NaX and NaY demonstrate applicability for the bulk separation of CO_2/CH_4 in a VPSA system. In addition the adsorbent NaLSX showed the highest capacity for CO_2 at elevated temperatures.

Following the adsorbent screening, the binary equilibrium behaviour of CO_2/CH_4 on NaLSX is investigated. Mixture gas adsorption behaviour is measured in a modified gas chromatograph at total mixture pressures of 1 and 3.3 atmospheres. The concentration pulse chromatography technique was used to observe the changes in the binary isotherm of the mixture at these two pressures. The results show an adsorbed phase that is dominated by CO_2 indicating a high selectivity for separation of CO_2 and CH_4. The increase in total pressure resulted in an increase in adsorbent capacity and a decrease in selectivity. The curvature of the binary isotherm is similar for both pressures although it differs significantly from pure isotherm models.

Finally, the binary equilibrium capacity is used in an economic analysis for the upgrading of Landfill gas (LFG). The size of the landfill and consequently the LFG throughput into the VPSA is varied to observe the relationship between process operational costs and returns. Currently the breakeven costs of upgrading LFG and reselling the product at current natural gas prices are not competitive with current utilization technologies based on laboratory experiments. However, PSA LFG upgrading projects at landfills greater than 4 million tonnes can be profitable when natural gas prices or renewable energy incentives increase substantially.

RÉSUMÉ

Les propriétés d'adsorption à l'équilibre de plusieurs matières adsorbantes sont étudiées dans l'application de l'amélioration des biogaz émanant des sites d'enfouissement. Cette étude débute avec l'examination de l'isotherme du dioxyde de carbone (CO_2) et du méthane (CH_4) purs sur divers adsorbants. Ces mesures sont réalisées avec un système de volume constant. Les différences de capacités à diverses températures sont étudiées. En plus des isothermes, les constantes d'Henry et la chaleur d'adsorption du Zeolite NaLSX sont déterminés à l'aide de la technique chromatographique d'une impulsion en concentration. Cette information expérimentale est combinée à un modèle dépendant de la température à l'équilibre pour évaluer la sélectivité de divers adsorbants basé sur la capacité de travail adiabatique d'un cycle VPSA. Les conclusions de ces analyses indiquent que les adsorbants NaLSX, NaX et NaY peuvent être appliqués à la séparation du CO_2/CH_4 dans un VPSA. De plus, l'adsorbant NaLSX a démontré la plus grande capacité pour le CO2 à des températures élevées.

Suite à l'examination des adsorbants, les isothermes d'adsorption de mélanges binaires sur le NaLSX sont investigués. L'isotherme binaire du CO_2/CH_4 est mesuré dans un chromatographe à gaz modifié aux pressions totales de 1.1 et 3.3 atmosphères. La technique chromatographique d'une impulsion en concentration fut utilisée pour observer les changements dans l'isotherme binaire à ces deux pressions. Les résultats démontrent une phase adsorbée dominée par le CO_2, indiquant une sélectivité significative. Une augmentation de la pression totale a conduit à une augmentation de la capacité d'adsorption et à une diminution de la sélectivité. La courbe de l'isotherme binaire est semblable aux deux pressions, bien que significativement différente des modèles d'isothermes purs.

Enfin, la capacité binaire à l'équilibre est utilisée dans une analyse économique pour l'amélioration des gaz émanant des sites d'enfouissement. La grandeur du site d'enfouissement est varié pour observer la relation entre les coûts opérationnels du processus et les profits. Basé sur des mesures de laboratoires, le seuil de rentabilité pour l'amélioration des gaz de sites d'enfouissement n'est pas compétitif avec les technologies utilisées à l'heure actuelle. Il est aussi conclu que les projets d'amélioration

des gaz des sites d'enfouissement PSA de plus de 4 millions de tonnes pourraient être profitables si les prix de l'énergie verte ou les incitations envers l'énergie renouvelable augmentent considérablement.

Declaration of Authorship

I hereby declare that I am the first author of this thesis project which was undertaken with the guidance of my supervisor, Dr. F. Handan Tezel. All experimental data, figures and tables are my work unless otherwise referenced.

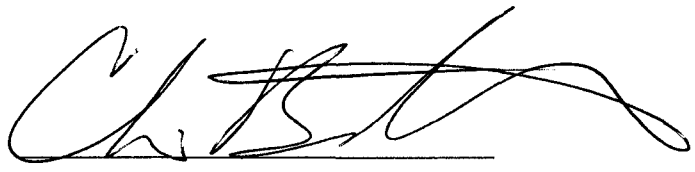

Chris Bestfather

September 9, 2009

Acknowledgements

First I would like to thank my supervisor, Dr. F. Handan Tezel. Her leadership, dedication to her students and family has been an inspiration to me. Without her understanding, guidance and patience I would not have been able to complete this endeavour.

I would like to thank the professors and technicians at the University of Ottawa for their help in my studies and trouble shooting my laboratory equipment. The staff and friendly administrative people at the University of Ottawa work hard to maintain a welcoming and comfortable learning environment.

Of course I would have had extreme difficulty starting graduate studies without financial support. I am forever indebted to the University of Ottawa's academic excellence scholarships, teaching assistance ships and the Ontario Graduate Studies program.

Finally and most importantly I would like to thank my friends and family for there encouragement and comfort. The members of the SMART group kept my spirits high when times were difficult. Special thanks to my friends Nathan and Estela who suffered through reading and editing my first drafts. Of course my family supported me throughout this challenge despite the distance. Most of all I would like to thank my wife for her endless understanding and patience with me. She inspires me to be a better person.

Table of Contents

APPENDICIES

List of Figures

List of Tables

Chapter I: Introduction

Introduction

Today's society is faced with the challenges of reducing green house gas (GHG) emissions globally. These emissions are contributing to quantifiable changes in global weather patterns, and temperature [1]. The anthropogenic sources of GHGs are largely made up of fossil fuel combustion by-products released in the sectors of energy supply, transport, industrial, and agriculture. Waste and wastewater decomposition represent only 2.8% of global GHG emissions [2]. The most common method for waste disposal, and coincidentally the most cost-effective, is landfilling. Roughly 50% of global waste is placed in large piles in the ground where it decomposes over many years [1]. The anaerobic decomposition of municipal solid waste releases landfill gas (LFG) a biogas that is mainly a binary mixture of methane (CH_4) and carbon dioxide (CO_2) as well as many trace gases listed in Table I -1. This biogas is released to the atmosphere as the organic fraction of waste decomposes in landfills over many decades after landfills have been closed. Both CH_4 and CO_2 are GHGs but methane has a global warming potential (GWP) 25 times that of CO_2 [3].

The release of LFG to the atmosphere has been identified as a significant source of GHGs and techniques for preventing its release are applied in some countries. The most common method of reducing the GWP of LFG is by capping the landfill and burning the gas in a flare. Flaring LFG is an effective method of GHG reduction in developing countries due to its relative low cost; however, the high energy content of LFG is largely wasted.

In developing countries LFG is being recognized as a renewable source of energy. Common technologies that change biogas into a useful energy form include steam boilers, modified natural gas engines and gas separators. Steam boilers allow for the thermal energy of LFG to be utilized locally. Gas engines are connected to turbines to produce electricity. Biogas is combusted in an engine or a steam boiler to produce electricity, however the gas requires pre-purification prior to combustion. The water and trace compounds in raw biogas can damage utilization equipment resulting in higher operational costs. An advantage of gas separators is that the energy density of biogas is increased by removing CO_2 as well as the unwanted trace impurities. Upgraded methane

from LFG can be sold on the energy market as a renewable fuel. Alternatively, if natural gas (NG) infrastructure is not available near the landfill, the CH_4 can be used as an alternative transportation fuel. For example, upgraded LFG in Puente Hills California is used to fuel waste processing equipment and garbage trucks with liquefied methane captured from the landfill. The application of upgrading LFG to natural gas quality is relatively new although the area of gas separations is well established.

LFG poses a challenging renewable resource to utilize via upgrading. Firstly the gas must be captured from the landfill. This is accomplished with wells and vacuum pumps at a maximum recovery rate of 50% [1]. Secondly the composition of LFG is mainly CO_2 and CH_4 in addition to many trace compounds that are a product of waste decomposition. The trace compounds include: air (N_2 and O_2), hydrogen sulphide (H_2S), carbon monoxide (CO), non-methane organic compounds (NMOCs), water vapour (H_20), siloxanes, and other compounds shown in Table I -1.

Table I -1 - Typical Landfill Gas Characteristics [4]

Component	Range
Methane (CH_4)	35% to 55%
Carbon Dioxide (CO_2)	20% to 50%
Nitrogen (N_2)	2% to 45%
Oxygen (O_2)	0.5% to 5%
Non-methane organic compounds (NMOCs)	200 to 2000 ppmv
Hydrogen Sulfide (H_2S)	20 to 500 ppmv
Carbon Monoxide (CO)	<10 ppmv
Siloxane	0.2 to 10 ppmv
Water (H_2O)	0-100% R.H.

The presence of the corrosive gases makes raw LFG difficult to store and burn without damaging energy utilization equipment [5]. In addition to troublesome compounds the composition of the LFG can vary depending on the climate, garbage type, and age of the landfill.

The field of adsorption separations is well established and is simple in its operation. The separation of LFG is carried out at an elevated pressure in a pressure swing adsorber (PSA). The binary mixture enters a packed column filled with porous adsorbent and the

CO_2 is retained in the bed as the relatively pure CH_4 exits the bed. Once the CO_2 begins to breakthrough the bed the feed mixture is redirected to another adsorbent bed. The adsorbed CO_2 in the saturated bed is desorbed by reducing the pressure in the column.

Purifying the LFG to NG quality involves three main steps. Removing unwanted trace compounds and drying the gas is first. This pre-purification is accomplished with a charcoal adsorbent bed that adsorbs and physically retains the trace elements and particulates in Table I -1. A desiccant bed in combination with a knockout drum removes H_2O from the raw biogas prior to pre-purification.

The second important step is the separation of CO_2. The separation of the main components of biogas can be performed by several technologies. There are several competing technologies for the bulk separation of CO_2 and CH_4. They include: cryogenic distillation, absorption (chemical or physical), membrane separation, and adsorption. For small to medium sized landfills adsorption separation has the advantages of being less energy intensive than cryogenic and absorption technologies [6]. PSAs are commonly used for gas bulk separations because of their simple operation and relatively low energy consumption [7]. A PSA also does not require water or liquid chemicals as in absorption processes. Membrane technologies are modular and adaptable although they are sensitive to variations in feed composition [8]. Adsorption processes are relatively flexible to variations in biogas composition and can be regenerated if accidentally contacted with raw LFG. Additionally, PSA is a proven separation technology that has been demonstrated for several decades [9].

The final purification of the CH_4 product elevates the purity to NG standards with N_2 removal. This third step is accomplished with membrane or adsorption processes. This paper explores the application of the bulk adsorption separation of LFG.

Bulk PSA separations are a challenging process because >10% (wt) of the feed is adsorbed, causing the temperature in the bed to increase and flow rate to decrease [10]. Physical adsorption is an exothermic process, thus the increase in system temperature results in a lower adsorption potential and a decreased PSA efficiency.

The adsorption of CO_2 is reversible because the mechanism of adsorption is physical and not chemical [9]. The adsorption process is scaled to the size required for a municipal landfill.

A successful LFG upgrading PSA requires an efficient separation of CO_2 from CH_4. This performance is mainly determined by the capacity and selectivity of the adsorbent bed [11]. These qualities are identified in laboratory experiments based on the screening of several materials.

In this study the adsorption equilibrium properties of several zeolite adsorbents are measured for the application of LFG bulk separation. The effect of the silica to alumina ratio (Si/Al) for zeolites are selected for analysis. The pure CO_2 and pure CH_4 adsorption isotherms are determined with the constant volume method at temperatures of 40 to 150 °C up to 5 atmospheres of pressure. The concentration pulse method is used to measure the Henry's Law Constant of pure CO_2 and CH_4 as well as the binary mixture adsorption isotherms for a candidate adsorbent. The results of these analyses have been applied to the operation of a PSA and the economics of a landfill gas separation.

Research Objectives

1. Identify an adsorbent with a high equilibrium capacity and selectivity for CO_2 at temperatures above 40 °C. The challenge is to find an adsorbent that applicable for a CO_2/CH_4 bulk separation with a PSA.
2. Incorporate the effects of temperature in adsorbent selection for a PSA bed designed for bulk equilibrium separation of CO_2 and CH_4. The challenge is to capture the change in equilibrium behaviour with temperature dependant isotherm models.
3. Measure the binary adsorption equilibrium behaviour of CO_2/CH_4 at atmospheric and elevated pressures. The challenge is to approximate the change in adsorption behaviour with pressure in a modified laboratory gas chromatograph.
4. Determine the economic expenses and returns with respect to landfill size for the PSA bulk separation of biogas. The challenge is to keep the analysis applicable to North America and compare the breakeven costs of upgrading LFG to other utilization technologies.

Thesis Structure

This thesis is presented in a paper format and includes four (4) chapters and five (5) Appendices. The first chapter introduces the topic of landfill gas upgrading by pressure swing adsorption and states the research objectives of the thesis. The second and third chapters consist of one paper each which will be submitted to be published in scientific journals. Their content is described in more detail below. The final chapter incorporates general conclusions and recommendations based on the findings of the two papers. The Appendices A and B have been added to compliment the analyses for chapter 2 and 3 respectfully. The restriction on journal article length does not allow a complete and transparent analysis of the experimental data therefore supplementary information has been located in the appendices. In addition, the methods of measurement and the details about the zeolite adsorbents used are included in the subsequent appendices.

Chapter II is composed of the paper by Bestfather, C. and Tezel, F.H.. The paper is entitled "Upgrading Landfill Gas by Adsorption: Adsorbent Selection and Equilibrium Data For the Bulk Separation of Carbon Dioxide and Methane" and is to be submitted for publication in the Journal of Energy & Fuels. This study identifies adsorbents that have potential for the separation of biogas based on the pure equilibrium behaviour and heats of adsorption. The pure isotherms of CO_2 and CH_4 are measured with a volumetric apparatus on CaX, NaY, and "NaLSX" (NaX zeolite with a Si/Al = 1.0) at temperatures of 40 to 150 °C and up to pressures of 4.5 atmospheres. Additionally, the concentration pulse chromatography technique is used to determine the Henry's Constants and limiting heat of adsorption for NaLSX. All of the adsorbents studied exhibit a favourable CO_2 isotherm and linear CH_4 isotherm although NaLSX has the highest CO_2 capacity at 40°C. The limiting heat of adsorption for NaLSX is 27.9 and 18.5 kJ/mol for CO_2 and CH_4 respectively.

The bulk separation of biogas in an adiabatic vacuum pressure swing adsorber (VPSA) exhibits a 70 to 140 °C increase in bed temperature for a pressure ratio of 80. The selectivity of CO_2 over CH_4 is favourable (5-20) based on a ratio of adiabatic working capacity. In conclusion NaLSX, NaX and NaY demonstrate applicability for the bulk separation of CO_2/CH_4 in a VPSA.

Chapter III is composed of the paper by Bestfather, C. and Tezel, F.H.. It is entitled: "Upgrading Landfill Gas by Adsorption: Economic Analysis and Binary Adsorption Behaviour of Carbon Dioxide and Methane on NaLSX" and is to be submitted for publication in the Journal of Environmental Science & Technology. This paper investigates the application of pressure swing adsorption for the bulk separation of biogases. The pure CO_2 and CH_4 gas adsorption equilibrium on NaLSX (Si/Al = 1.0) at 150 °C and up to 4.5 atm is compared with the binary equilibrium at 150 °C and total pressures of 1 and 3.3 atm. The binary equilibrium was successfully measured with concentration pulse chromatography in a gas chromatograph modified for total system pressures above 1 atm. The results show the domination of CO_2 in the adsorbed phase with comparable capacity at elevated temperatures of the experiments. The ideal separation factor of NaLSX ranges from 20 to 103 for the experimental conditions.

The results of the binary adsorption equilibrium experiments were applied to an economic analysis of a bulk PSA separation for LFG. The analysis included the sale of natural gas and the benefits of carbon credits for landfills sized from 0.2 to 10 Million tonnes. The results of the analysis indicate that upgrading LFG is not competitive with other utilization methods at current prices. It also suggests that if renewable fuel and green house gas economic incentives do increase, upgrading landfill gas is better suited for landfills above 4 million tonnes.

References

1. IPCC - Intergovernmental Panel on Climate Change *Waste Management & Research* **2008**, 26, 11-32.

2. Bogner, J.; Pipatti, R.; Hashimoto, S.; Diaz, C.; Mareckova, K.; Diaz, L.; Kjeldsen, P.; Monni, S.; Faaij, A.; Gao, Q.; Zhang, T.; Ahmed, M.M.; Sutamihardja, R.T.M.; Gregory, R. *Waste Management Research* **2008,** *26*, 11-32.

3. Forster, P.; Ramaswamy, V.; Artaxo, P.; Berntsen, T.; Betts, R.; Fahey, D.W.; Haywood, J.; Lean, J.; Lowe, D.C.; Myhre, G.; Nganga, J.; Prinn, R.; Raga, G.; Schulz, M.; Van Dorland, R. 2007: Changes in Atmospheric Constituents and in Radiative Forcing. *In: Climate Change **2007**: The Physical Science Basis. Contribution of Working Group I to the Fourth Assessment Report of the Intergovernmental Panel on Climate Change* [Solomon, S., D. Qin, M. Manning, Z. Chen, M. Marquis, K.B. Averyt, M.Tignor and H.L. Miller (eds.)]. Cambridge University Press, Cambridge, United Kingdom and New York, NY, USA.

4. Sulivan, P. *California Biomass Collaborative: 4th Annual Forum, Sacramento, California*, **2007**, March 28.

5. Ghoufi, A.; Gaberova, L.; Rouquerol, J.; Vincent, D.; Llewellyn, P.L.; Maurin, G. *Microporous and Mesoporous Materials* **2009**, *119*, 117-128.

6. Cavenati, S.; Grande, C.A.; Rodrigues, A.E. *Energy and Fuels* **2006**, *20*, 2648-2659.

7. Shin, H. *Adsorption* **1995**, *1*, 321-333.

8. Hagen, M.; Polman, E.; Myken, A.; Jensen, J.; Jönsson, O.; Dahl, A. *Swedish Gas Centre, Report SGC* **2001**, *118*, 1-142.

9. Ruthven, D.M.; *Principles of Adsorption and Adsorption Processes*; Wiley: New York, **1984**; pp 1–433.

10. Yang Ralph, *Adsorbents: Fundamentals and Applications*; John Wiley and Sons, Inc: New Jersey, **2003**.

11. Li, P.; Tezel, F.H. *Journal of Colloid and Interface Science* **2007**, *313*, 12-17.

Chapter II

Upgrading Landfill Gas by Adsorption: Adsorbent Selection and Equilibrium Data For the Bulk Separation of Carbon Dioxide and Methane

Bestfather, C.J.[*] and Tezel, F.H.[*a]

[*] Department of Chemical and Biological Engineering, University of Ottawa, 161, Louis Pasteur, Ottawa. K1N 6N5. Canada

[a] Author to which correspondence should be addressed

To be submitted for publication in *Energy & Fuels* journal, 2009.

Presented at the 58th Canadian Chemical Engineering Conference October 19-22, 2008, Ottawa, Ontario.

Abstract

Biogas is a significant green house gas that can be utilized as a renewable source of methane (CH_4) when it is separated from carbon dioxide (CO_2). In this study adsorption separation of these gases has been considered. The equilibrium adsorption behaviour of pure CO_2 and CH_4 was studied on various adsorbents to screen materials for a bulk separation of CO_2/CH_4. The pure adsorption isotherms of CO_2 and CH_4 were measured with a constant volume system on zeolites CaX, NaY, and NaLSX (Si/Al = 1.0) at temperatures of 40 to 100 °C and up to 4.5 atmospheres of pressure. Additionally, the concentration pulse chromatography technique was used to determine the Henry's Law constants and limiting heat of adsorption for NaLSX.

All of the adsorbents exhibited a favourable CO_2 isotherm and linear CH_4 isotherm. The limiting heats of adsorption for NaLSX were determined to be 27.9 and 18.5 kJ/mol for CO_2 and CH_4 respectively. The bulk separation of biogas in an adiabatic vacuum pressure swing adsorber (VPSA) cycle (pressure ratio of 80) exhibited 70 to 140 °C increase in bed temperature. The selectivity for CO_2 over CH_4 was favourable (5-20) based on a ratio of adiabatic working capacity. In conclusion NaLSX, NaX and NaY have applicability for the bulk separation of CO_2/CH_4 in a VPSA.

Introduction

Biogas from landfills and waste water sludge is a renewable energy resource that can be upgraded to an alternative fuel source. Biogas is a result of the anaerobic digestion of organic waste in bioreactor vessels and landfills. It is our environmental responsibility to capture this gas before it is released to the atmosphere because it is composed of several greenhouse gases (GHG) that contribute to global warming and climate change. The main component is methane (CH_4) that makes up approximately half of the mixture with carbon dioxide (CO_2). The composition of Landfill Gas (LFG) varies with waste type, climate, and landfill age and contains a wide variety of trace compounds and saturated water vapour shown in Table II - 1.

Table II - 1 - Typical Landfill Gas Characteristics [1]

Component	Range
Methane (CH_4)	35% to 55%
Carbon Dioxide (CO_2)	20% to 50%
Nitrogen (N_2)	2% to 45%
Oxygen (O_2)	0.5% to 5%
Non-methane organic compounds (NMOCs)	200 to 2000 ppmv
Hydrogen Sulfide (H_2S)	20 to 500 ppmv
Carbon Monoxide (CO)	<10 ppmv
Siloxane	0.2 to 10 ppmv
Water (H_2O)	0-100% R.H.

At landfills biogas is flared to reduce its global warming potential (GWP). Methane has a GWP of 25 (assuming a 100 year lifetime in the atmosphere) compared to carbon dioxide with a GWP of 1 [2]. Therefore the combustion of LFG significantly reduces its GHG impact. Alternatively, if the methane in biogas is upgraded, it can be piped directly into natural gas (NG) pipelines or used as an alternative fuel for waste disposal vehicles and landfill equipment [1].

The bulk separation of CO_2 and CH_4 is an important step of the biogas upgrading processes. The CO_2 must be removed to increase the energy content of the gas and to prevent corrosion in NG transportation and equipment [3]. There exist several competing technologies for the bulk separation of CO_2 and CH_4. They include: cryogenic

distillation, absorption (chemical or physical), membrane separation, and adsorption. For small to medium sized landfills adsorption separation has the advantages of being less energy intensive than cryogenic and absorption technologies [4]. As a promising separation technology, a Pressure Swing Adsorber (PSA) also does not require water or liquid chemicals in its operation as in absorption processes.

Adsorption processes separate gas mixtures by differences in adsorbent capacity, electrostatic properties, and diffusion rates. The physical interaction of van der Waals forces between the gas "adsorbate" and solid "adsorbent" create a potential for adsorption. This interaction between the adsorbent and the adsorbate is a very important factor in determining the size of the packed bed for PSA and the overall efficiency.

Table II - 2 - Physical properties of CO_2 and CH_4 [5]

Adsorbate	CH_4	CO_2
MW (kg/kmol)	16.04	44.01
$D_{gas\text{-}He}$ x 10^5 (m^2/s)	6.76	5.65
Kinetic Diameter (Å)	3.80	3.30
Polarizability (10^{-40} $J^{-1}C^2m^2$)	2.93	2.89
Dipole Moment ($Å^3$)	0.0	0.0
Quadrupole moment ($Å^3$)	0.00	0.64
T_b Boiling Temperature (K)	111	195
T_c Critical Temperature (K)	190.6	304.2
P_c Critical Pressure (atm)	45.4	72.9

Table II - 2 compares the properties of the main components of LFG. CO_2 has a larger molecular weight and is more linear in shape than the spherical CH_4 [5]. Both gases share a similar kinetic diameters and lack dipoles. The main difference is the quadrupole moment of CO_2 whereas CH_4 has none. A significant potential for adsorption for CO_2 over CH_4 is a result of this difference, especially on heterogeneous adsorbent surfaces.

Zeolite adsorbents are used commercially for gas mixture separation. Synthetic zeolites have a stable crystal structure with surface areas of 500-800 m^2/g [7]. X and Y type zeolites are selected based on their adsorption behaviour with pure CO_2 and CH_4 gases. These zeolites have a uniform pore size of 8.1 Å [7]. Adsorbent selection is the most important part of PSA design [6]. A more detailed description of zeolite structure is provided in Appendix C.

In this paper adsorbents for the bulk separation of CO_2/CH_4 from LFG are screened based on equilibrium parameters. The properties measured in the laboratory include the selectivity, capacity, heat of adsorption, and adiabatic working capacity (AWC). Selectivity for CO_2 is necessary to produce a high purity methane product stream. The ideal selectivity for CO_2 is determined from a ratio of Henry's Law constants. The capacity for CO_2 determines the size of the adsorbent bed and the regeneration time. The heat of adsorption is released in the transition from the gas phase to the adsorbed phase for the adsorbate. It quantifies the energy required to reverse the physical adsorption process and regenerate the saturated adsorbent bed. Finally, the adiabatic working capacity and selectivity are determined from the adsorption isotherms and heat of adsorption data. These screening parameters indicate the applicability of an adsorbent for CO_2/CH_4 separation by adsorption.

Literature Review

Interest in renewable sources of energy like LFG began to rise when oil prices increased suddenly in the 1980's. Today, fossil fuel prices are on the rise again and international environmental regulations are encouraging GHG emissions reductions [8]. Demand for renewable and alternative fuels is also increasing and natural gas produced from biogas is an example. It can be marketed as a green fuel for electricity production, heating, or transportation fuel. For example, incentives for alternative fuel use in California have led to the development of 8 LFG to pipeline quality NG plants [1]. Currently, rising fuel prices and GHG emission regulations have set the stage for renewable fuels like upgraded landfill gas to become feasible on the green economical stage.

Upgrading LFG by adsorption separation is a well proven technology and a growing field [7]. The adsorption separation of landfill gas by pressure swing adsorption was first patented by Sircar, et al. in the late 80's [9]. Continuous development of new adsorbents has led to further research into CO_2/CH_4 separations with activated carbons, carbon molecular sieves (CMS), zeolites (natural and synthetic), and silicalites. In addition to capacity, adsorbents for LFG separation require selectivity and low heat of adsorption. Table II - 3 identifies the ranges of these properties.

Table II - 3 - Common CO_2 adsorbent properties

	Si/Al	Surface Area (m^2/g)[10]	Surface Polarity[10]	Pore size (Å)[10]	ΔH_{CO2} (kJ/mol)	CO_2 Selectivity*	Reference
Zeolite NaX	1-1.5	500 to 800	Hydrophilic	7 to 8.1	-26.2 to -54.73	20 - 75	[11]; [12]
Zeolite NaY	1.5-3	500 to 800	Hydrophilic	7 to 8.1	-30 to -33	N/A	[13]; [14]
Activated Carbon	N/A	100 to 3000	Non-polar	10 to 10^4	-16 to -26	1 - 5	[15]
Carbon Molecular Sieve (CMS)	N/A	500	Non-polar	4 to 9	-11 to -39	1 - 40	[5]; [12]; [16]
Silicalite	>1000	800 to 900	Hydrophobic	7 to 30	-20 to -27.4	2 - 3	[17]

*Equilibrium selectivity based on ratio of CO_2/CH_4 capacity at 1 atm.[10]

Activated carbon is widely used in PSA systems as a hydrophobic adsorbent [7]. It has a wide pore size distribution and has been used in the trace removal of LFG due to its organophilic surface. CMS are used for the kinetic separation of CO_2 from CH_4 although they require the diameter of the adsorbate to be comparable to the diameter of the pore [10]. The closing of the carbon pores results in a decreased CMS surface area however the surface is energetically homogeneous for CO_2 adsorption [5]. Synthetic zeolites are most commonly used for CO_2 bulk gas separations because of their selectivity. X and Y zeolites are types of faujasites that have a narrow pore size distribution and exchangeable cations within a crystalline structure [7]. Ackley et al. argue that natural zeolites have applications for the trace removal of CO_2, however not in the application of bulk separations due to their impurities and low reproducibility [18]. As a result, the majority of industrial applications for CO_2 adsorption utilize synthetic zeolites like CECA 13X (herein referred to as NaX).

Zeolites are crystalline aluminosilicates and are composed of SiO_4 and AlO_4 tetrahedra [7]. They contain cations that can be exchanged to modify the selectivity for components in gas mixtures. The zeolite Si/Al atomic ratio determines the number of ions within the framework to balance the overall charge. Cation type and Si/Al ratio are customized to optimize a PSA separation like LFG. In the case of CO_2/CH_4 separation the electrostatic field of the cation interacts directly with the quadrupole of the CO_2 to

increase the potential for adsorption [7]. The result is a high degree of localized adsorption around the cation sites in the zeolite crystals [19]. An example of this application is the commercial use of NaX to remove CO_2 from air before cryogenic separation of O_2 and N_2 [7].

NaLSX (Si/Al = 1.0) is an example of an adsorbent that has a high cation density and capacity for CO_2. Currently, there exists little CO_2 equilibrium data for this adsorbent (at pressures above 0.4 atm) and no CH_4 adsorption data due to a patent on zeolite manufacture with Si/Al ratios below 1.15 [20]. This is in sharp contrast to the well used and published NaX (Si/Al > 1.15). NaLSX represents the upper limit of cation density for zeolites due to the low quantity of silica within its structure.

Heat effects in bulk separations pose a challenging separation problem when compared to trace removal. Industrial PSA systems operate under adiabatic conditions where the heat released from adsorption directly heats the gas and adsorbent bed [4]. Since adsorption is an exothermic process the increase in temperature results in a decrease in capacity [21]. Temperature changes of up to 70 K have been observed in bulk separations of CO_2 [6]. Significantly larger heat of adsorption has the consequence of high PSA operational costs due to the energy input required for regeneration. Therefore an adsorbent with a high capacity and a low heat of adsorption can exhibit a superior working capacity that is advantageous in a PSA separation. The difference between the adsorption equilibrium capacities at the end of the high pressure feed and at the end of the low pressure regeneration is the working capacity. The effect of thermal conditions in a PSA cycle is conveniently measured with the adiabatic working capacity (AWC) [22]. This paper will examine the properties of NaLSX and compare its CO_2 adsorption behaviour with other zeolites for the bulk separation of landfill gas.

Experimental & Theory

In this section the method of experimentation and data analysis is described for: adsorbent capacity, selectivity at low pressures, heat of adsorption and adiabatic working capacity.

Constant Volume System (CVS)

The constant volume system evaluates the equilibrium capacity of an adsorbent by measuring the pressure change due to adsorption in a fixed volume. It is the oldest method of adsorption measurement and has been used since 1777 [23]. This system calculates the volume of gas adsorbed in contact with an adsorbent at various pressures and a fixed temperature [23]. An Accusorb 2100E Physical Adsorption Analyser (manufactured by Micromeritics Instrument Corporation) was equipped with two MKS pressure transducers at high (260 psi ±0.02) and low (1000 Torr ± 0.7) pressure ranges that measured the pressure change in a sample cell containing 4 to 5 g of out gassed adsorbent (W_s).

Prior to experiments, the adsorbent was regenerated under vacuum overnight at 350 °C to remove any water and impurities adsorbed in its structure. Then, the sample was cooled to the desired temperature and the dead volume (V_s) in the sample cell was estimated twice and an average used (±0.2 ml) with non-adsorbing Helium (He) gas. The temperature of the isotherm was maintained within ±0.4 °C with a thermal jacket and measured with thermocouples in the manifold and sample cell. Pressure and temperature were recorded with Labview software. The adsorbate gas was allowed 20 hrs to reach equilibrium with the adsorbent at which time the pressure in the system was observed to remain constant. Details on the operation of the constant volume system are provided in Appendix A.1.

The regeneration of the adsorbent determines the PSA operation cycle time and the greater part of energy required for system operation. The reversibility of the CO_2 adsorption isotherm is demonstrated with a desorption isotherm. This method is commonly used for equilibrium separations [24; 25].

Concentration Pulse Chromatography (CPC)

In this study Concentration Pulse Chromatography (CPC) has been used to measure Henry's Law constants and heat of adsorption [21; 26-28]. The linear relationship between the adsorbed phase and the gas phase at equilibrium is expressed as the Henry's Law Constant (K_P).

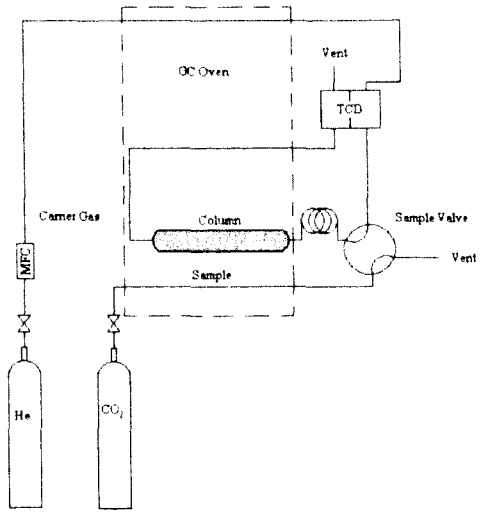

Figure II - 1 - Gas Chromatographic system with He carrier gas controlled by mass flow controller (MFC), CO_2 sorbate, and thermal conductivity detector (TCD).

A Varian 3300 Gas Chromatograph (GC) was employed to measure Henry's Law constants for various adsorbents. A He gas carrier was passed through a 10.5 cm long (L) stainless steel column (1.677 cm^3) filled with approximately 1 g of crushed (20x60 mesh) adsorbent. The carrier gas flow was controlled by an MKS mass flow controller (MFC) and verified with a bubble flow meter at the system outlet. The concentration of the gas was measured at the column outlet at atmospheric pressure with a thermal conductivity detector (TCD) and its signal (c) was recorded with Labview software installed on an Intel based computer. The helium gas entered the reference side of the TCD, then passed through the oven for heating and subsequently through a sample valve in which a pulse (1 ml sample) of adsorbate gas was injected into the carrier gas. The pulse passed through the column filled with crushed adsorbent and the sample gas was adsorbed causing a delay in the time the pulse remained in the column. The dimensionless Henry's Law constant (K) is determined from the first moment (μ) according to the following relationships [29]:

$$\mu = \frac{\int_0^\infty c(t-\mu_D)dt}{\int_0^\infty c dt} \tag{1}$$

$$\mu = \frac{L}{v}\left[1+\left(\frac{1-\varepsilon}{\varepsilon}\right)K\right] \tag{2}$$

The system dead time (μ_D) is the time (t) from injection to column exit determined for a pulse of a non-adsorbing gas. For these studies μ_D was deducted from the measured system retention time, as shown in Equation (1). The adsorbent was regenerated at 350 °C under a He purge for 24 hrs prior to experiments. The GC experiments were conducted in a 0.451 cm diameter and 10.5 cm long column, at volumetric flow rates between 5 and 30 cm^3/min (STP). The porosity (ε = 0.421) of the crushed adsorbent was determined with glass beads that have the same particle size (20x60 mesh) as the adsorbent packed in the column. The interstitial velocity (v) was calculated from the porosity, volumetric flowrate and column volume. The dimensionless Henry's Law constant (K) is related to the dimensional Henry's Law constant (K_p) at the experimental temperature (T) of the gas (R = ideal gas constant) as follows [30]:

$$K = K_p RT\rho_{ads} \tag{3}$$

The absolute density of the adsorbent pellets (ρ_{ads} = 2.23 g/cm^3 excluding the volume of the pores) was measure with non-adsorbing He gas at room temperature.

The pulse size of the CPC experiments was sufficiently small to ensure that the measurements were made in the Henry's Law region. The uncertainty in the Henry's Law constant measurements were determined by repeating the injections (after regeneration) at different flow rates for the same temperature and pressure for different samples of the same adsorbent.

The limiting heat of adsorption at low adsorbent coverage (ΔH_0) is calculated from the change in Henry's Law constant due to temperature. This follows the vant Hoff equation [10]:

$$\frac{d\ln K_p}{dT} = \frac{\Delta H_0}{RT^2} \tag{4}$$

Adiabatic Working Capacity (AWC)

The packed bed adsorbent increases in temperature adiabatically because the porous adsorbent behaves as an insulator. Therefore the majority of the heat released during the PSA operation goes into heating the bed [4]. The capacity and temperature changes in the bed are correlated with the adiabatic working capacity (AWC). For a PSA cycle the low and high pressures are predetermined and the adsorbent behaviour with respect to temperature is evaluated from an isobar plot (amount adsorbed vs temperature for lines of constant partial pressure). The PSA operating line intersects the isobar plot at the feed conditions (partial pressure of adsorbate species at feed temperature conditions) with a slope of $\Delta H/C_{ps}$ [18]. This method assumes all of the heat generated due to adsorption goes into heating the adsorbent bed with solid heat capacity C_{ps}. The difference between the capacity at the end of the high pressure feed and the end of the low pressure regeneration provides the pure gas adiabatic working capacity and an approximation of the bed temperature swing.

VSA-PSA systems (herein shortened to VPSA) are commonly regenerated at 0.1 atm because any lower pressures increase vacuum pump operating costs [4]. The changes in capacity and temperature are directly related to the operation cycle and a 4 step VPSA cycle is used [31]:

1. Feed pressure (1 atm) and temperature (5 to 100 °C)
2. Pressurization (8 atm)
3. Counter-current blow down (1 atm)
4. Vacuum Regeneration (0.1 atm)

To generate the isobar plot the adsorption isotherm data at several temperatures are used. The isotherms have been "fit" (by minimizing the *SSR*) to the Temperature Dependant (TD) Toth Isotherm Model [32]. The amount of data available for fitting the isotherms to the TD Toth isotherm model varied depending on the adsorbent. In most cases only two isotherms were available whereas NaLSX has up to four isotherms, NaX [33] and silicalite [17] has three isotherms. Additionally, the heats of adsorption measured in the laboratory were used where ever possible and literature values are

supplemented where necessary. Utilizing the TD model allows for the equilibrium adsorption capacity (q) to be interpolated at various temperatures and pressures as follows [32].

$$\theta = \frac{q}{q_s} = \frac{bP}{\left[1+(bP)^t\right]^{\frac{1}{t}}} \quad (5)$$

Where P is the pressure (atm) and the other parameters can be written as functions of temperature as follows:

$$q_s = q_{so} \exp\left[\chi\left(1-\frac{T}{T_0}\right)\right] \quad (6)$$

$$b = b_\infty \exp\left(\frac{Q}{RT}\right) = b_o \exp\left[\frac{Q}{RT_o}\left(\frac{T_o}{T}-1\right)\right] \quad (7)$$

$$t = t_o + \alpha\left(1-\frac{T_0}{T}\right) \quad (8)$$

Q is the heat of adsorption (kJ/kmol)

T_o is the reference temperature (K)

q_{so}, χ, b_o, t_o, and α are all constants

The parameters for the model are determined by a least squares minimization technique utilizing the non-linear solver tool in MS Excel for all of the experimental temperatures. Initial estimates of these parameters were based on single isotherm behaviour and common sense. After the determination of these parameters, a spreadsheet was used to calculate the capacity and temperature at which lines of constant pressure could be drawn. Although the isobar plots are constructed only from the CO_2 pure isotherm data. Since the CO_2/CH_4 mixture adsorption was mostly dominated by CO_2 on zeolites, the isobars provide a good estimation of the mixture behaviour [17; 33].

Adsorbent Selection

A simple method is used in this work for selecting an adsorbent for the bulk separation of CO_2/CH_4 from biogas. Comparing isotherm capacities or Henry's Law constants of CO_2 and CH_4 can indicate the equilibrium selectivity (α_{eq}) for CO_2 on various adsorbents [7].

$$\alpha_{eq} \approx \frac{q_{CO2}}{q_{CH4}} \tag{9}$$

$$\alpha_{eq} = \frac{K_{CO2}}{K_{CH4}} \cong \frac{(q_S b)_{CO2}}{(q_S b)_{CH4}} \tag{10}$$

This relatively simple method of selection does not take into account the VPSA operating conditions or the change in bed temperature for bulk separations. Additionally the mixture behaviour and competition for adsorption sites is largely overlooked. The relatively simple adsorbent selection practice of Ackley [22] that takes operating conditions, temperature change, and mixture behaviour into account is the AWC selectivity method.

The AWC selectivity is based on the ratio of the AWC evaluated at the adsorption ($_{ADS}$) and desorption ($_{DES}$) conditions (mole fraction, bed temperature, and pressure). The AWC for a pure gas is given by the following equation [22]:

$$\Delta AWC = q(P,T)_{ADS} - q(P,T)_{DES} \tag{11}$$

The selectivity for a given adsorbent, binary mixture, and PSA cycle can be compared in the form of a ratio of AWCs in the following manner [22]:

$$\alpha_{AWC} = \frac{\Delta AWC_{CO2}}{\Delta AWC_{CH4}} = \frac{[q(y,P,T)_{ADS} - q(y,P,T)_{DES}]_{CO2}}{[q(y,P,T)_{ADS} - q(y,P,T)_{DES}]_{CH4}} \tag{12}$$

Where the adsorbent capacities are evaluated with a multi-component model at the molar composition (y), temperature (T) and pressure (P) at the end of the adsorption and desorption steps. The temperature change in the bed is based on the adsorption of CO_2 and not in combination with CH_4. This assumption was made because the adsorbents studied have a greater capacity and larger heat of adsorption for CO_2. The above

selectivity parameter is shown to have good predictive capabilities of recovery for equilibrium bulk separations [7; 18].

Materials

The adsorbents used in this study were graciously provided by Air Products and UOP. Table II - 4 gives the physical properties of the adsorbents considered in this study. The zeolite NaX (Si/Al = 1.0) is known as "NaLSX" where the LSX represents a low silica to alumina ratio.

Table II - 4 – Physical Properties of the Adsorbents considered in this study.

	Supplier	Si/Al Ratio	Cation Density (ions/cage)	Size	ρ_{Bulk} (g/cm^3)	C_{ps} (J/g K)
NaLSX	Zeochem	1.0	96.0	8x14 mesh	0.632	0.92
NaY	UOP	1.8	68.6	8x14 mesh	0.729	0.92
CaX*	Air Products	1.17	53.1	8x14 mesh	0.645	0.92
NaX[33]	CECA	1.17	88.5	8x14 mesh	0.659	0.92
Silicalite[17]	UOP	>1000	0.0	1/16" extrudate	1.070	1.00

*The CaX is 80% substitution of NaX.

All bulk densities (ρ_{Bulk}) were measured in the laboratory (±0.001 g/cm^3). The zeolite heat capacity was assumed to be similar and the value for NaX (0.920 J/g K) was used for all zeolites [34]. This assumption was made since the heat of adsorption is the main contribution to the AWC calculations. Similarly the Si/Al ratio was obtained from the manufacturer and subsequent literature. CaX is supplied by Air Products and is made from NaX by ion exchanging with Ca^{2+} cations (up to 80% substitution). As a result the CaX zeolite has the same adsorbent Si/Al ratio as NaX although the cation density is lower due to the divalent cation substitution. Volumetric experiments for NaX and Silicalite were performed in our laboratory by Mulgundmath et al [33] and Li and Tezel [17] respectively. The isotherms (at 40, 70, and 100 °C) and heat of adsorption for CO_2 and CH_4 have been used in this paper to compare the selectivity of NaLSX (measured by present author) to other adsorbents with elevated Si/Al ratios.

The adsorbents in Table II - 4 were selected to provide a comparison of Si/Al ratios for the CO_2/CH_4 mixture separation. The gases used in this study were provided by BOC GASES®. The CO_2 was of Bone Dry Grade 3.0 (99.9% purity), CH_4 of Ultra High Purity 3.7 (99.97% purity), and Helium of Ultra High Purity 5.0 (99.999% purity).

Results & Discussion

The zeolite adsorbents listed in Table II - 4 are presented as isotherms at 40 °C. The isotherms of NaLSX, NaY, and CaX were measured and compared with the isotherms of NaX [33] and silicalite [17] from literature. Because NaLSX has, theoretically, the lowest Si/Al the adsorbent was selected to comparing its isotherm behaviour at various temperatures, regeneration, Henry's Law constants, and limiting heat of adsorption to silicalite [17], NaX [33], CaX and NaY. In addition a detailed analysis of NaLSX was chosen because of its high capacity for CO_2 and the absence of adsorption equilibrium data on this zeolite at high pressures. Finally, adiabatic CO_2 working capacities are presented for the adsorbents studied.

Isotherms at 40 °C

The isotherms at 40 °C and up to 4 atm in Figure II - 2 demonstrate that CO_2 is adsorbed with much higher capacity than CH_4 on all of the zeolites studied. This figure illustrates the rectangular isotherm shape of CO_2 at low pressures compared to the linear isotherms of CH_4. At 1 atm pressure, CO_2 adsorbent equilibrium capacity begins levelling off at 3-5 mol/kg whereas CH_4 capacity is around 0.5 mol/kg. At these conditions the bulk separation has an equilibrium selectivity of 6-10 (according to equation 9 and depending on temperature) which increases as the partial pressure of CO_2 decreases.

In LFG, CO_2 has a partial pressure of 0.5 atm and the capacity of CO_2 follows NaLSX>CaX>NaX>NaY in decreasing order. Under these conditions the capacity of CH_4 at 40 °C is relatively similar for the three zeolites and followed the order: CaX>NaLSX>NaX>NaY.

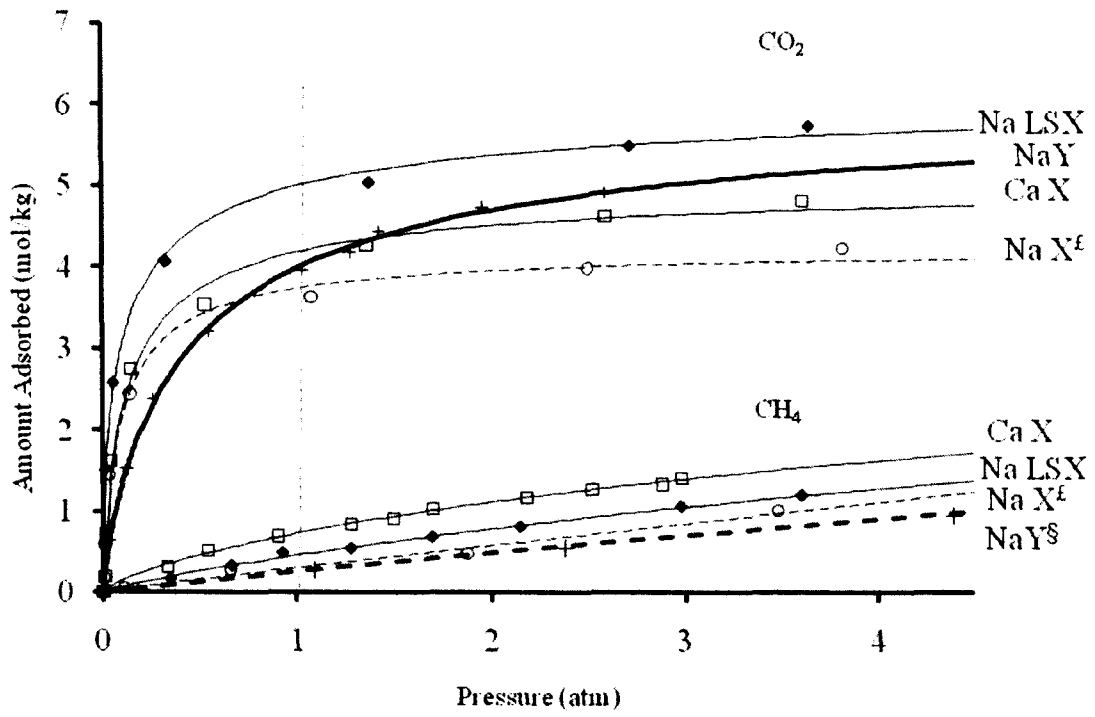

Figure II - 2 – CO_2 & CH_4 isotherms NaLSX and CaX at 40 °C. NaY-CO_2 isotherm at 40°C was measured with the CVS. The broken curves - NaY§-CH_4 and NaX£ (CO_2 and CH_4) isotherms are from Talu et al. [14] and Mulgundmath et al[33] respectively. All data are fit to the Toth isotherm model.

The differences in CH_4 capacity between the four zeolites studied are relatively small. Literature data for NaY-CH_4 [14] isotherm at 40 °C was fit to the Toth isotherm model and was found to behave similarly to the other zeolites. They all increase linearly with increasing partial pressure within the pressure range presented in this study. Therefore the equilibrium selectivity for CO_2 will decrease as pressure is increased for the PSA at higher pressures because capacity for CH_4 adsorption increases, whereas that for CO_2 starts levelling off.

NaLSX-CO_2 isotherm is rectangular compared to the NaY-CO_2 isotherm which behaves in a less rectangular fashion due to its low cation density. There are less high energy adsorption sites in NaY and CO_2 has a relatively low adsorption potential at low partial pressures when compared to the other zeolites. Similar observations have been made for CO_2 adsorption by NaX and NaY at 22 °C [21].

At pressures below 0.7 atm the 3 Na^+ zeolites have CO_2 capacities that increase with cation density (NaLSX>NaX>NaY). This follows the Si/Al ratio; as it decreases, the equilibrium capacity for CO_2 increases. This behaviour is due to the interaction of the quadrupole moment of CO_2 with the electrostatic field of the Na^+ cations. The predominant electrostatic interaction of CO_2 and Na^+ cations in zeolites is identified by Ghoufi et al. [3] The presence of more cations within the unit cell increases the potential for adsorption for CO_2. Once the high energy adsorption sites adjacent to the cations become occupied, the remaining sites are available as pressure increases. As the amount of CO_2 adsorbed increases the distance between the adsorbed molecules decreases [3] resulting in a higher interaction energy. This causes the adsorption potential to decrease and the isotherm to level off at pressures above 0.7 atm.

In summary, the equilibrium results at 40 °C suggest all of the zeolite adsorbents presented above have a high capacity and selectivity for CO_2 which is necessary for the CO_2/CH_4 bulk separation. Of the zeolites studied, NaLSX has the largest potential for CO_2 adsorption and the following measurements further examine this adsorbent.

NaLSX CO_2 and CH_4 Isotherms

CO_2 and CH_4 isotherms for NaLSX were measured at 40, 70, 100, and 150 °C with the CVS up to 4.5 atm and the results are shown in Figure II - 3. Four temperatures were chosen to characterize the adsorbent equilibrium behaviour as temperature increases. There is a significant potential for CO_2 adsorption at low pressures which is why X type zeolites are commonly used for trace removal [7]. NaLSX shows high equilibrium capacity at temperatures above ambient (25 °C) conditions. Therefore it can be beneficial to operate the bulk separation VPSA at a higher operating temperature and forego inter-stage cooling during feed compression.

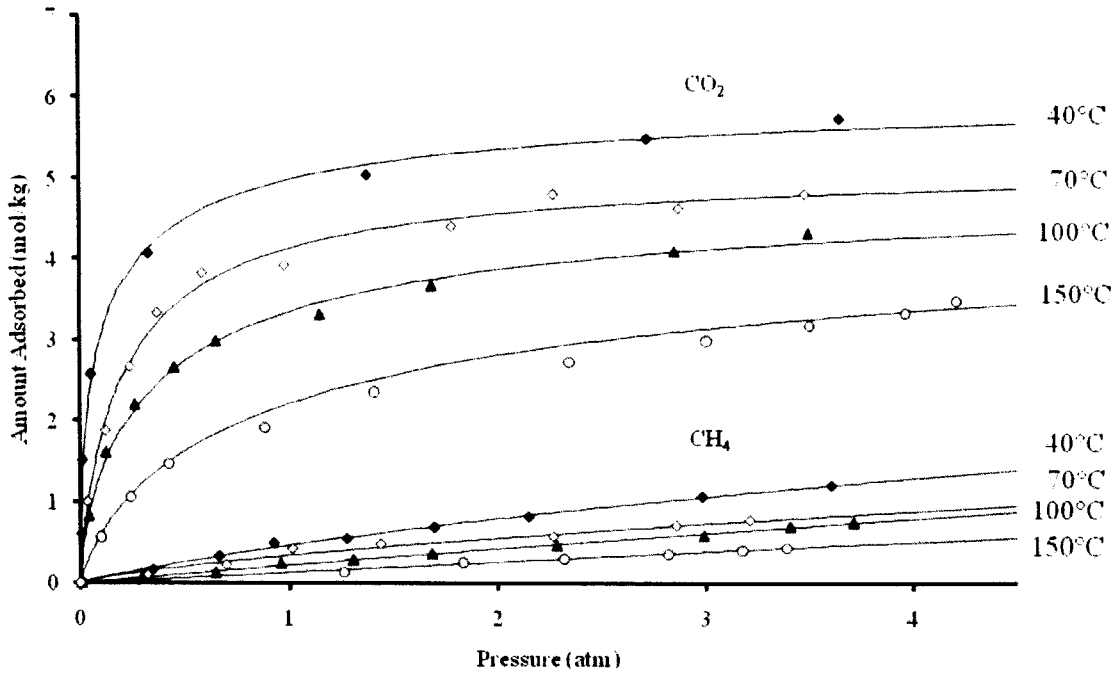

Figure II - 3 – CO_2 & CH_4 NaLSX isotherms measured with the CVS at 40 (◆), 70 (◇), 100 (▲), and 150 (○) °C and fit with TD Toth isotherm model.

Figure II - 3 shows the adverse effect of temperature on the equilibrium capacity for NaLSX adsorption of CO_2 and CH_4 as expected because physical adsorption is an exothermic process [10]. The NaLSX-CO_2 isotherm becomes less rectangular as temperature increases whereas the CH_4 isotherms retain their linear shape. In addition, the reduction in CO_2 capacity due to temperature is larger than that of CH_4 implying CO_2 capacity is more sensitive to temperature effects with a larger heat of adsorption. This behaviour suggests a decrease in NaLSX equilibrium selectivity at higher temperatures. Therefore operating the VPSA at temperatures above ambient will decrease equilibrium capacity and selectivity for CO_2.

Table II - 5 - TD Toth parameters for CO_2 and CH_4 on NaLSX at 40 to 150 °C

	n_{so} (mol/kg)	χ	b_o (atm^{-1})	t_o	α	Q/RT_o (kJ/mol)	T_o (K)
CO_2	6.09	0.62	24.99	0.63	0.04	9.91	313.15
CH_4	2.48	0.00	0.21	1.14	0.47	4.62	313.15

The TD Toth isotherm model describes the NaLSX CO_2 & CH_4 system well with minor deviation from the measured data. Table II - 5 contains the six parameters of the temperature dependant Toth isotherm model that describe the variation of n_s, b, and t over the temperature range measured (see equations 5 – 8). The raw isotherm data is located in Appendix A. It should be noted that extrapolating this model to temperature and pressure ranges outside of the present study invites uncertainty.

NaY and CaX CO_2 and CH_4 Isotherms

CO_2 and CH_4 isotherms for CaX and NaY were measured at 40 and 100 °C by the CVS up to 4.5 atm and are shown in Figure II - 4.

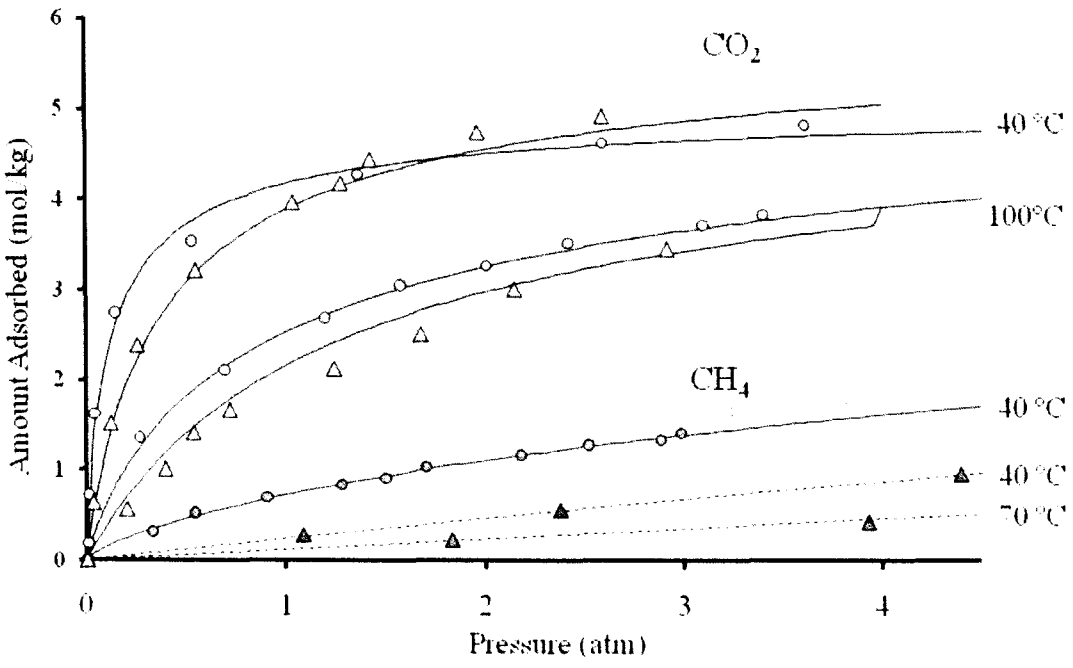

Figure II - 4 – CaX- CO_2 isotherms with (○) @ 40 & 100 °C & CaX-CH_4 (●) isotherm @ 40 °C measured with the CVS. NaY-CO_2 isotherms @ 40 & 100 °C (△) measured with the CVS & NaY-CH_4 (▲) isotherm data at 40 and 70 °C from Talu et al.[14] All curve fits with TD Toth isotherm equation.

The capacity of both CaX and NaY for CO_2 exhibit similar temperature dependence. The capacity of CaX for CH_4 is relatively larger than NaY and the temperature dependence is relatively small when compared to the behaviour of CO_2.

The TD Toth adsorption isotherm model accurately represents the equilibrium behaviour of NaLSX, CaX and NaY. Table II - 6 shows the parameter values used to fit the isotherms presented in Figure II - 4. In addition, the isotherms of NaX [33], Silicalite [17] and NaY (CH_4 only) [14] from literature are also fit to the TD Toth isotherm based on the single isotherm data. The raw isotherm data for NaLSX, CaX and NaY is located in Appendix A along with data and figures of the Toth model for NaX [33], silicalite [17], and NaY (CH_4) [14].

Table II - 6 - TD Toth parameters for CO_2 and CH_4 on CaX, NaY, NaX, and Silicalite at 40 to 100 °C

	n_{so} (mol/kg)	χ	b_o (atm^{-1})	t_o	α	Q/RT_o (kJ/mmol)	T_o	Reference
CO_2								
CaX	5.20	0.00	14.33	0.68	-0.47	13.97	313	Present study
NaY	5.86	0.73	3.26	0.80	-0.59	8.58	313	
NaX	4.36	0.00	18.12	0.72	-0.05	10.18	313	[33]
Silicalite	3.72	0.00	1.66	0.49	0.87	10.87	313	[17]
CH_4								
NaY	4.22	2.53	0.06	1.31	2.91	5.54	313	[14]
NaX	1.80	0.80	0.20	1.65	-1.00	6.00	313	[33]
Silicalite	2.03	0.00	0.26	1.07	1.07	4.81	313	[17]

NaLSX Vacuum Regeneration

NaLSX has the highest capacity and potential for adsorption of the zeolites studied. A desorption isotherm at 40 °C was measured after saturating and then vacuuming the same adsorbent sample. The reversibility of the NaLSX adsorbent is demonstrated in Figure II - 5 with an adsorption and desorption isotherm. To do that, the CO_2 adsorption isotherm at 40 °C was measured with the CVS up to 4 atm and was followed by the desorption isotherm (measured down to 0.045 atm). For each desorption point the system was left up to a maximum of 48 hrs to reach equilibrium (no significant change in pressure). CO_2 was selected from the CO_2/CH_4 bulk mixture for this desorption study since it is the adsorbed component to be removed from the VPSA with vacuum regeneration. Only one desorption cycle was performed to show that the adsorbent could be regenerated with only a vacuum and without the addition of temperature.

The capacity for CO_2 is shown in Figure II - 5 to be replicated well within the theoretical operational range of the VPSA (0.1 atm to 8 atm). Therefore pure CO_2 can be regenerated from the NaLSX adsorbent via equilibrium at 40°C in a vacuum although the kinetics of the regeneration and temperature drop in the bed require further investigation.

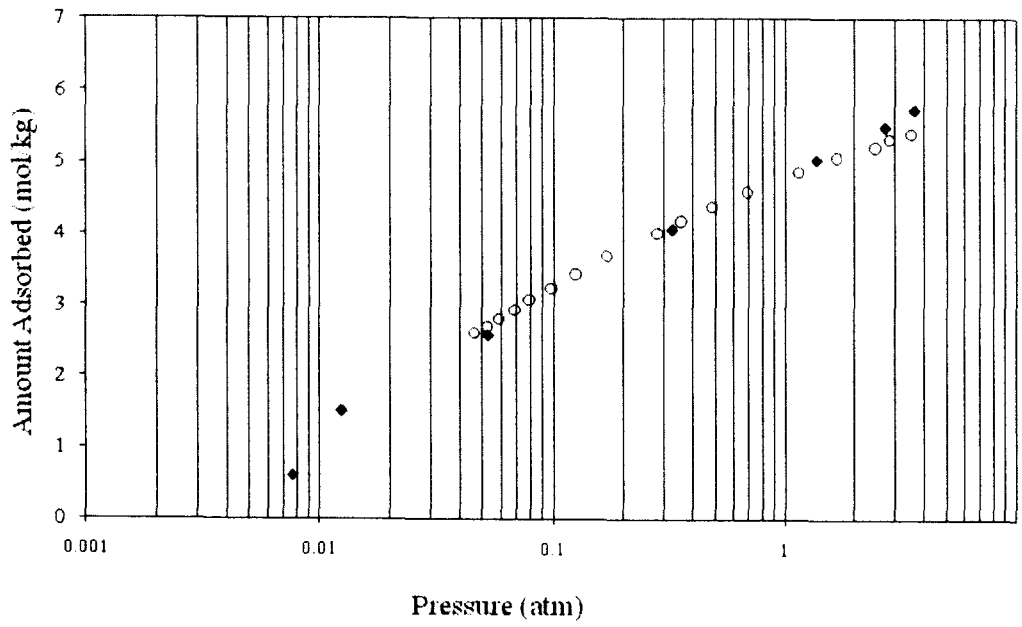

Figure II - 5 – NaLSX adsorption (♦) and desorption (O) isotherm (CO_2 vacuum regeneration at 40 °C).

Literature Comparison of NaLSX isotherm results

As stated earlier, few experimental results have been published for CO_2 and CH_4 adsorption isotherms on NaLSX. Three references to NaLSX (Si/Al ≈ 1.0 assumed) were found [20; 36; 37] and all contained data at pressures below 0.4 atm. The isotherm data of Brandani et al [37] was measured with the zero length column method up to partial pressures of 0.03 atm. This pressure is too low to compare with the CVS data since the CVS is better suited to measure equilibrium capacity above pressures of 0.1 atm and the comparisons below reflect this.

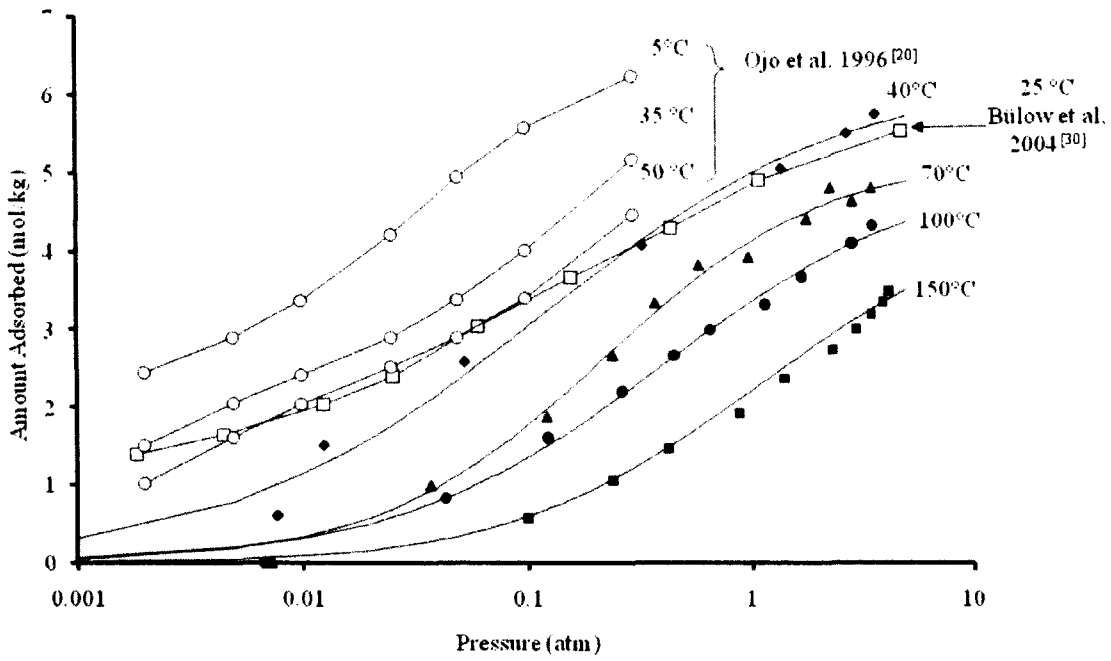

Figure II - 6 – NaLSX CO_2 isotherm comparison. CVS present study at 40 (◆), 70 (▲), 100 (●), and 150 (■) °C (fit with TD Toth model), Bülow [36] at 25 °C (□), and Ojo et al [20] at 5, 35, and 50 °C (○).

The CO_2-NaLSX isotherms are compared with the gravimetric results of Bülow et al [36] on the adsorbent FAU-I or "NaLSX" at 25 °C in Figure II - 6. The CO_2 capacity (at 40 °C) of NaLSX in the present study is comparable to the results they obtained above pressures of 0.1 atm. As expected, their lower temperature (25 °C) results are higher than the capacity of the present study at 40 °C. The capacity of the 50 °C isotherm from Ojo et al [20] is higher than that measured with the CVS at 40 °C in the present study. In comparison, the 40 °C isotherm is up to 1 mol/kg lower than their results at 50 °C. The comparisons above show higher CO_2 capacity than measured in the present study. The discrepancies are likely due to differences in NaLSX sample Si/Al ratio and equilibrium measurement techniques. Despite this plausible difference, in general they show a similar trend of CO_2 equilibrium capacity increasing as temperature decreases. A detailed CVS uncertainty analysis is provided in Appendix A.

Literature data high NaLSX CO_2 capacity at temperatures lower than those measured in the present study. This implies that CO_2 equilibrium selectivity is likely to extend into

lower operational temperatures, which can be the condition for LFG due to its seasonal temperature variation.

Henry's Law Constant (K_p)

The Henry's Law constants for NaLSX are measured with the CPC and the CO_2 values are compared to the low pressure literature values. The Henry's Law Constants of CO_2 in Figure II - 7 are several magnitudes higher than CH_4 indicating a high selectivity for CO_2 at low partial pressures. This was expected based on the steep CO_2 isotherm compared to the linear CH_4 isotherm. The high selectivity for CO_2 at low partial pressures will warrant a pure CH_4 product from the bulk separation.

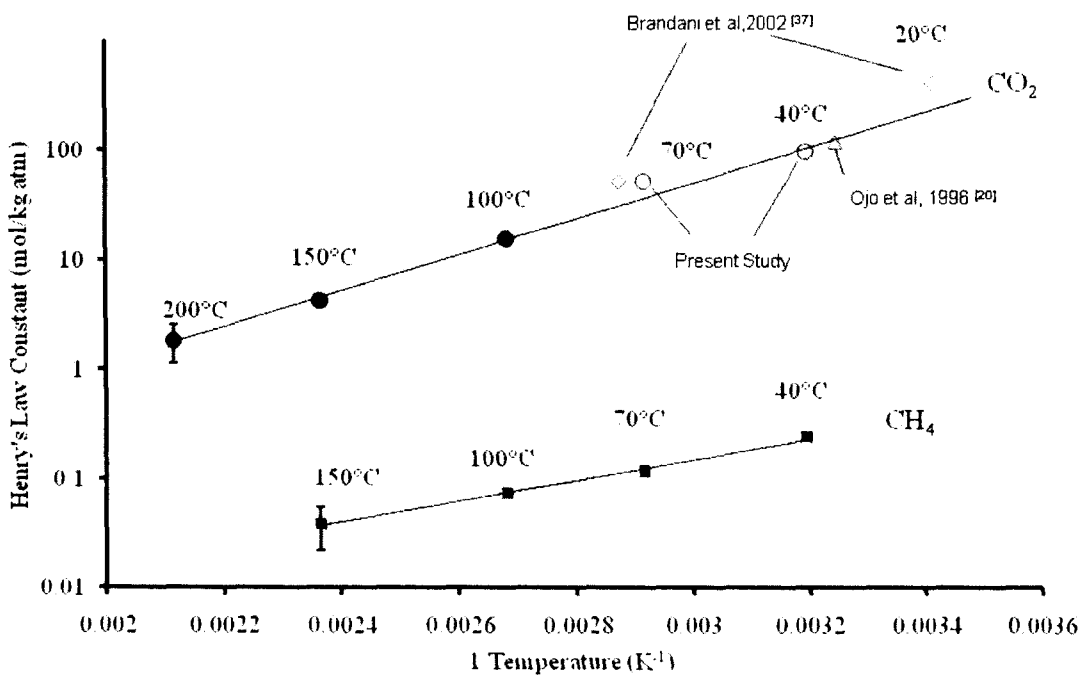

Figure II - 7 - Henry's Law constant results for NaLSX on CH_4 (■) and CO_2 (● - measured with CPC experimental data; ○ - estimated from initial slope of the isotherm) compared with literature (estimated from initial slope of the isotherm).

The Henry's Law constant measurements were repeated a minimum of 3 times and the 95% confidence interval associated with these replicates is illustrated with error bars in Figure II - 7. The raw CPC data is provided in Appendix A. The comparison of the

Henry's Law constants obtained in the present study with literature values was possible with the low pressure results shown in Figure II - 6. The NaLSX-CO_2 isotherms from literature were fitted to a Langmuir isotherm model [24] and the Henry's Law constants for these systems were determined from the initial slope of the isotherm. The results of Brandani et al [37] show reasonable agreement to the line of best fit determined with the CPC technique. The Henry's Law constant of Ojo et al [20] at 35 °C lies directly on the line of best fit. In the same fashion, the CO_2-NaLSX isotherms measured with the CVS at temperatures of 70 and 40 °C were also found to follow the line of best fit. The Henry's Law constants for CO_2 on NaLSX were not measured at temperatures below 100 °C because of the limited TCD sensitivity in combination of the high potential for adsorption at low temperatures. Even at high temperatures, NaLSX exhibits very high equilibrium selectivity (equation 10) of 400 to 100 for CO_2 at low partial pressures. This high selectivity indicates a favourable CO_2 separation although isothermal operation is not likely to be the situation for the bulk separation of CO_2/CH_4.

Limiting Heat of Adsorption ($-\Delta H_o$)

The limiting heat of adsorption values were calculated for CO_2 and CH_4 on NaLSX adsorbent from the slope of the van't Hoff plots given in Figure II - 7, as mentioned in the Experimental and Theory section. The results along with the 95% confidence interval are presented in Table II - 7 together with corresponding values from literature.

Table II - 7 – Limiting Heat of adsorption, $-\Delta H_0$ measured in kJ/mol (±95% confidence interval).

Adsorbent	Reference	CO_2	CH_4
NaLSX	**present study**	**27.9 (± 5.21)**	**18.37 (± 0.03)**
NaLSX	[37]	41.60	-
Zeochem NaX	[17]	34.9	-
Zeochem NaX	[39]	49.1	19.2
CECA 13X	[40]	37.22	15.29
NaX	[34]	54.73	15.68
CECA 13X	[17]	26.2	-
LiLSX	[37]	48.1	-
CaX	[37]	53.3	-
NaX	[41]	8.2	3.3
NaY	[17]	33.6	-
Silicalite (HiSiv-3000)	[17]	28.31	12.52

CO_2-NaLSX heat of adsorption value is greater than CH_4 as expected from the differences in the slopes of the van't Hoff plots in Figure II - 7. The greater heat of adsorption is due to the dominant electro static interactions of the Na^+ cation electric field with the quadrupole moment of CO_2. The CO_2 95% confidence interval (± 5.21 kJ/mol) is significantly large due to the variation of K_p data. This difficulty in CO_2 replication is a result of the considerable adsorption potential and uncertainty in the first moment analysis. Similar difficulty in CPC analysis of strong CO_2 adsorption on zeolites is observed by Triebe and Tezel [27].

Comparatively, the CO_2 limiting heat of adsorption on NaLSX is much lower than that of Brandani et al [37] even when accounting for the experimental uncertainty. This discrepancy is due to differences in measurement techniques. Differences of 10 to 20% are observed in heat of adsorption measurements at multiple laboratories for the same sample [38]. In contrast, the CH_4 limiting heat of adsorption is comparable to other zeolites and has a small degree of uncertainty. An isosteric heat of adsorption analysis is provided in Appendix A for CO_2 and CH_4 on NaLSX.

Adiabatic CO_2 Working Capacity (AWC)

The adiabatic CO_2 working capacity and bed temperature range is approximated with equation (12) for VPSA operating conditions. These conditions are a feed at 1 atm, pressurization to 8 atm, and a regeneration pressure of 0.1 atm [42]. This cycle represents a bulk VPSA separation with a pressure ratio of 80. The regeneration at low pressure increases the CO_2 working capacity by removing the largest fraction of the adsorbed CO_2. In addition, the adsorption stage pressurization has been shown to increase methane purity (for pressure ratios of 30 to 50) [4]. For the LFG scenario, the feed temperature is dependent upon the season. The effect of these operating conditions on bed working capacity and bed temperature are quantified in an isobar plot. Figure II - 8 illustrates an isobar plot of CO_2-NaLSX from 0.01 up to 10 atm with a VPSA operating line at 40 °C.

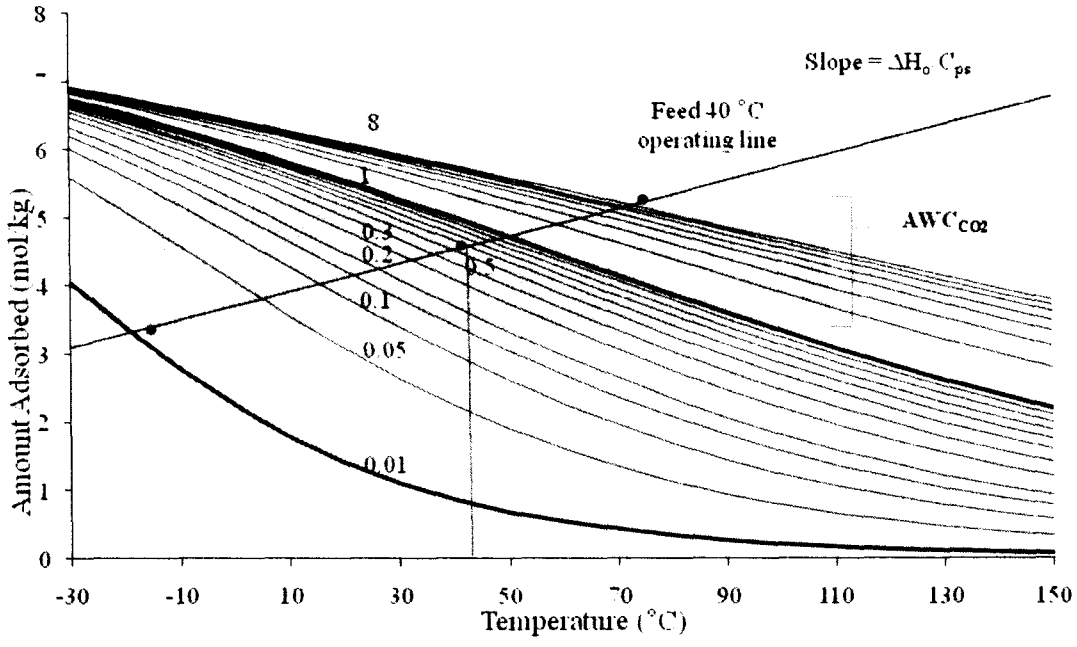

Figure II - 8 – NaLSX-CO_2 isobars (0.01 – 10 atm) from TD Toth isotherm fit. 40 °C operating line has slope of $\Delta H_o/C_{ps}$ (from Table 4 & 7) and intercept at LFG feed conditions (P_{CO2} = 0.5 atm).

Figure II - 8 demonstrates the relationship of NaLSX-CO_2 capacity with adsorbent temperature and pressure. The amount of CO_2 adsorbed on NaLSX decreases as adsorbent temperature increases. As pressure increases equilibrium capacity increases along the operating line and the largest changes in capacity occur as pressure decreases from 0.1 to 0.01 atm. This behaviour reflects the rectangular shape of the CO_2 isotherm observed for CO_2 on X-type zeolites.

For NaLSX and all of the other zeolites, as feed temperature is increased, the CO_2 AWC increases. This behaviour can be observed in Figure II - 8, where the AWC is calculated from equation (11). The isobars remain fixed and as the operating line intercept is shifted based on the inlet feed temperature (intercept remains on the P_{CO2} = 0.5 atm isobar). As feed temperature increased the operating line (with fixed slope $\Delta H_o/C_{ps}$) gets longer and hence the CO_2 AWC increases. This property is a result of the CO_2 equilibrium isotherm shape becoming more linear as temperature increases and the distribution of the capacity over a greater pressure range. Figure II - 9 illustrates the

increasing CO_2 AWC and decreasing CH_4 AWC as the feed temperature and subsequently the bed temperature at the end of the adsorption cycle rise.

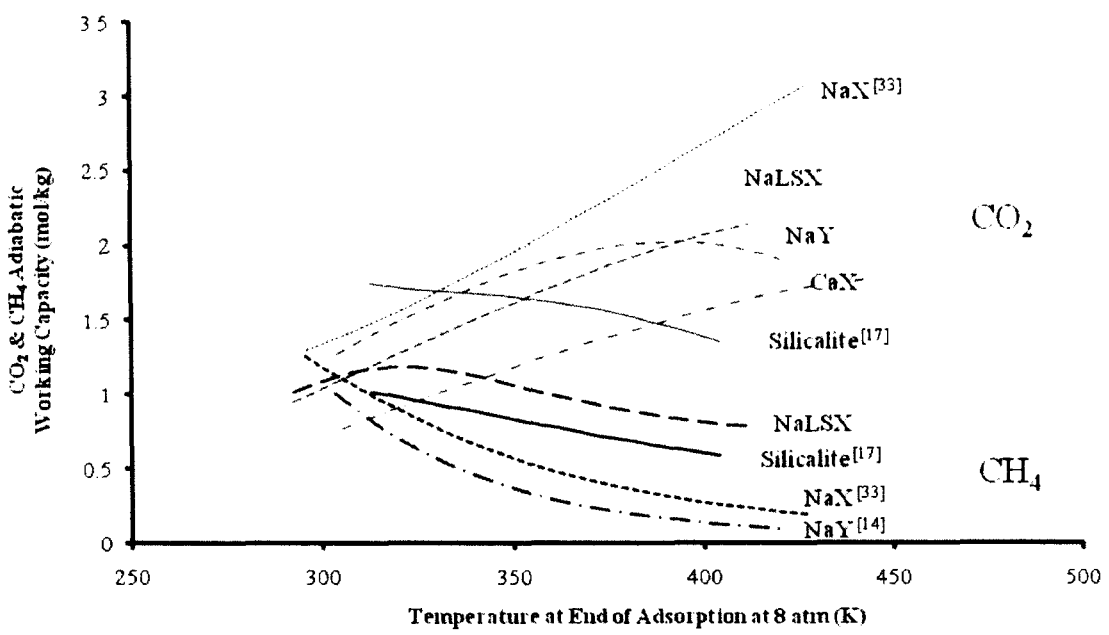

Figure II - 9 – CO_2 and CH_4 AWC behaviour as feed temperature is increased (HP – 8 atm, LP = 0.1 atm). The following isotherms data were fit to the TD Toth model: NaY-CH_4 from Talu et al.[14], NaX (CO_2 and CH_4) from Mulgundmath et al[33], and Silicalite (CO_2 and CH_4) from Li et al[17].

The CO_2 working capacities of all the zeolites increase with temperature in the adiabatic bed except for silicalite. The silicalite isobars differ from other zeolites in that the isobars narrow as temperature increases (See Appendix A). NaX exhibits the highest AWC for CO_2 although all the zeolites have relatively high values. Ackley et al [22] observed AWC for N_2 in the range of 0.8 to 0.2 (mol/kg) for the bulk separation of N_2/O_2 at a pressure ratio of 5. The values observed here are significantly higher due to the greater pressure ratio and differences in gases.

The CH_4 AWC decreases with temperature for all adsorbents as shown in Figure II - 9. NaY shows the lowest CH_4 AWC capacity. Conversely, NaLSX has the highest CH_4 adiabatic working capacity for the operating conditions proposed. The ratio of the CO_2 AWC to the CH_4 AWC from equation (12) gives the adiabatic working capacity selectivity which is shown in Figure II - 10.

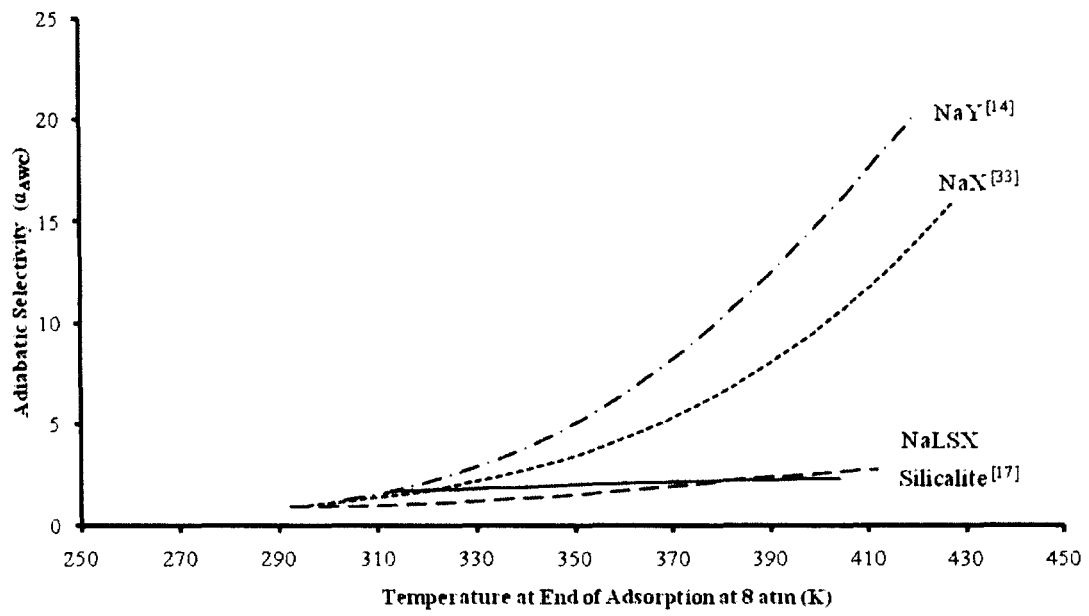

Figure II - 10 – CO_2 and CH_4 AWC selectivity as feed temperature is increased (HP = 8 atm, LP = 0.1 atm). The following isotherms data were fit to the TD Toth model: NaY-CH_4 from Talu et al.[14], NaX (CO_2 and CH_4) from Mulgundmath et al[33], and Silicalite (CO_2 and CH_4) from Li et al[17].

The selectivity of the four adsorbents in Figure II - 10 are favourable for the separation of CO_2 from CH_4. NaY and NaX have CO_2 selectivity that increases with temperature above 20 for the proposed VPSA operating conditions. For the bulk separation of N_2/O_2 on zeolites and pressure ratio of 5, selectivity of 5 to 12 is observed [22]. The high selectivity observed in the present study is a result of low CH_4 AWC. The numerator of equation (12) can reach very small numbers from minor differences in CH_4 capacity which artificially inflates the selectivity [18]. In comparison, silicalite and NaLSX have adiabatic selectivity for CO_2 that is favourable and relatively stable with respect to changes in bed temperature. This thermal stability is important for bulk VPSA separation process because as the adsorbent bed is cycled through several adsorption cyles, the bed temperature can change. If the adsorbent is not thermally stable the operation time and conditions will change which can result in process instability.[22]

The isobar results above are based on pure gas equilibrium and are used to approximate the multicomponent mixture behaviour. This assumption has been made because CO_2 is adsorbed much more strongly than CH_4 and controls the mixture behaviour). Based on the higher adsorption potential of CO_2 shown in Figure II - 3 & 4,

it is assumed that CO_2 dominates the binary system. Binary adsorption equilibrium studies show this to be true for silicalite [17], NaX [4, 33], NaY [3] and ZSM-5 zeolites [28].

Selecting an ideal adsorbent for VPSA bulk separation of CO_2/CH_4 is based on the adsorbent characteristics and their ability to be related to the adiabatic working capacity and selectivity. In this study NaX and NaY exhibit the highest selectivities although they lack thermal stability with variations in feed temperature. On the other hand, NaLSX shows high CO_2 capacity although low selectivity. In comparison to NaX and NaY, the thermal stability of NaLSX would be favourable for stability of the LFG VPSA bulk separation.

Capacity is the most important property to decrease the capital costs of a LFG PSA system; whereas selectivity is important for the process operational costs. It is preferable to have an adsorbent that exhibits both elevated selectivity at the PSA operating conditions and a high capacity. The zeolite adsorbents in the present study exhibit comparable capacity and selectivity with pure gases. An examination of their mixture capacity and selectivity for PSA conditions is necessary to complete the selection.

Conclusions

The equilibrium adsorption properties of three zeolites (NaLSX, NaY and CaX) were measured as screening parameters for the bulk separation of CO_2 and CH_4. All of the adsorbents showed high selectivity for CO_2 at low partial pressures due to the high potential of CO_2 relative to CH_4. The equilibrium isotherms exhibited high capacity for CO_2 and low capacity for CH_4.

NaLSX was studied in more detail because it has the highest cation density of all the zeolites studied and limited data is available for this adsorbent behaviour at pressures above atmospheric. Therefore measurements of its isothermal capacity from 40-150 °C up to 4 atm and the limiting heat of adsorption and Henry's Law constant were determined. NaLSX exhibited the highest capacity for CO_2 even at elevated temperatures due to its low Si/Al ratio and high density of cations. However the high potential for CO_2 adsorption also showed it to have a higher limiting heat of adsorption.

The ideal selectivity for NaLSX-CO_2 was shown to range from very favourable (up to 400 with ratio of Henry's Law Constants) to slightly favourable (5-20 with AWC selectivity). The large difference in these selectivities indicates the significant effect bed heating has on a bulk separation. VPSA bed temperature changes were in the magnitude of 70 to 140 °C based on adiabatic process for a pressure ratio of 80.

The zeolite equilibrium isotherms were used to evaluate expected working capacity and adiabatic working capacity for various VPSA operating conditions. NaLSX was shown to have the highest CO_2 working capacity for a bulk separation of LFG. The adiabatic working capacity was much smaller in comparison due to the heating effects that occur in a VPSA. As such NaX and NaY showed the highest AWC for the conditions selected although their selectivity increases with bed temperature. This suggests that the VPSA could be operated at higher temperatures effectively for the bulk separation of CO_2/CH_4 if the operation remains thermally stable.

In conclusion NaLSX, NaX and NaY show applicability for the bulk separation of CO_2/CH_4. All the zeolites studied have selectivity for CO_2 adsorption at low partial pressures due to the quadrupole moment. This bulk separation is sensitive to heating and it should be an important consideration in designing the separation process. Additionally all of the zeolites used are sensitive to water and NMOC adsorption therefore the pre-treatment of the landfill gas is an important step before the bulk separation. The result of a VPSA application to upgrade LFG will reduce GHG emissions, as well as produce high purity carbon dioxide and methane products.

Nomenclature

b	Equilibrium Constant	(atm^{-1})
b_s, b_o	Equilibrium Constant Parameter for TD Toth Isotherm	(atm^{-1})
c	Concentration Signal from GC	(volts)
C_p	Heat Capacity	(J/g K)
$D_{gas\text{-}He}$	Diffusion of gas into Helium	(m^2/s)
K	Dimensionless Henry's Constant	(-)
K_P	Dimensional Henry's Constant	(mol/kg atm)
L	Column Length	(m)
MW	Molecular Weight	(kg/kmol)
p	Partial Pressure	(atm)
P	Total Pressure	(atm)
P_c	Critical Pressure	(atm)
Q	Heat of Adsorption in TD Toth Isotherm Model	(kJ/mol)
q	Amount Adsorbed or Capacity	(mol/kg)
q_s	Saturation Capacity	(mol/kg)
q_{so}	Saturation Capacity Parameter for TD Toth Isotherm	(mol/kg)
R	Ideal Gas Constant	(J/mol K)
t, dt	Time or Time Step	(s)
t, to, α, χ	Constants in TD Toth Isotherm Model	(-)
T	Temperature	(K)
T_b	Boiling Temperature	(K)
T_c	Critical Temperature	(K)
T_d	Manifold Temperature	(K)
T_i	Interconnecting Tubing Temperature	(K)
T_o	Reference Temperature (TD Toth Isotherm Model)	(K)
T_s	Sample Cell Temperature	(K)
V	Volume	(ml)
V_d	Manifold Volume	(ml)
V_i	Interconnecting Tubing Volume	(ml)
V_s	Sample Cell Volume	(ml)
W_s	Adsorbent Sample Weight	(g)
ΔH	Isosteric Heat of Adsorption	(kJ/mol)
ΔH_0	Limiting Heat of Adsorption (zero coverage)	(kJ/mol)

Greek Letters

ε	Porosity or Void Fraction of Packed Bed	(-)
μ	First Moment	(s)
μ_D	First Moment (System Retention)	(s)
v	Interstitial Velocity	(m/s)
ρ_{ads}	Absolute Density of Adsorbent (excluding pore volume)	(g/cm^3)
ρ_{bulk}	Bulk Density of Adsorbent	(g/cm^3)

Abbreviations

AWC	Adiabatic Working Capacity
AlO_4	Alumina Tetrahedral
Si/Al	Atomic Ratio of Silica to Alumina
Ca^{2+}	Calcium Cation
CH_4	Methane
CO_2	Carbon Dioxide
CMS	Carbon Molecular Sieves
CO	Carbon Monoxide
CCX	Chicago Climate Exchange
CPC	Concentration Pulse Chromatography
CI	Confidence Interval
CVS	Constant Colume System
ECX	European Climate Exchange
EWC	Expected Working Capacity
GC	Gas Chromatogaph
GHG	Greenhouse Gas
GWP	Global Warming Potential
He	Helium Gas
H_2S	Hydrogen Sulphide
HP	High Pressure for Adsorption Stage of VPSA Cycle
JCR	Joint Confidence Region
LFG	Landfill Gas
Li^+	Lithium Cation
LP	Low Pressure Regeneration Stage of VPSA Cycle
MFC	Mass Flow Controller
CH_4	Methane
NG	Natural Gas
N_2	Nitrogen
NMOC	Non-methane Organic Compounds
O_2	Oxygen

PSA	Pressure Swing Adsorber
VSA-PSA or VPSA	Pressure Swing Adsorber (above 1 atm) with Vacuum Regeneration
SiO_4	Silicalite Tetrahedral
Na^+	Sodium Cation
STP	Standard Temperature and Pressure
SSR	Sum of Squared Residuals
TD	Temperature Dependant (Toth isotherm model)
TCD	Thermal Conductivity Detector
UOP	Universal Oil Products
H_2O	Water
ZLC	Zero Length Column

References

1. Sulivan, P. California Biomass Collaborative: 4th Annual Forum, Sacramento, California, 2007, March 28.

2. Forster, P.; Ramaswamy, V.; Artaxo, P.; Berntsen, T.; Betts, R.; Fahey, D.W.; Haywood, J.; Lean, J.; Lowe, D.C.; Myhre, G.; Nganga, J.; Prinn, R.; Raga, G.; Schulz, M.; Van Dorland, R. **2007**: Changes in Atmospheric Constituents and in Radiative Forcing. *In: Climate Change 2007: The Physical Science Basis. Contribution of Working Group I to the Fourth Assessment Report of the Intergovernmental Panel on Climate Change* [Solomon, S., D. Qin, M. Manning, Z. Chen, M. Marquis, K.B. Averyt, M.Tignor and H.L. Miller (eds.)]. Cambridge University Press, Cambridge, United Kingdom and New York, NY, USA.

3. Ghoufi, A.; Gaberova, L.; Rouquerol, J.; Vincent, D.; Llewellyn, P.L.; Maurin, G. *Microporous and Mesoporous Materials* **2009**, *119*, 117-128.

4. Cavenati, S.; Grande, C.A.; Rodrigues, A.E. *Energy and Fuels* **2006**, *20*, 2648-2659.

5. Bae, Y.S.; Lee, C.H. *Carbon* **2005**, *43*, 95-107.

6. Ruthven, D.M.; Farooq, S.; Knaebel K.S. *Pressure Swing Adsorption*; Wiley: Toronto, 1994; pp 1-350.

7. Yang R.T.; *Adsorbents: Fundamentals and Applications*, John Wiley and Sons, Inc: New Jersey, 2003.

8. Williams, T. Climate Change: Credit Trading and the Kyoto Protocol. Library of Parliament PRB 05-47E, December 2005; www.parl.gc.ca/information/library/PRBpubs/prb0547-e.htm, accessed November 2008.

9. Sircar, S.; Kumar, R.; Koch, W.R.; Van Sloun, J. Recovery of Methane from Land Fill Gas. US Patent 4,770,676, 1988.

10. Ruthven, D.M.; *Principles of Adsorption and Adsorption Processes*; Wiley: New York, 1984; pp 1–433.

11. Choudhary, V.R.; Mayadevi S. *Sep. Sci. and Tech.* **1993**, *28*, 2197-2209.

12. Cavenati, S.; Grande, C.A.; Rodrigues, A.E. *Energy and Fuels* **2005**, *19*, 2545-2555.

13. Pires, J.; Brotas de Carvalho, M. *Journal of Molecular Catalysis* **1993**, *85*, 95-303.

14. Talu, O.; Zhang, S.; Hayhurst, D.T. *Journal of Physical Chemistry* **1993**, *97*, 12894-12898.

15. Himeno, S.; Komatsu, T.; Fujita, S. *Journal of Chemical Engineering Data* **2005**, *50*, 369-376.

16. Nabais, J.M.V.; Carrott, P.J.M.; Ribeiro Carrott, A.M.; Padre-Eterno, J.A.; Menéndez, A.; Dominguez, and A.L. Ortiz. *Carbon* **2006**, *44*, 1158–1165.

17. Li, P.; Tezel, F.H. *Journal of Colloid and Interface Science* **2007**, *313*, 12-17.

18. Ackley, M.W.; Rege, S.U.; Saxena, H. *Microporous and Mesoporous Materials* **2003**, *6*, 25-42.

19. Ruthven, D.M.; Kumar, R. *Industrial Engineering Chemical Fundamentals* **1980**, *19*, 27-32.

20. Ojo, A. F.; Fitch, R.F.; Bülow, M. Removal of Carbon Dioxide from Gas Streams. US Patent 5,531,808, 1996.

21. Harlick, P.J.E.; Tezel, F.H. *Microporous and Mesoporous Materials* **2004**, *76*, 71-79.

22. Ackley, W.M. Multilayer Adsorbent Beds for PSA gas Separation. US Patent 6,152,991, 2000.

23. Keller, J.; Staudt, R. *Springer* **2005**, 1-420.

24. Langmuir, I. *Journal of the American Chemical Society* **1918**, *40*, 1361-1403.

25. Golden, T.; Sircar, S. *Journal of Colloid and Interface Science* **1994**, *162*, 182-188.

26. Triebe, R.W.; Tezel, F. H.; Khulbe, K.C. *Gas Separation and Purification Technology* **1996**, *10*, 81-84.

27. Triebe, R.W.; Tezel, F. H. *Gas Separation and Purification Technology* **1995**, *9*, 223-230.

28. Harlick, P.J.E.; Tezel, F.H. *Separation and Purification Technology* **2003**, *33*, 199-210.

29. Shah, D.B.; Ruthven, D.M. *AICHE Journal* **1977**, *23*, 804-809.

30. Harlick, P.J.E.; Tezel, F.H. *Adsorption* **2000**, *6*, 293–309.

31. Skarstrom, C.W. Method and Apparatus for Fractionating Gaseous Mixtures by Adsorption. US Patent 2,944,627, 1960.

32. Malek, A.; Farooq, S. *AICHE Journal* **1996**, *42*, 3191-3201.

33. Mulgundmath, V.P.; Tezel, F.H.; Saatcioglu, T.; Golden, T.C. *The Canadian Journal of Chemical Engineering*, Article in press Jan 2009.

34. Cavenati, S.; Grande, C.A.; Rodrigues, A.E. *Adsorption*, **2005**, *11*, 549-554.

35. Walton, K.S.; Abney, M.B.; LeVan, M.D. *Microporous and Mesoporous Materials* **2006**, *91*, 78-84.

36. Bülow, M.; Shen, D.; Jale, S.R. *Colloids and Surfaces A: Physicochem. Eng. Aspects* **2004**, *241*, 59–65.

37. Brandani, F.; Ruthven, D.; Coe, C.G. *Industrial & Engineering Chemistry Research* **2003**, *42*, 1451-1461.

38. Shen, D.; Bülow, M.; Siperstein, F.; Engelhard, M.; Myers, A. *Adsorption* **2000**, *6*, 275-286.

39. Dunne, J.A.; Rao, M.; Sircar, S.; Gorte, R.J.; Myers, A.L. *Langmuir* **1996**, *12*, 5896-5904.

40. Cavenati, S.; Grande, C.A.; Rodrigues, A.E. *J. of Chem. Eng. Data* **2004**, *49*, 1095-1101.

41. Rege, S.U.; Yang, R.T.; Buzanowski, M.A. *Chemical Engineering Science* **2000**, *55*, 4827-4838.

42. Golden, T. Air Products and Chemicals, Inc. Various personal communications 2006-2008.

Chapter III

Upgrading Landfill Gas by Adsorption: Economic Analysis and Binary Adsorption Behaviour of Carbon Dioxide and Methane on NaLSX

Bestfather, C.J.[*] and Tezel, F.H.[*a]

[*] Department of Chemical and Biological Engineering, University of Ottawa, 161, Louis Pasteur, Ottawa. K1N 6N5. Canada

[a] Author to which correspondence should be addressed

To be submitted for publication in *Environmental Science & Technology* journal, 2009.

Abstract

Upgrading landfill gas (LFG) to natural gas purity is a beneficial method of reducing greenhouse gas (GHG) emissions and utilizing a renewable fuel. This paper investigates the application of pressure swing adsorption to the bulk separation of biogas. The pure carbon dioxide (CO_2) and methane (CH_4) gas adsorption equilibrium on NaLSX (Si/Al = 1.0) at 150 °C and up to 4.5 atm is compared with the binary equilibrium at 150 °C and total pressures of 1 and 3.3 atm. The binary equilibrium was successfully measured with concentration pulse chromatography in a gas chromatograph modified for total system pressures above atmospheric. The results show the domination of CO_2 in the adsorbed phase with comparable capacity at elevated temperatures of the experiments. The separation factor of NaLSX ranges from 20 to 103.

The results of the binary adsorption equilibrium experiments were applied to an economic analysis of a bulk Pressure Swing Adsorber (PSA) separation for LFG. The analysis included the resale of natural gas and the benefits of carbon credits for landfills sized from 0.2 to 10 Million tonnes. The results of the analysis indicate that upgrading LFG is not competitive with other utilization methods at current prices. It also suggests that if renewable fuel and greenhouse gas economic incentives do increase, upgrading landfill gas is best suited for landfills above 4 million tonnes of waste.

Introduction

The current global environment suggests that there is a need to reduce greenhouse gas (GHG) emissions and increase renewable resource utilization. Biogas is one of the largest anthropogenic sources of CH_4 emitted to the atmosphere world wide. Biogas is typically a binary mixture of carbon dioxide (CO_2) and methane (CH_4) is a by-product of anaerobic digestion of organic waste in landfills and sewage. The composition is 50/50 CO_2/CH_4 although it can contain numerous other trace gases. The methane content of biogas is a significant source of renewable energy that has historically been wasted by emission to the atmosphere or combustion in a flare. The energy density of landfill gas (LFG) can be increased to that of natural gas (NG) by separating the CO_2. The economics of this process of separation can be prohibitive to upgrading biogas to NG for small landfills. However, rising energy costs and motivational factors are creating a greater emphasis on utilizing renewable sources of energy and are beginning to make these projects more feasible.

Renewable energy incentives and programs to reduce greenhouse gas (GHG) emissions are increasing locally and globally. Provincial examples, within Canada, of government incentives to boost renewable energy reliance and decrease GHG emissions include the Ontario Renewable Energy Standard Offer Program [1] and the Ontario Green Energy Act [2]. Internationally, the carbon credit market is open to trading CO_2 emission reductions [3; 4]. These credits are distributed to regulated programs that reduce GHG emissions, otherwise emitted into the atmosphere. LFG capture and combustion is a well established carbon credit program that is economical and growing in acceptance. The landfill that implements LFG combustion is required to monitor the quantitiy of GHGs that are diverted from the atmosphere and is credited for each ton of CO_2 equivalent. The advantage of LFG upgrading is that the methane is sold on the energy market in addition to renewable incentives. The price of NG has risen in the last decade to peak prices of 6 to 16 $US/mmBTU (2000-2009) [5]. These revenues can offset the costs of the equipment and infrastructure required to separate and refine LFG to NG standards. The economics for renewable energy projects are improving, costs of LFG capture and upgrading can be offset by carbon credits, as well as, incentives to utilize renewable fuels.

The utilization of LFG can take many forms that depend on the location and size of the landfill as well as the infrastructure available for energy utilization. The breakeven costs (revenue required to sustain project without deficit) associated with the utilization of LFG are shown in Table III - 1:

Table III - 1 - Breakeven costs for GHG abatement by emission controls [6].

Breakeven GHG abatement Costs	(CAD/tCO_2$e)
On-site electrical generation	105
Industrial boilers	-30
Flaring	38

The breakeven costs are measured in tons of CO_2 equivalent (CAD/tCO_2$e) because each GHG has a relative global warming potential (GWP) that is compared to that of CO_2 (GWP_{CO2} = 1). Of the three examples above, industrial boilers are the utilization technology that offers a profit. Upgrading renewable fuel to NG pipeline quality (CH_4 with maximum of 2-4% N_2 and 2% CO_2) for resale is an option for LFG utilization that is not in the table above [7]. The costs of separating biogas are relatively greater than the technologies in Table III - 1; although the infrastructure and market for NG is well established (e.g. high efficiency appliances and automobiles). In Puente Hills California, LFG is upgraded to compressed natural gas and utilized locally as an alternative fuel. The gas is stored at the landfill site and used to power garbage trucks and heavy landfill equipment [8].

The difficulties of LFG separation can be overcome with proven gas separation technologies like adsorption. CO_2/CH_4 separation has been favourably performed in a pressure swing adsorber (PSA) for "small to medium" sized volumes of biogas [7]. Adsorption separation offers an economical method of upgrading with a higher degree of automation [9]. In addition, LFG upgrading provides a source of NG which can be piped directly into local infrastructure. The separation technology used to upgrade the LFG needs to be economical enough to make a profit from the sale of NG.

The PSA operation, size and efficiency vary depending on the adsorbent within the column. A highly selective adsorbent for CO_2 is desirable for the separation of the mixture to produce a high pressure CH_4 enriched product. Many types of adsorbents are

available and screening studies identify potential candidate adsorbents. The equilibrium capacity, selectivity and heat of adsorption for the mixture gas are measured for materials in the laboratory. These experiments are commonly performed with pure gases and not CO_2/CH_4 or LFG mixtures. Mixture component gas equilibrium data is time and labour intensive to obtain, but it is valuable for non-ideal mixtures like CO_2/CH_4 because it demonstrates the interaction of the gas species as well as the competition for the adsorption sites. Binary equilibrium data reflect the conditions in the PSA, which differ greatly from pure component behaviour. Therefore, a screening process based only on pure component behaviour is unwise for the bulk separation of biogas. Additionally, the screening experiments should consider the temperature and pressure range of the PSA. An industrial PSA behaves adiabatically, especially for bulk separations, and exhibits up to 70 °C changes in adsorbent bed and gas temperature [10]. Similarly, the pressure of the PSA changes as the adsorbent bed becomes saturated; the process cycles through at least 4 stages: Pressurization (above atmospheric), Adsorption, Depressurization, and Regeneration (at low pressure or high temperature). The cyclic process is carried out in several adsorbent beds that operate in sequence so that a constant product stream is produced.

In this paper, the binary adsorption equilibrium of CO_2/CH_4 is measured with the concentration pulse chromatographic technique at 1.0 and 3.3 atm total pressure and an elevated temperature of 150 °C. For the purposes of CO_2/CH_4 separation, a zeolite adsorbent is selected because of its favourable CO_2 capacity and selectivity over CH_4. The objective is to characterise the PSA operational efficiency of NaLSX based on the equilibrium capacity and selectivity for CO_2 at the selected conditions. The binary isotherm is compared to a simple mixture model and an economic analysis is performed for the case study of a bulk landfill gas separation and upgrading process.

Literature Review

PSA design for bulk separation requires an adsorbent that is both high in CO_2 adsorption capacity and selectivity under mixture conditions [10]. Many pure gas equilibrium results are available in literature to identify adsorbents with these properties. However, the available mixture adsorption data is significantly less. There is binary data

available for CO_2/CH_4 on zeolites [11; 12; 13], silicalite [14], and activated carbon [15; 16; 17; 18]. These studies show the CO_2/CH_4 mixture behaves as a non-ideal adsorbate on zeolites, silicalites and activated carbon.

The potential for CO_2 adsorption is much more significant than CH_4 largely due to the presence of the CO_2 quadruple moment. Electrostatic interactions govern CO_2 adsorption potential whereas CH_4 has significantly less interactions. This difference in electromagnetic property is exploited at the cation sites in various adsorbents. For example, adsorbents exhibit CO_2 separation factors above 3 for H-ZSM-5 [12], up to 17 on silicalite [14], and 2 to 6 on activated carbon [15; 16; 17; 18]. Of these binary studies, those done on activated carbon were measured above and below atmospheric pressure (total). Increasing the equilibrium pressure reflects the conditions in a PSA as well as increasing the adsorbent capacity. The large pore distribution of activated carbon exhibits a binary CO_2 capacity of 2 to 9 (mol/kg), at 1 and 10 atm respectively [15; 16; 17; 18]. The increase in pressure also results in a change in selectivity which is a consequence of CH_4 adsorption.

The Concentration Pulse Chromatography (CPC) technique is useful for binary measurements and is employed in this study. It is a reliable method and is shown to replicate gravimetric results [19]. This method has been examined in detail and several papers are published on its use [11; 12; 19-26]. Of the CPC binary studies, those focused on zeolites are measured at varied temperatures and a fixed pressure. These conditions do not reflect the combination of variable temperature and pressure within an operational PSA.

The difference between experimental conditions and operational conditions are far from identical but the disparities can be minimized. For example, the CPC technique allows for the binary equilibrium to be measured at total pressures above atmospheric. These high pressure measurements illustrate the change in binary capacity and selectivity. Binary equilibrium measurements at varied pressures have been performed on various carbons but remain to be determined for a uniformly porous molecular sieve zeolite.

Zeolites have favourable adsorption properties due to their uniformly porous structure and heterogeneous surface properties. More specifically, zeolite CECA 13X (Si/Al = 1.17) has been used commercially in CO_2 removal for air pre-purification [10]. In very

recent studies the CO_2/CH_4 selectivity and capacity of CECA 13X has been measured with the CPC technique at 40, 100 °C and atmospheric pressure [13]. The NaX adsorbent exhibited an equilibrium separation factor above 40 and CO_2 capacity of 2.5 and 1.5 mol/kg for temperatures of 40 and 100 °C respectively. The adsorbent selected for binary research in this study is a form of NaX that has a Si/Al ratio of 1.0. It is referred to as Low Silica NaX (or NaLSX) and represents the lowest theoretical limit of Si/Al ratio. Studies have shown that decreasing the Si/Al maximises the CO_2 adsorption potential due to the increased cation density and heterogeneity of the zeolite surface [27]. Limited CO_2 adsorption data is available for NaLSX due to a patent on the manufacture of zeolites with Si/Al ratio below 1.15 [28]. Therefore the potential for application of this zeolite in bulk separation of CO_2/CH_4 is explored in this paper with the chromatographic technique. More details on zeolite structure are provided in Appendix C.

In this paper isothermal adsorbent bed operating characteristics are determined for the bulk separation of CO_2/CH_4 on NaLSX. Bestfather and Tezel [29] have determined the properties of various adsorbents for the bulk separation of CO_2/CH_4 based on pure gas isotherms. For example, the temperature swing in the bed can be approximated by binary working capacity, the heat of adsorption, and the adsorbent heat capacity [30]. This paper furthers the research of this separation by exploring the binary equilibrium behaviour at atmospheric and higher pressures with the chromatographic system.

In addition to binary measurements, a PSA operation economic analysis identifies whether LFG upgrading is profitable for landfills. Currently there are limited economic studies on upgrading landfill gas with adsorption because of the high separation costs. A general analysis based on PSA size relative to landfill size will identify the potential for the proposed separation. The landfill gas production rate and landfill size are related with the well established US EPA LANDGEM model [31]. The economics of upgrading LFG to natural gas are compared to the breakeven costs of other LFG utilization technologies. Thus the capital and operational costs of the upgrading facilities are weighed against the returns from the sale of NG and Carbon credits.

Experimental & Theory

The CPC technique is based on the following principles. A carrier gas composed of two species (for binary system) passes through a column packed with adsorbent at a fixed flowrate, temperature, and pressure. The carrier gas composition is then changed by adding a pulse of adsorbate gas species which is sufficiently small enough that the carrier gas remains in equilibrium with the adsorbent. The delay of this pulse within the adsorbent column indicates the equilibrium behaviour of the adsorbent and adsorbed phase. This relationship is linear at low concentrations and is referred to as the Henry's Law Constant.

The dimensionless Henry's Law constant (K) is determined from a material balance on the adsorbent column. The first moment (μ) provides a direct calculation of the Henry's Law constant [21].

$$\mu = \frac{L}{v}\left[1+\left(\frac{1-\varepsilon}{\varepsilon}\right)K\right] \tag{1}$$

The first moment of the pulse is measured at the experimental conditions in the column of known length (L), fixed interstitial velocity (v), and adsorbent void fraction (ε). The material balance assumes no mass transfer resistance within the zeolite and that the pulse is sufficiently small that it is in linear equilibrium phase range [21]. The dimensionless Henry's Law constant (K) represents the effective binary mixture slope (a combination of both species in the adsorbed phase). Where the dimensionless Henry's Law Constant (K) is related to the dimensional Henry's Law constant (K_P) at the experimental temperature (T) and the absolute density of the adsorbent pellets (ρ_{ads} = 2.23 g/cm^3) by the following formula [26]:

$$K = K_P RT\rho_{ads} \tag{2}$$

The absolute density of NaLSX (exluding the pore volume) was measured with non-adsorbing He gas at room temperature.

The effective binary equilibrium slope (K_p) is a measure of the linear equilibrium relationship between the binary gas phase and the adsorbed phase. This measure is a combination of the binary adsorption isotherm slopes of CO_2 (dq_1/dP_1) and CH_4 and (dq_2/dP_2). The effective binary equilibrium slope is described for a gaseous equilibrium as follows [20]:

$$K_{P} = (1 - Y_1)\frac{dq_1}{dP_1} + Y_1\frac{dq_2}{dP_2} \tag{3}$$

K_P is determined experimentally for various compositions (Y_1) of carrier gas and the relationship for the individual equilibrium isotherm slopes are unknown. The binary isotherm slopes are resolved by assuming a functional form that captures the variation in K_P with respect to composition [20; 32; 33]. A result is that the binary equilibrium assumes a similar form that is related to the first form with several parameters. The functional form of Harlick and Tezel [34] is shown to capture large variations in the effective slope for systems like CO_2/CH_4 on ZSM-5 [11; 12], silicalite [14], and CECA 13X [13]. The effective slope functional form is also known as HT-CPM [34]:

$$K_{P} = A_1 + A_2 Y_1 + A_3 Y_1^2 + A_4 \ln\left|Y_1 + \lambda\right| \tag{4}$$

Where A_i and λ are coefficients ($\lambda \neq 0$) with no physical meaning. The slopes of the binary isotherms are described by the following equations [34].

$$\frac{dq_1}{dP_1} = B_1 + 2B_2 Y_1 + \frac{B_3}{\left(\left|Y_1 + \lambda\right|\right)} \tag{5}$$

$$\frac{dq_2}{dP_2} = C_1 + 2C_2 Y_1 + \frac{C_3}{\left(\left|Y_1 + \lambda\right|\right)} \tag{6}$$

Where B_i's, C_i's and λ are constants. The functional form for the experimental binary effective slope contains 6 unknown coefficients (B_i and C_i). When equations (5) and (6) are substituted into equation (4) these coefficients are determined by the objective function of minimizing the sum of square residuals (SSR) defined by equation (7). The non-linear solver function in MS Excel was utilized to vary the parameters and achieve the objective function.

$$SSR = \sum\left[K_{P}(Experimental) - K_{P}(B_i, C_i)\right]^2 \tag{7}$$

The final solution was resolved by achieving the objective function with the formula for K_P with the B_i and C_i coefficients in the following formula:

$$K_{P}(Experimental) = (1 - Y_1)\left[B_1 + 2B_2 Y_1 + \frac{B_3}{\left|Y_1 + \lambda\right|}\right] + Y_1\left[C_1 + 2C_2 Y_1 + \frac{C_3}{\left|Y_1 + \lambda\right|}\right] \tag{8}$$

Multiple combinations of solutions and local minimums are possible when minimizing the objective function; therefore the final solution is confined. The following

constraints are imposed to maintain the solution represents the physical adsorption that is actually occurring, [26]:

1. The pure isotherm capacity (q_i^o) must match the binary isotherm capacity (q_i) at the endpoints.

$$\left(q_1^0\right)_{P_i} = \left(q_1\right)_{Y_1=1.0} \qquad \left(q_2^0\right)_{P_i} = \left(q_2\right)_{Y_1=0.0} \tag{9}$$

2. The effective binary slope of the mixture (K_P) must match the Henry's Law constant of the pure component (K_P^o).

$$\left(K_P\right)_{Y_1=1.0} = \left(K_P^0\right)_1 \qquad \left(K_P\right)_{Y_1=0.0} = \left(K_P^0\right)_2 \tag{10}$$

3. The slope of the binary isotherm is positive for both species and all compositions.

$$\frac{dq_1}{dP_1} \geq 0 \quad and \quad \frac{dq_2}{dP_2} \geq 0 \quad for\ all\ 0 \leq Y_1 \leq 1.0 \tag{11}$$

Integrating over the composition of the system provides the binary isotherms, after the determination of B_i and C_i coefficients as follows:

$$q_1 = \left[B_1 Y_1 + B_2 Y_1^2 + B_3 \ln\left(\left|\frac{Y_1 + \lambda}{\lambda}\right|\right)\right] P \tag{12}$$

$$q_2 = \left[C_1\left(1 - Y_1\right) + C_2\left(1 - Y_1^2\right) - C_3 \ln\left(\left|\frac{Y_1 + \lambda}{1 + \lambda}\right|\right)\right] P \tag{13}$$

CPC Experiment

The CPC technique was carried out in a modified Varian 3300 Gas Chromatograph (GC) equipped with a thermal conductivity detector (TCD). The experiments were conducted in a 0.451 cm diameter stainless steel column (10.5 cm length) at volumetric flow rates between 10 and 30 cm^3/min (STP). The porosity (ε = 0.421) of the column filled with crushed adsorbent particles (20x60 mesh) was determined with 20x60 mesh glass beads. The column of adsorbent was equilibrated at 150 °C with the carrier gas stream composition (Y) for a period of 24 hours. The size of the sample loop is (1 ml) and was sufficiently small enough that the carrier gas remained in equilibrium with the adsorbent.

The first moment (μ) of the pulse is given by:

$$\mu = \frac{\int_0^\infty c(t-\mu_D)dt}{\int_0^\infty c\,dt} \tag{14}$$

Where the concentration of the gas at the column exit (c) is measured with respect to time (t) and the first moment is corrected for the system retention time (μ_D). The system retention time accounts for the delay in the system tubing and detector. μ_D was calculated from a pulse of non-adsorbing gas through the adsorbent column. A simplified schematic of the apparatus is shown in Figure III - 1.

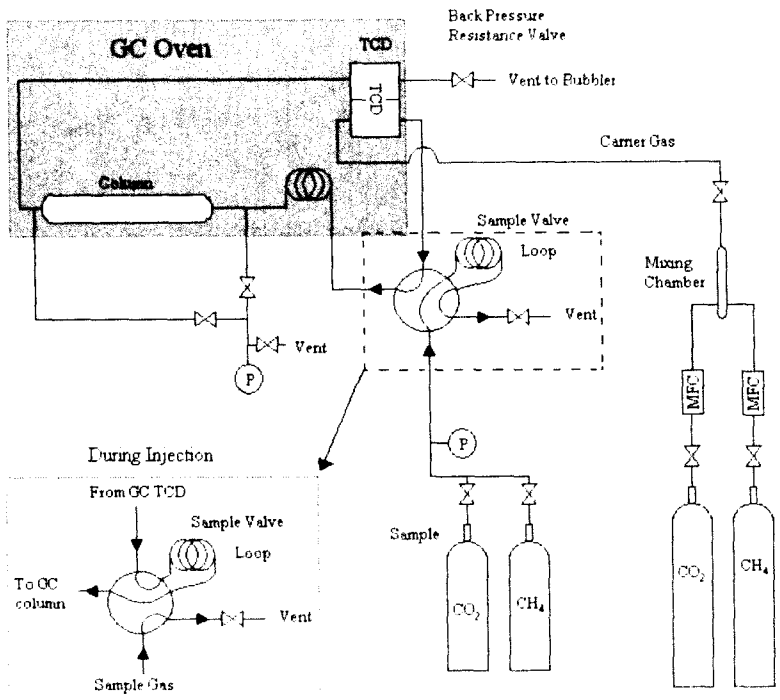

Figure III - 1 - CPC schematic with modifications for high pressure.

The carrier flow rate was measured with a bubble flow meter and regulated with two MKS Type M100B Mass-Flo® Controllers (MFC). A mixing chamber was positioned before the GC entrance to ensure a well mixed CO_2/CH_4 carrier gas. The mixture carrier gas passed through the oven and reference side of TCD before entering the sample valve. The GC is equipped with an oven and thermocouples to ensure the adsorbent column and gas temperature are constant (±0.1 °C). A 6 port sample valve injects a 1 ml sample into the carrier gas and a Burgess micro switch was used to record the injection time. The carrier and sample then passed through the column (1.677 cm^3) filled with approximately

1 to 1.5 g of crushed (20x60 mesh) adsorbent. The composition of the gas exiting the column was measured with a TCD to determine the first moment of the pulse within the adsorbent column and system. All data from TCD was recorded with Labview software on an IBM Intel based computer.

The Varian 3300 GC was modified with back pressure valves to allow the system to be increased above atmospheric pressure. Prior to all experiments the internal system tubing was replaced with 1/8 Stainless steel tubing and Swagelok fittings such that system was capable of being pressurized to 4.0 atm without any leaks. The modifications include several high pressure metering valves (Series 31) manufactured by Whitey Tool and Die Company. The valves shown in Figure III - 1 maintain a constant back pressure on the system and on the sample injection loop. The outlet side of GC was modified with a needle valve to provide a constant resistance to flow at outlet. The pressure at the column entrance and exit was monitored with one 100 psi pressure Gauge (Grade 3A) from Omega Engineering Inc. Two binary experiments were carried out at a total pressure of 1 and 3.3 (± 0.11 atm). At the beginning of the high pressure experiments, the system was pressurized and the back pressure valve adjusted to maintain an approximate flow of 15 cm^3/min STP (± 0.07 cm^3/min).

Prior to experimentation the adsorbent was regenerated at 350 °C under a He purge at atmospheric pressure for 24 hrs. The carrier gas composition was adjusted with the MFCs to maintain a fixed flowrate and mixture concentration. The measurement of the effective slope was performed when the TCD baseline was observed to remain unchanged. The experiments covered the entire range of mixture compositions and commenced with pure CH_4 carrier gas and the mole fraction of CO_2 was increased at regular intervals. Injections of CO_2 and CH_4 were repeated at each mixture concentration to estimate uncertainty of results.

Materials

The NaLSX (NaX zeolite with a Si/Al = 1.0) zeolite adsorbent selected for binary equilibrium measurement with the bulk mixture was graciously supplied by Air Products. The physical properties of this zeolite are presented in Table III - 2.

Table III - 2 – Physical Properties of Current Study Adsorbents

	NaLSX
Manufacturer	Zeochem
Si/Al Molecular Ratio	1.0
Cation Density (ions/cage)	96.0
Pellet Size (as received)	8 x 14 mesh
Particle Size (experimental)	20 x 60 mesh
Bulk Density ρ_{Bulk} (g/cm^3)	0.632
Heat Capacity C_{ps} (J/g K)	0.920*

* Heat capacity for NaX zeolite assumed for NaLSX from [7].

All gases were supplied by BOC Canada Limited and the quality of each is listed in Table III - 3.

Table III - 3 - Gas Grade and Purity used in this Study

Gas	Grade	Purity
Helium (He)	5.0 (Ultra High Purity)	99.999%
Carbon Dioxide (CO_2)	Bone Dry	99.85%
Methane (CH_4)	3.7 (Ultra High Purity)	99.97%

Extended Langmuir Isotherm Model

The Langmuir isotherm model is commonly used to describe pure and multi-component mixtures. It is explained in detail by Yang [35] and Ruthven [36]. The pure component equilibrium capacity is measured as a function of pressure for component *i* at a constant temperature. The Langmuir [37] isotherm model is fit to the data:

$$q_i = \frac{q_{s,i} b_i P_i}{1 + b_i P_i} \tag{15}$$

The parameters for CO_2 and CH_4 are determined from the pure isotherm data with a best fit plot of P_i/q_i vs P_i, a slope of $1/q_{s,i}$ and an intercept of $1/q_{s,i}b_i$. Where $q_{s,i}$ is the saturation capacity, b_i is the equilibrium constant, and P_i is the partial pressure (total pressure for pure isotherms) of the gas species *i*. The Henry's Law Constant (K_P) is approximated from the pure Langmuir parameters with the relationship [36]:

$$K_{P,i} = q_{s,i} b_i \tag{16}$$

The Extended Langmuir (EL) isotherm model follows directly from the pure isotherm parameters. For a mixture of *N* gases the amount adsorbed (q_i) of component *i* is as follows:

$$q_i = \frac{q_{\infty i} b_i P_i}{1 + \sum_{i}^{N} b_i P_i} \tag{17}$$

The mixture isotherm parameters are taken from the pure Langmuir isotherm model. The selectivity (α_i) gives an indication of how selective an adsorbent is for a mixture. For LFG, the ideal selectivity for CO_2 is given by [36]:

$$\alpha_{CO_2} = \frac{(K_P)_{CO_2}}{(K_P)_{CH_4}} = \frac{(q_\infty b)_{CO_2}}{(q_\infty b)_{CH_4}} \tag{18}$$

The ratio of Henry's Law constants can be measured with the CPC method directly (K_P) and as a ratio of the Langmuir parameters.

Economic Analysis

The break even costs of LFG upgrading were evaluated for several landfill sizes. The LFG production relative to landfill size was related with the US EPA LANDGEM model [31]. The economics encompassed the capital costs of the adsorption system (including compressors, vacuum pumps, heat exchanger, adsorption vessels and adsorbent) and the operational costs (utilities, labour, maintenance, and bed replacement). The present value of the project was evaluated (benefits vs costs) to determine the breakeven cost for the operation with the method of Delhotal et al [38]:

$$\sum_{t=1}^{T}\left[\frac{\theta\delta(1-\chi)+\psi(1-\chi)+\beta}{(1+\gamma)^t}\right] = \kappa + \sum_{t=1}^{T}\left[\frac{\sigma(1-\chi)}{(1+\gamma)^t}\right] \tag{19}$$

Where θ is the break even price ($ CAD/t CO_2e)

δ is the emissions reductions for CH_4 and CO_2 (tCO_2e)

ψ is the revenue generated from sale of NG ($12 CAD/mmBtu)

β is the tax break ($\kappa/T\chi$)

γ is the discount rate (20%)

χ is the tax rate (40%)

κ is the capital cost ($CAD)

σ is the reoccurring operational and maintenance costs ($CAD)

T is the project lifetime (15 years)

The parameters above are selected for comparison to the results in Table III - 1 which are based on a 15 year project lifetime and an industrial perspective of 20% discount rate and 40% tax rate [38]. The analysis does not include pre-purification and assumes instantaneous adsorption, 100% recovery of all CH_4 at NG purity. No inflation or changes in operation costs are assumed and NG prices are from recent (2008) market values.

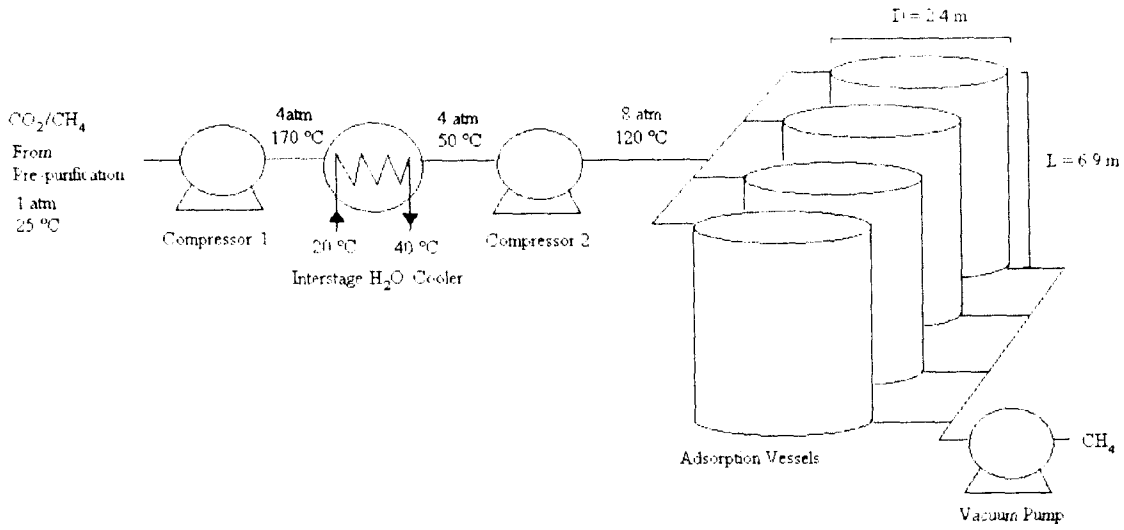

Figure III - 2 - LFG VPSA bulk separation process

Capital costs

The schematic of the VPSA separation process is illustrated in Figure III - 2. The capital costs for this system was determined based on the input flow rate and scaled according to equipment heuristics. The inlet gas passes through two compression stages and one interstage cooler. The adsorbent capacity was calculated from the adiabatic working capacity (2.5 mol CO_2/kg NaLSX) which assumes all of the heat goes into heating the adsorbent bed and an average feed temperature of 120 °C. The adsorbent price of NaLSX ($6.60 CAD/kg) [39] was used to determine the total adsorber and adsorbent cost. The ratio of the total adsorption system cost (includes valves, piping, instrumentation, etc.) to the adsorbent cost is related to the volumetric flowrate with the method of Cooper and Alley [40]. A two stage compressor was selected to elevate the feed pressure from 1 to 8 atm in combination with a stainless steel (304) shell and tube water heat exchanger. The vacuum pump was sized for adsorbent regeneration from 1 to

0.1 atm for an adsorption cycle time of 15 minutes. The purchased equipment cost was then multiplied by three factors from Keller [41] to account for the delivery costs (18%), direct installation costs (44%) and indirect installation costs (31%). The details of theses calculations are provided in Appendix B.

Operational Costs

The operational costs are based on 24 hr operation, 350 days/year for labour ($22.60 CAD/hr), supervision (15% of the labour) and maintenance (5% of the total installed cost). The utilities include electricity ($0.06/kWh) and cooling water ($0.02/1000 L) available at 20 °C. The power demand is determined from the compressor and vacuum pump horsepower with an adiabatic efficiency of 80%. The cooling water rate is controlled such that the compressed gas enters the second stage of compression (4 to 8 atm) at 50 °C. This PSA cycle was selected as a typical industrial LFG separation cycle [39]. The exhaust gas enters the adsorbent column at a temperature of approximately 120 °C. Adsorbent bed replacement is also considered every 8 years and the cost is distributed over the 15 year project lifetime at an interest rate of 7%. The details of theses calculations are provided in Appendix B.

Results & Discussion

Pure Isotherms for CO_2/CH_4 on NaLSX

The isotherms of CO_2 and CH_4 on NaLSX at 150 °C were obtained in our previous studies [29] and are shown in Figure III - 3:

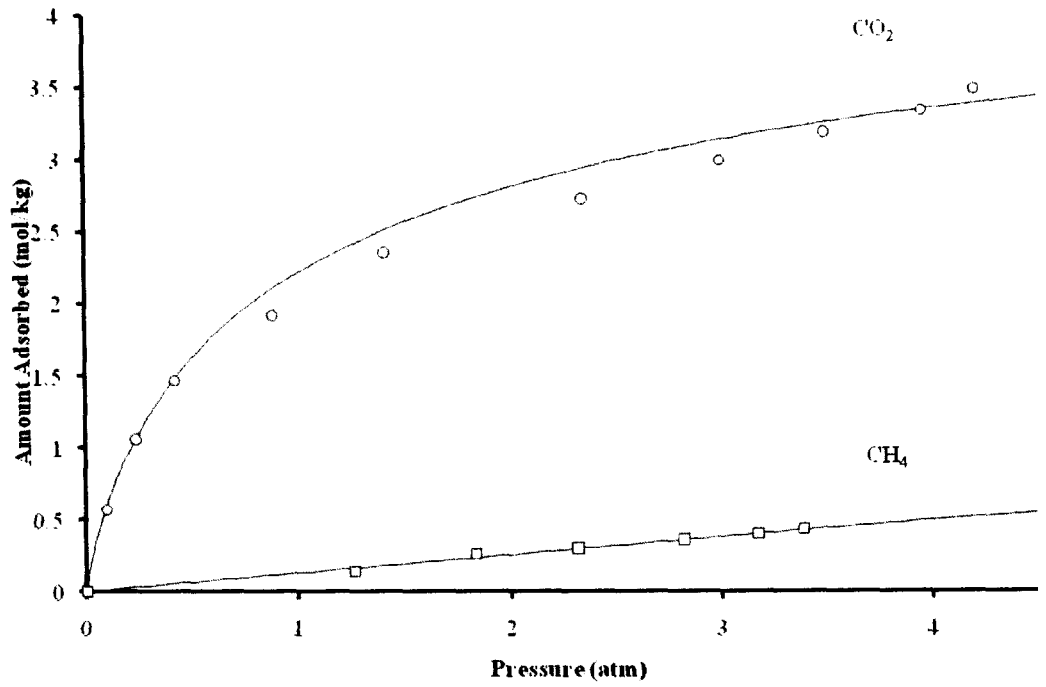

Figure III - 3 – Experimental NaLSX CO_2 (○) and CH_4 (□) isotherms at 150 °C [29] data points compared with the solid lines of the Langmuir isotherm model.

The two parameter Langmuir model follows the variation of the data although the CO_2 isotherm is slightly over and under predicted. The parameters of the Langmuir isotherm, as well as the Henry's Law constant (K_P) and heat of adsorption (measured with the CPC method) are presented in Table III - 4. The ideal selectivity for CO_2 is greater than 28 at 150 °C, indicating a favourable CO_2 separation at elevated temperatures.

Table III - 4 - Langmuir parameters and adsorption properties for NaLSX on CO_2 and CH_4 at 150 °C [29].

	NaLSX CH_4	NaLSX CO_2
Temperature (°C)	150	150
$q_{s,i}$ (mol/kg)	2.42	4.07
B_i (atm^{-1})	0.06	1.05
$q_{s,i} B_i$ (mol/kg atm)	0.15	4.27
K_p measured with CPC* (mol/kg atm)	0.15	4.13
Heat of Adsorption* (kJ/mol)	18.4	27.9

*Data obtained from Bestfather and Tezel [29], curve fitted to Langmuir isotherm model in present study.

The Henry's Law constant for CO_2 is much greater than that of CH_4 which reflects the difference in isotherm shape. The Langmuir parameters for CO_2 saturation capacity and equilibrium constant are greater than those for CH_4. Similarly the Henry's Law Constant and limiting Heat of adsorption determined with the CPC technique are significantly higher for CO_2 [29]. The difference is due to the greater potential for CO_2 adsorption. The CPC measurement of the K_p is comparable to the value obtained from the Langmuir parameters above in equation (16) for CH_4 and CO_2.

Concentration pulse chromatography for Binary Adsorption Isotherms

The effective binary mixture slope of CO_2/CH_4 was measured for NaLSX at 150 °C, 1 and 3.3 atm total pressure with the CPC technique. The capacity at two pressures exhibited similar behaviours which are illustrated in Figure III - 4 as a semi-log plot.

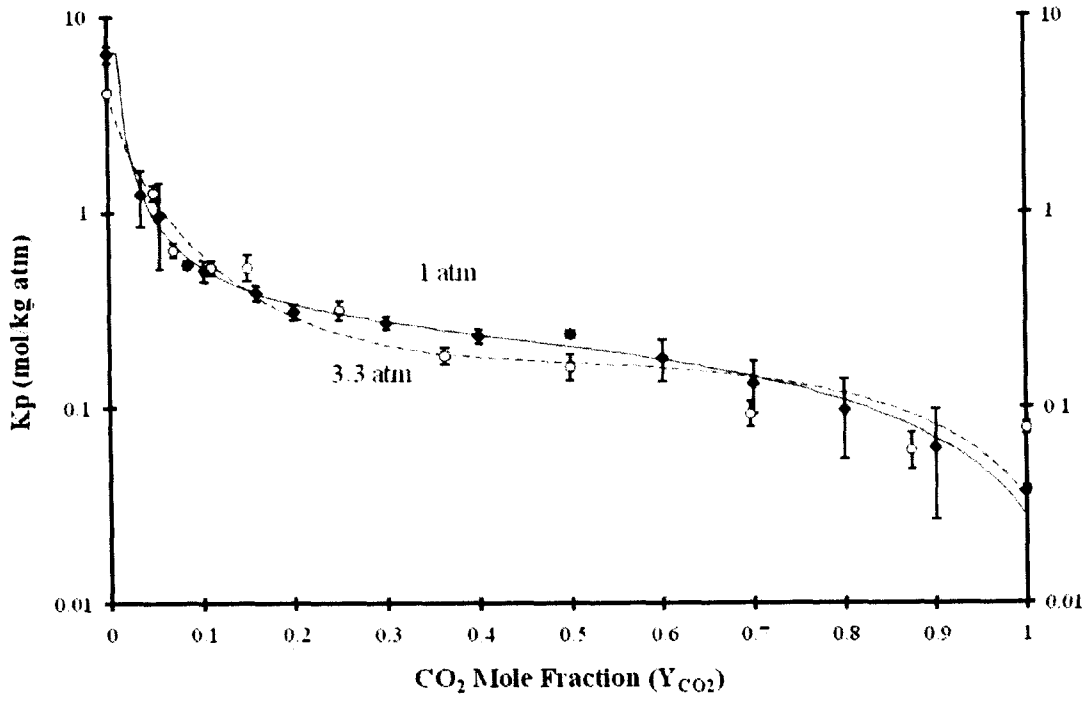

Figure III - 4 - CO_2/CH_4 effective slope at 150 °C, 1 atm (◆) and 3.3 atm (○).

At low CO_2 concentrations, CO_2 out competes CH_4 for adsorption sites. This is reflected in the high adsorption potential and high effective slope at low CO_2 mole fractions indicating selectivity for CO_2. The effective slope decreases sharply as the CO_2 fraction increases to 20 % and then remains relatively unchanging for the remaining binary mixture fraction. This decrease in potential for CO_2 adsorption at low CO_2 fractions is due to limited available high energy cation adsorption sites. The high energy adsorption sites are occupied first (i.e. at low CO_2 mole fractions) around the cations, and then the lower energy sites (further from the cations). This property is common to non-ideal binary systems where CO_2 experiences significantly stronger electromagnetic interactions with the cations due to its quadrupole moment.

As the pressure increases, the Henry's Law constant of the pure gases decreases as illustrated at the endpoints of both effective slopes. The shape of the effective slope is similar to that observed by Mulgundmath et al [13] for CO_2/CH_4 on 13X. They found that the system behaviour at 40 and 100 °C only differed significantly below mole fractions of 0.2 for CO_2.

The effective slope was measured with CO_2 and CH_4 injections at different carrier gas compositions of CO_2 and CH_4. Additionally, the effective slope was measured a minimum of 3 times with each species injection. On average 11% variability was observed and the confidence intervals reflect this in Figure III - 4Figure III - . At CO_2 mixture fractions below 0.2 the high potential for adsorption caused the sample pulse to spread out within the column and the change in concentration at the TCD was more difficult to interpret.

The effective slope obtained from the methane injection was consistently higher than the CO_2 injection. This difference can be explained with two reasons related to the greater potential for CO_2 adsorption and the heat of adsorption (see Table III - 4). First, looking at Figure III - 4, it can be observed that the effective slope decreases as the CO_2 mixture fraction is increased. Therefore as CO_2 is injected into the carrier gas at any mixture fraction the effective slope will decreases. Correspondingly, for a CH_4 injection the effective slope increases. Secondly, the difference in the heat of adsorption also contributes to the differences in first moment. The CO_2 sample injection increases the partial pressure, resulting in CO_2 adsorption and heat being released. Because physical adsorption is an exothermic process, the increase in available energy within the column encourages CO_2 desorption. This increase in heat due to CO_2 adsorption is significantly greater than that released when CH_4 is injected. Finally, as the CH_4 sample is injected, the increase in partial pressure results in some CH_4 adsorption. The potential for adsorption is much less than CO_2 as is the heat released due to CH_4 adsorption. Therefore there is less energy available for desorption within the column resulting in a longer CH_4 first moment and larger effective slope. This systematic difference between injections accounted for the largest fraction of variability and remained below 10% for the majority of measurements. The propagation of measurement errors for the CPC technique is provided in Appendix B.

The change in effective slope across the mixture fraction is modeled to the functional form in equation (8). By capturing the behaviour of the effective slope the slopes of the binary isotherms can be evaluated. However, these adsorption isotherms are not a result of individual measurements but rather of the behaviour of the system and the binary equilibrium relation between the binary gases. The trend of the effective slope in Figure

III - 4 was well described by the HT-CPM form. Mulgundmath et al [13] also found the HT-CPM form for K_P captured the behaviour of the 13X biogas binary mixture at atmospheric pressure similarly to the NaLSX system above. The trend of the effective slope is captured with the purposed functional form within the variability of the measurements.

It was found that the solution to the algorithm that "fit" the data was highly dependant upon the λ parameter in equations (4) to (6), (12) and (13). Details of this data analysis are provided in Appendix B. The following procedure was followed:

1. For various values of λ:
    a. Using equation (4) the objective function (equation (7)) was minimized holding λ constant and allowing A_i parameters to vary.
    b. A plot of SSR vs λ demonstrated a minimum region and this range of values for λ was constrained.
2. With the constrained value of λ equation (8) was used to minimize equation (7) by varying the B_i and C_i parameters while subjected to the constraints of equation (9) to (11).

The application of the constraints in equation (9) to (11) were found to significantly limit the number of possible solutions to the objective function. The method above shortened the trial and error that occurs when all parameters in equation (8) are allowed to vary which leads to numerous local minimums that do not necessarily conform to the constraints.

Binary Isotherm

The CO_2/CH_4 binary isotherms for NaLSX at 150 °C are determined from the best fit to the effective slope in Figure III - 4 and are described by equation (12) and (13). They are illustrated at total pressures of 1 and 3.3 atm in Figure III - 5 and Figure III - 6 respectively.

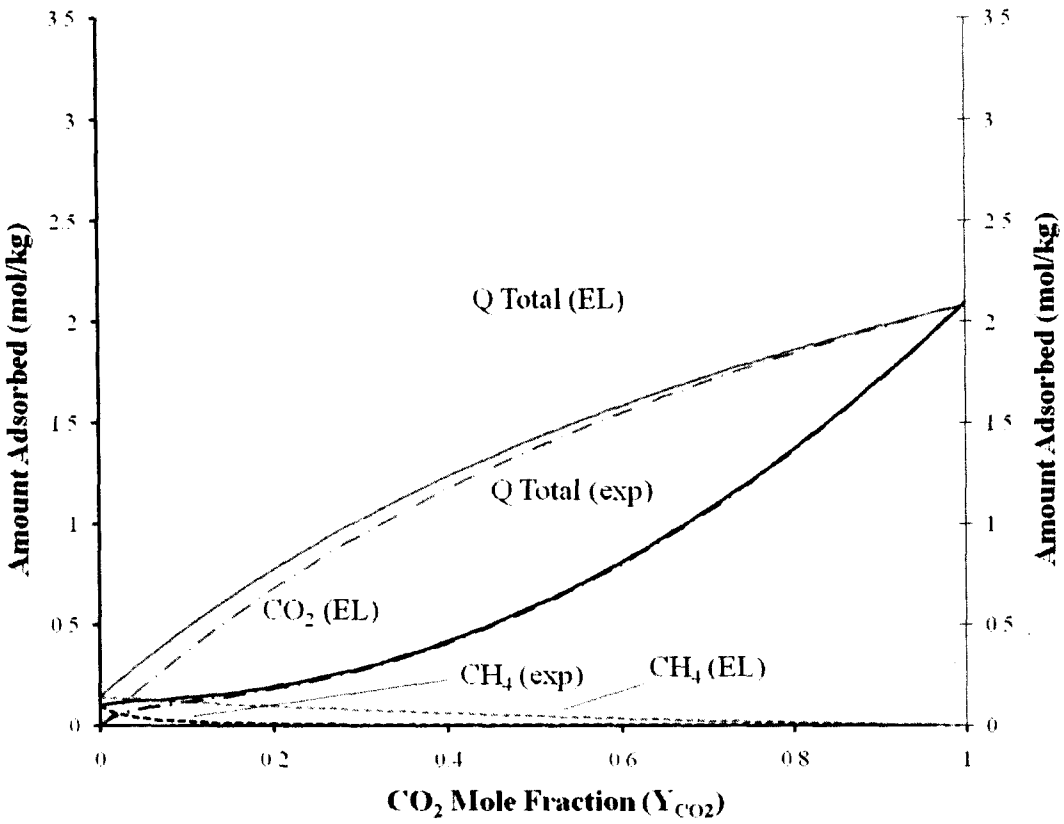

Figure III - 5 – Experimental CO_2/CH_4 binary adsorption equilibrium at 150 °C, 1 atm (black) compared with predicted Extended Langmuir (grey).

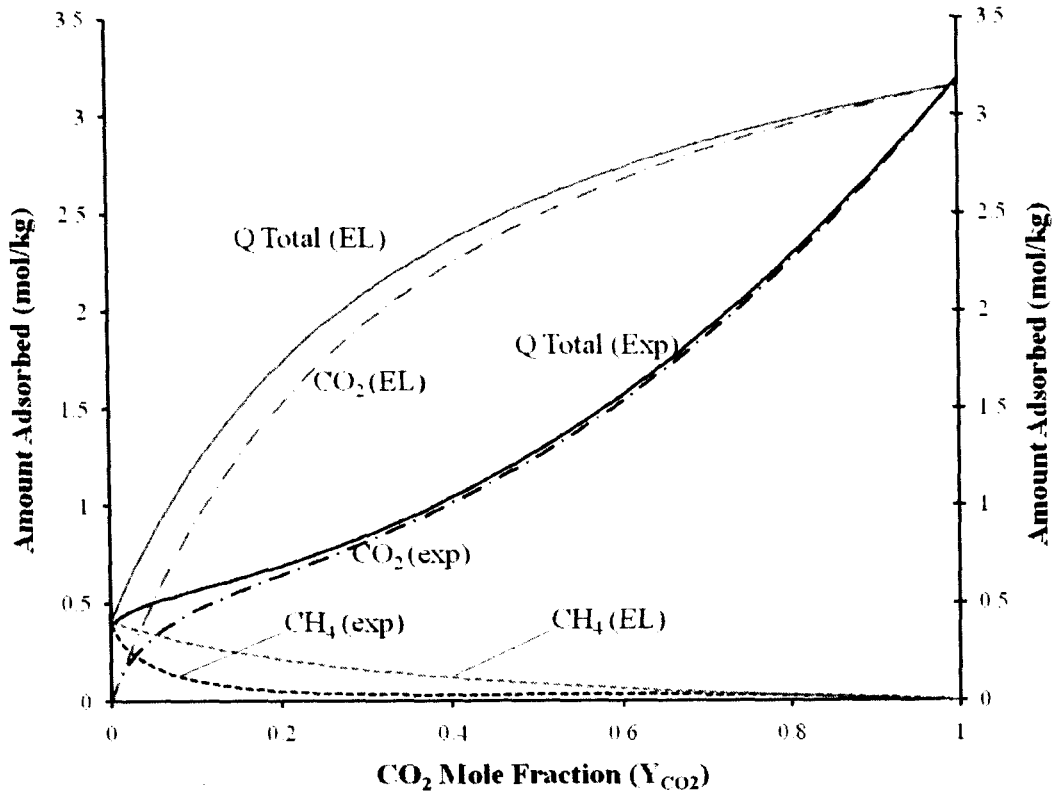

Figure III - 6 - Experimental CO_2/CH_4 binary adsorption equilibrium at 150 °C, 3.3 atm (black) compared with predicted Extended Langmuir (grey).

The CO_2/CH_4 binary equilibrium on NaLSX contains an adsorbed phase that is composed primarily of CO_2. The total amount adsorbed increases fairly linearly as the carbon dioxide fraction in the mixture increases. Only at methane fractions below 90% does methane compose a significant fraction of the adsorbed phase equilibrium. This behaviour suggests that NaLSX is highly selective for CO_2 adsorption at both pressures studied. The behaviour of CO_2 dominating the adsorbed phase is well documented on H-ZSM-5 [11; 12; 34], activated carbon [15-18], and less so on silicalite [14]. For biogas (Y_{CO2} = 0.5), the capacity of NaLSX is greater than 1 and 0.4 mol/kg for 3.3 and 1 atm respectively. In comparison, the binary CO_2 capacity is 1 mol/kg on H-ZSM-5 [11; 34], 1.5 mol/kg for activated carbon [18] and 0.7 to 0.3 mol/kg for silicalite [14] at lower temperatures. Mulgundmath et al [13] observe a concave up CO_2 binary isotherm capacity on 13X at atmospheric pressure at 40 and 100 °C. The capacity for 13X is also significantly higher (1.5 to 2.5 mol/kg), at 40 to 100 °C and 1 atm total pressure. This

difference suggests at equivalent temperatures and pressures 13X has higher binary CO_2 capacity than NaLSX. It also suggests that decreasing the Si/Al ratio or similarly increasing the surface heterogeneity of NaX is less important at high temperatures and pressures for LFG bulk separations. Therefore, the amount of NaLSX required to separate CO_2 from biogas may be similar to 13X and significantly less than non-zeolites.

The increase in total pressure from 1 to 3.3 atm results in less CO_2 selectivity. Since this increase in pressure results in 4 to 5 times the amount of CH_4 and 1.5 to 3 times the amount of CO_2 being adsorbed. The shape of the isotherm is similar at both pressures and differs due to the constraints for capacity at the endpoints. This similarity in shape is also reflected in Figure III - 4. The increase in capacity for CO_2/CH_4 on activated carbon is observed by Buss [15], Dreisbach et al [16], Van der Vaart et al [17], and Goetz [18]. The pressure range considered for these studies was greater (1 up to 60 atm) than that in this paper and the temperatures were also much closer to 298 K. Similar to the results above, Van der Vaart et al [17] observed roughly twice the activated carbon capacity with a pressure change from 1 to 3 atm at 303 K, although CO_2 did not dominate the adsorbed phase in activated carbon as it does in NaLSX. The increase in pressure has resulted in roughly 2x the CO_2 capacity. The CO_2 selectivity is lost due to CH_4 potential for adsorption although the increase is small relative to CO_2. Therefore there is a balance between CO_2 capacity and selectivity that can be explored with dynamic experiments and a cost analysis focused on PSA operating cycles and conditions. This analysis is not included in the present study.

The NaLSX CO_2/CH_4 adsorption isotherms are tested for their thermodynamic consistency in Appendix B.

Extended Langmuir

The EL isotherm model is utilized for comparison of binary isotherm CO_2/CH_4 capacity on NaLSX at different total pressures. Figure III - 5 and Figure III - 6 illustrate the EL binary isotherm at 1.0 and 3.3 atm modeled from equation (7) and the parameters in Table III - 4. The model predicts an adsorbed phase that is dominated by CO_2 and is highly favourable for bulk mixture separation. The total capacity of the adsorbent is overestimated with the EL model when compared to the adsorption isotherms measured

with the CPC method. CH_4 potential for adsorption is only significant in mixtures of mainly methane (<80%). As the pressure is increased, the capacity of NaLSX increases for both CO_2 and CH_4 (although CO_2 continues to dominate the adsorbed phase). At total pressures of 1 and 3.3 atm CO_2 mimics its pure isotherm rectangular behaviour.

In Figure III - 5 and Figure III - 6 the extended Langmuir isotherm model over predicts the adsorption equilibrium capacity of CO_2/CH_4 at 150 °C, 1.0 and 3.3 atm. The binary isotherm measured with the CPC method exhibits concave up adsorption and decreasing capacity across the composition range. The reduction in modelled capacity is due to the ideal adsorption assumption and the interaction of adsorbed phase molecules. The adsorption of CO_2 on zeolites is not ideal and is highly localized around the cation sites as shown by [9]. The non-ideality of CO_2/CH_4 is especially difficult to model because multicomponent forms of pure isotherm models are limited [42]. Li and Tezel [14] show that six different multicomponent adsorption models fail to capture CO_2/CH_4 adsorption mixture behaviour on silicalite. Despite these conclusions, the Langmuir adsorption model is derived from basic principles and its multisite form is commonly used to describe adsorption behaviour successfully [7, 43, 44]. The EL isotherm model implies much higher CO_2 capacity than measured suggesting it should not be used for PSA scaling.

Phase diagram

The phase diagram indicates the favourability of the separation of CO_2 from CH_4 on NaLSX at 150 °C. The adsorbed phase CO_2 fraction vs the gas phase CO_2 fraction is shown in Figure III - 7.

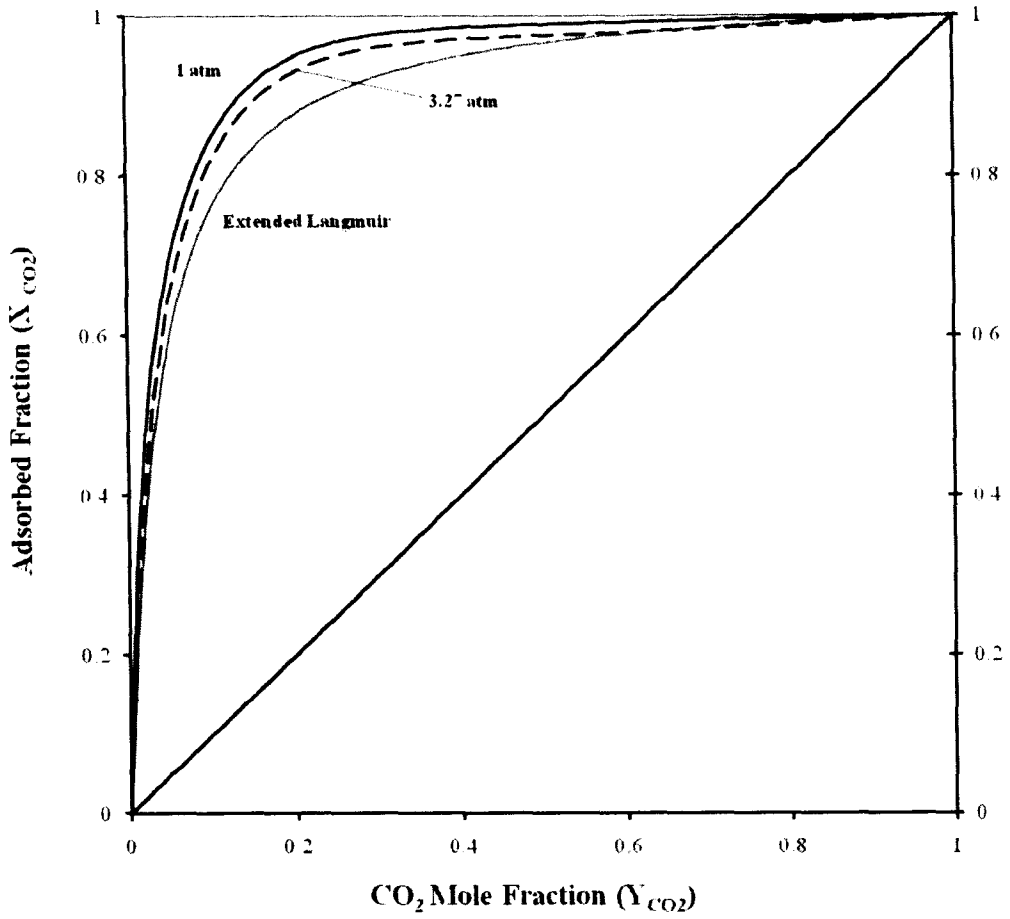

Figure III - 7 - CO_2/CH_4 phase diagram 150 °C, 1 atm (black), 3.3 atm (dashed) and EL (grey).

The phase diagram is calculated from the adsorption isotherms curves and reflects the domination of CO_2 in the adsorbed phase. There is a slight decrease in CO_2 selectivity at total pressure of 3.3 atm. Similarily, Van der Vaart et al [17] observed little change in the phase diagram for CO_2/CH_4 at 303 K from 0.5 to 5 atm. The Extended Langmuir isotherm model shows a less favourable separation of CO_2 than measured in this study. All three lines in Figure III - 7 suggest NaLSX is a selective adsorbent for CO_2.

Equilibrium Separation factor

The equilibrium separation factor ($\alpha_{equilibrium}$) is determined from a ratio of the adsorbed (x_i) and fluid (y_i) phase fractions.

$$\alpha_{equilibrium} = \frac{x_1 y_2}{x_2 y_1} \tag{20}$$

The equilibrium separation factor is calculated for the binary equilibrium for both pressures and for the EL model.

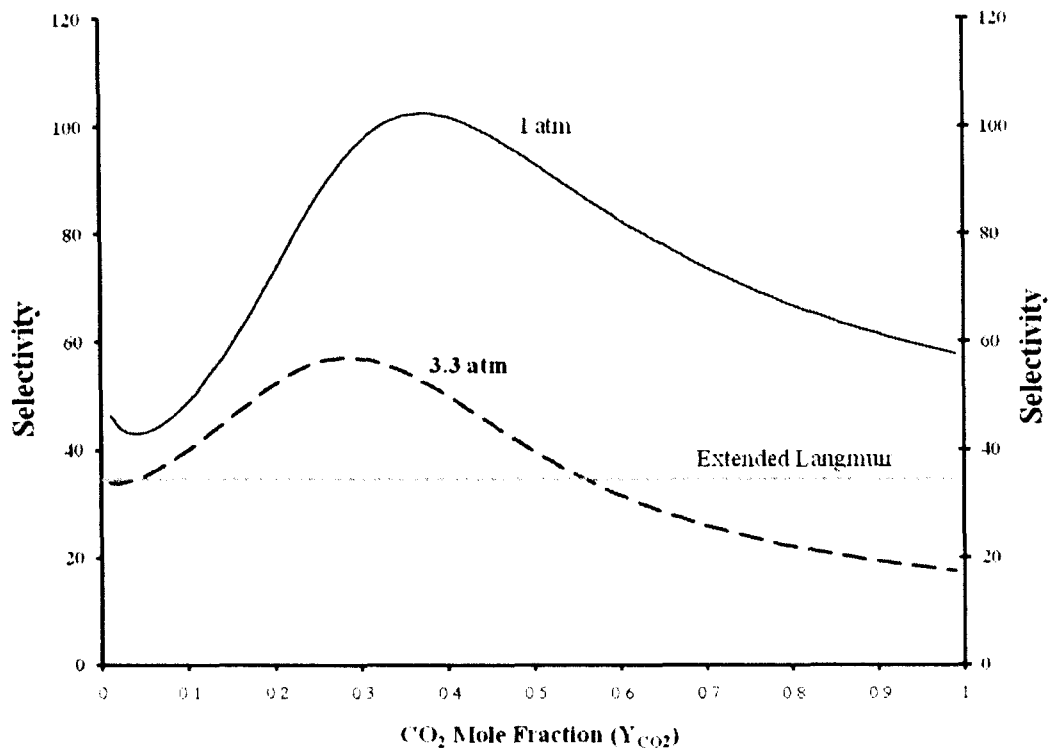

Figure III - 8 - NaLSX CO_2/CH_4 selectivity at 150 °C, 1 and 3.3 atm.

Figure III - 8 illustrates the favourable equilibrium selectivity for CO_2 adsorption across the range of binary compositions. The separation factor is highest (103) at atmospheric pressure and 0.37 CO_2 mole fraction. At the total pressure of 3.3 atm, the selectivity is significantly lower, although above 20, and has a maximum of 57 at a mole fraction of 0.29. The increase is due to the significant change in CO_2 adsorbed phase at low CO2 concentrations. The peak is a result of the adsorbed phase CO_2 ratio not increasing as quickly as the gaseous phase CO_2 ratio. Similar maximums in separation

factor have been documented for CO_2/CH_4 by Li and Tezel [14] on silicalite and Mulgundmath et al [13] for CECA 13X. At elevated pressures, the decrease in separation factor is due to the higher potential for adsorption of methane. The constant selectivity provided by the Extended Langmuir CO_2/CH_4 isotherm model does not change with composition or mole fraction. This is a result of the ideal adsorbed phase assumptions of the model. The separation factor for this system, which is based on the effective slope measurement fits, exhibits an increase and decrease with increasing CO_2 composition.

At LFG composition NaLSX exhibits a separation factor above 40 at both pressures. This is high relative to other studies shown in Table III - 5.

Table III - 5 – Equilibrium separation factors for CO_2/CH_4 on various adsorbents.

Adsorbent	$\alpha_{equilibrium}$	Pressure	Temperature (°C)
NaLSX	20 to 103	1 to 3.3 atm	Present Study (150 °C)
CECA 13X	40 to 100	1 atm	[13] 40 to 100 °C
H-ZSM-5	3 to 3.5	1 atm	[11] 40 °C
Silicalite	5 to 17	1 atm	[14] 25 to 100 °C
Activated Carbon	2 to 9	1 to 60 atm	[16] 25 °C

In comparison NaLSX has the highest separation factor for CO_2. The other separation factors were all measured at lower temperatures and the CO_2/CH_4 separation factor on silicalite is shown to be maximum at 70 °C [14]. The capacity of NaLSX for CO_2 is comparable to the other adsorbents although they are measured at lower temperatures. The measurements of capacity of NaLSX at lower temperatures requires sensitive equipment due to the high potential for adsorption. The high temperature results presented in this study are limited in their application. Despite this fact the behaviour of the binary system is described on the zeolite with a low Si/Al ratio. Therefore at high temperatures NaLSX has considerable selectivity and the CO_2 capacity can be increased somewhat by increasing the PSA adsorption pressure.

Economic Analysis

The breakeven costs of the landfill upgrading project were evaluated for various sized landfills and LFG feed flowrates based on the LandGem model. The PSA operating parameters were fixed at a feed pressure of 8 atm a regeneration pressure of 0.1 atm and a cycle time of 15 minutes to maximize the NaLSX working capacity. The number of

adsorption vessels was increased to accommodate the increase in LFG volume which is also reflected in the capital and operational costs. It was found that industrial scenario of a 40% tax rate and 0% discount rate resulted in the lowest breakeven costs. The breakeven costs for upgrading LFG are presented in Table III - 6.

Table III - 6 - Breakeven costs of LFG upgrading for 15 year project timeline.

Landfill Size (Mt)	Average LFG flow (m^3/hr)	Number of Adsorbers	capital $CAD (2008)	operation $CAD (2008)/year	Breakeven ($/$tCO_2e$)	$/$m^3$ LFG
0.2	50	1	$ 457,846	$ 280,022	$ 20,187	0.92
1.2	250	3	$ 1,389,354	$ 481,853	$ 5,303	0.56
2.3	500	4	$ 2,136,341	$ 713,271	$ 3,072	0.41
4.7	1000	8	$ 3,906,188	$ 1,189,902	$ 2,079	0.35
9.4	2000	16	$ 7,187,191	$ 2,130,228	$ 1,525	0.32

The breakeven cost for LFG upgrading is the highest for small landfills and well above $1,500 CAD (2008) for landfills above 9 Mt. This is significantly higher than the current resale price of carbon credits in Canada [3]. The maximum costs/tCO_2e occurs for landfills below 1 million tonnes and decreases exponentially for landfills up to 10 million tonnes. The amount of LFG increases proportionally with landfill size although the current scenario assumes a 50% recovery rate.

The capital costs ($7 M) are spread out over the 15 year project timeline and are composed mainly of the adsorber vessels, equipment, and adsorbent. The operational costs are roughly 30% of the total capital costs. The operational costs are considered constant and are comprised mainly of utilities and depreciation.

This cost analysis is limited in scope. It only takes into account one type of adsorbent, a fixed cycle and assumes instantaneous adsorption. In addition there is no pre-purification or post-purification of the LFG product and the adsorbent working capacity was limited due to the high operational temperature.

Based on the current study, the economics of LFG upgrading are not competitive with other utilization technologies for the largest of landfills at current carbon prices. They do however stand a chance at feasibility if the price of NG continues to increase with energy demand. The breakeven costs for various sized landfills with respect to NG prices is illustrated in Figure III - 9:

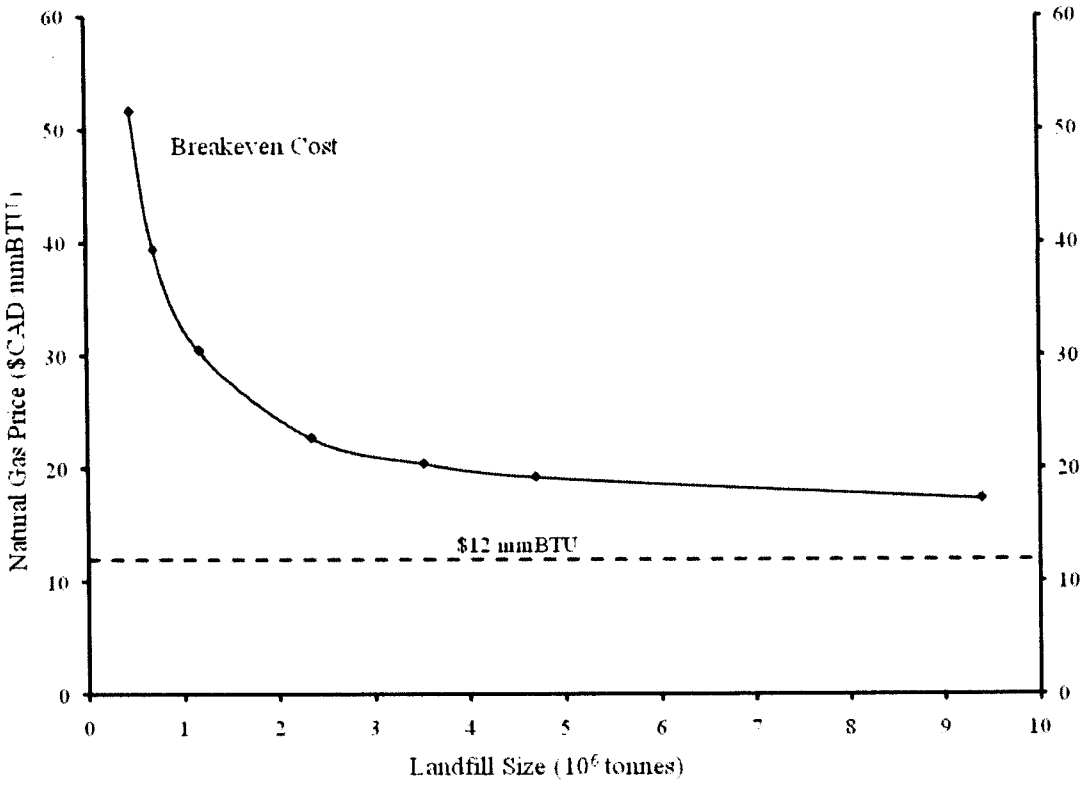

Figure III - 9 - Breakeven LFG upgrading costs with respect to landfill size and NG price.

The breakeven costs of LFG upgrading increase exponentially for landfills below 4 Mt. Currently a 10 Mt landfill would require over $ 1,500/tCO_2e to break even at NG prices of $12/mmBTU. If prices increase above $20/mmBTU upgrading LFG can be profitable for landfills over 4 Mt. Historically NG prices can rise up to $15/mmBTU and even higher considering the fossil fuel has a finite supply. However this study suggests that LFG upgrading would only be feasible for landfills over 4 Mt.

A small change in NG price can result in large returns for biogas recovery operations like LFG upgrading. They do however run the financial risk of returns that are volatile based upon consumer demand for NG. These operations require a more steady income from governmental bodies to remain sustainable for longer periods of time.

In addition to the revenues from NG there are several government incentives to utilize renewable sources of energy like biogas. An example of an Ontario incentive is the Standing Offer program where renewable sources of energy are guaranteed rates of

energy production. LFG upgrading is not competitive with other landfill gas technologies based on the case study which is applicable to North America.

Conclusions

The CO_2/CH_4 equilibrium adsorption behaviour on NaLSX is highly selective for CO_2 with high capacities. A LFG separation factor of 40 is observed at the LFG composition and the experimental conditions of this study. The binary isotherms exhibit capacity that is comparable to other binary adsorbents at temperatures below 150 °C.

Increasing the total pressure increased the CO_2 capacity and selectivity was maintained above 20. The CPC technique for binary measurement was adapted relatively simply to measure binary equilibrium at pressures above atmospheric. These conditions reflect the actual PSA operating which are significantly different from results based on pure isotherms and extended Langmuir model.

Based on the present study conditions LFG upgrading by adsorption is not as cost effective as are other LFG utilization technologies. Future increases in NG prices up to $20/mmBTU would make LFG upgrading profitable for landfills greater than 4 Mt for the conditions studied. The energy put into separating LFG is greater than that recovered. Therefore government incentives are required to encourage the utilization of this renewable biogas as an alternative fuel source.

Nomenclature

A_i	Coefficients in equation (4)	(mol/kg atm)
b *or* b_i	Equilibrium Constant	(atm^{-1})
b_r, b_o	Equilibrium Constant Parameter for TD Toth Isotherm	(atm^{-1})
B_i *and* C_i	Coefficients in equations (5) to	(mol/kg atm)
c	Concentration Signal from GC	(-)
C_{ps}	Heat Capacity	(J/g K)
k	Biogas Generation Decreasing Rate Constant	(yr^{-1})
K	Dimensionless Henry's Constant	(-)
K_P	Dimensional Henry's Constant	(mol/kg atm)
L	Column Length	(m)
L_o	Waste Methane Potential Production	(m^3/ton)
P *or* P_T	Total Pressure	(atm)
P_i	Partial Gas Pressure of Species *i*	(atm)
Q_t	Volume of Biogas Produced from the Landfill	(m^3/yr)
Q	Volumetric Flowrate to the Adsorber Column	(ft^3/min)
q_i	Amount Adsorbed or Binary Capacity of Species *i*	(mol/kg)
q_i^0	Amount Adsorbed of Species *i* in Pure Gas Isotherm	(mol/kg)
q_{sat}	Saturation Capacity of Species *i*	(mol/kg)
R	Ideal Gas Law Constant	(J/mol K)
R_c	Ratio of Adsorber System Cost to Adsorbent Cost	(-)
SSR	Sum of Squared Residuals	(mol/kg atm)
t, dt	Time or Time Step	(s)
t *and* ti	Time in equation (19)	(yr)
T	Temperature or projects lifetime in equation (20)	(K) or (yr)
W	Landfill Waste Receipts	(tonnes)
x_i *or* Xi	Mole Fraction in adsorbed Phase of Component *i*	(-)
y_i *or* Y_i	Mole Fraction in Gas Phase of Component *i*	(-)

Greek Letters

$\alpha_{equilibrium}$	Equilibrium separation factor	(-)
β	Tax Break	($CAD/year)
γ	Discount Rate (20%)	(%)
δ	Emission Reductions of CO_2 (or equivalent CO_2) to the atmosphere	(tCO_2e)
ε	Porosity or Void Fraction of Packed Bed	(-)
θ	Break Even Price when costs equal revenues	($ CAD/t CO_2e)
κ	Capital Cost	($CAD)
λ	Logarithmic Coefficient in equations (4) to (8)	(-)
μ	First Moment	(s)
μ_{ID}	System Retention time	(s)

v	Interstitial Velocity	(m/s)
ρ_{ads}	Absolute Density of Adsorbent (excluding pore volume)	(g/cm^3)
ρ_{bulk}	Bulk Density of Adsorbent	(g/cm^3)
σ	Reoccurring Operational and Maintenance Costs	($CAD/year)
χ	Tax Rate (40%)	(%)
ψ	Revenues Generated From Sale of NG	($CAD/mmBtu)

Abbreviations

atm	Atmospheres (measurement of pressure)
AWC	Adiabatic Working Capacity
AlO_4	Alumina Tetrahedral
Si/Al	Atomic Ratio of Silica to Alumina
BOC	British Oxygen Company (part of Linde Group)
$ CAD	2008 Canadian Dollars
CO_2	Carbon Dioxide
CECA 13X	CECA France NaX (Si/Al = 1.17)
CPC	Concentration Pulse Chromatography
EL	Extended Langmuir Binary Isotherm Model
GC	Gas Chromatogaph
GHG	Greenhouse Gas
GWP	Global Warming Potential
He	Helium Gas
HT-CPM	Harlick Tezel Concentration Pulse Method
IPCC	Intergovernmental Panel on Climate Change
LFG	Landfill Gas
MFC	Mass Flow Controller
mmBtu	Million British Thermal Units
Mt	Million tonnes
NaLSX	NaX (Si/Al ratio = 1.0)
CH_4	Methane
NG	Natural Gas
N_2	Nitrogen
NYME	New York Mercantile Exchange (NG prices)
OGEA	Ontario Green Energy Act
OPA	Ontario Power Authority
O_2	Oxygen
PSA	Pressure Swing Adsorber
SiO_4	Silicalite Tetrahedral
Na^+	Sodium Cation
STP	Standard Temperature and Pressure

SSR	Sum of Squared Residuals
t CO_2 e	Equivalent tonnes of CO_2 (based on GWP)
TCD	Thermal Conductivity Detector
US EPA	United States Environmental Protection Agency
ZSM-5	Pentasil Zeolite Adsorbent

References

1. OPA - Ontario Power Authority, A Progress Report on Renewable Energy Standard Offer Program, 2009: www.powerauthority.on.ca/sop, accessed on February, 2009.

2. OGEA - Ontario Green Energy Act, February 2009, www.greenenergyact.ca, accessed on February 2009.

3. Chicago Climate Exchange (CCX). Renewable Energy Emission Offsets and Landfill Methane Emission Offsets. January 2004; www.chicagoclimatex.com, accessed November 2008.

4. European Climate Exchange (ECX). Historical data – ECX EUA Futures Contract. January 2004; www.europeanclimateexchange.com/default_flash.asp, accessed November 2008.

5. NYME - New York Mercantile Exchange: Natural Gas Prices - Monthly graph 1980-2009, www.nymex.com/ng_pre_agree.aspx, accessed on Feb 2009.

6. IPCC, Mitigation of global greenhouse gas emissions from waste: conclusions and strategies from the Intergovernmental Panel on Climate Change (IPCC) Fourth Assessment Report. Working Group III (Mitigation). *Waste Management & Research* **2008**, 26, 11-32.

7. Cavenati, S.; Grande, C.A.; Rodrigues, A.E. Removal of Carbon Dioxide from Natural Gas by Vacuum Pressure Swing Adsorption. *Energy and Fuels* **2006**, *20*, 2648-2659.

8. Sulivan, P. *California Biomass Collaborative: 4th Annual Forum, Sacramento, California*, **2007**, March 28.

9. Ghoufi, A.; Gaberova, L.; Rouquerol, J.; Vincent, D.; Llewellyn, P.L.; Maurin, G. Adsorption of CO_2, CH_4 and their binary mixture in Faujasite NaY: A combination of molecular simulations with gravimetry–manometry and microcalorimetry measurements. *Microporous and Mesoporous Materials* **2009**, 119, 117-128.

10. Kerry, F.G. *Industrial Gas Handbook: Gas Separation and Purification*; CRC Press, Taylor and Francis Group: New York, 2007.

11. Harlick, P.J.E.; Tezel, F.H. Adsorption of carbon dioxide, methane and nitrogen: pure and binary mixture adsorption for ZSM-5 with SiO_2/Al_2O_3 ratio of 30. *Separation Science and Technology* **2002**, 37, 33-60.

12. Harlick, P.J.E.; Tezel, F.H. Adsorption of carbon dioxide, methane and nitrogen: pure and binary mixture adsorption for ZSM-5 with $SiO_2/Al2O_3$ ratio of 280. *Separation and Purification Technology* **2003**, *33*, 199-210.

13. Mulgundmath, V.P.; Tezel, F.H.; Saatcioglu, T.; Golden, T.C. Adsorption and Separation of CO_2/N_2 and CO_2/CH_4 by 13X Zeolite. *The Canadian Journal of Chemical Engineering*, Article in press Jan 2009.

14. Li, P.; Tezel, F.H. Equilibrium and kinetic analysis of CO_2–N_2 adsorption separation by concentration pulse chromatography. *Journal of Colloid and Interface Science* **2007**, *313*, 12-17.

15. Buss, E. Gravimetric measurement of binary gas adsorption equilibria of methane-carbon dioxide mixtures on activated carbon. *Gas Sep. Purif.* **1995**, 9 (3), 189-197.

16. Dreisbach, F.; Staudt, R.; Keller, J.U. High Pressure Adsorption Data of Methane, Nitrogen, Carbon Dioxide and their Binary and Ternary Mixtures on Activated Carbon. *Adsorption* **1999**, 5, 215-227.

17. Van der Vaart, R.; Huiskes, C.; Bosch, H.; Reith, T. Single and Mixed Gas Adsorption Equilibria of Carbon Dioxide/Methane on Activated Carbon. *Adsorption* **2000**, 6, 311-323.

18. Goetz, V.; Pupier, O.; Guillot, A. Carbon dioxide-methane mixture adsorption on activated carbon. *Adsorption*, **2006**, 12, 55-63.

19. Buffham, B.A; Mason, G.; Heslop, M.J. Binary Adsorption Isotherms from Chromatographic Retention Times. *Industrial & Engineering Chemistry Research.* **1999**, 38 (3), 1114-1124.

20. Van Der Vlist, E.; Van Der Meijden, J. Determination of Adsorption Isotherms of the Components of Binary Gas Mixtures by Gas Chromatography. *Journal of Chromatography* **1973**, 79, 1-13.

21. Shah, D.B.; Ruthven, D.M. Measurement of Zeolitic Diffusivities and Equilibrium Isotherms by Chromatography. *AIChE Journal* **1977**, 23, 804-809.

22. Tezel, F.H.; Tezel, H.O.; Ruthven, D.M. Determination of Pure and Binary Isotherms for Nitrogen and Krypton. *Journal of Colloid and Interface Science* **1992**, 149, 197-207.

23. Heslop, M.J.; Buffham, B.A.; Mason, G. A Test of the Polynomial-Fitting Method of Determining Binary-Gas-Mixture Adsorption Equilibria *Industrial & Engineering Chemistry Research* **1996**, 35, 1456-1466.

24. Heslop, M.J.; Buffham, B.A.; Mason, G. Tests of the Consistency between Binary Gas Adsorption Isotherms and Binary Chromatographic Retention Volumes. *Industrial & Engineering Chemistry Research* **2000**, 39, 1514-1519.

25. Heslop, M.J; Richardson, D.J.; Russell, P.A.; Mason, G.; Buffham, B.A.; Guo, J. Chromatographic Retention Times Using Mixture Pulses of Different Compositions. *Adsorption* **2005**, 11, 127–131.

26. Harlick, P.J.E.; Tezel, F.H. A Novel Solution Method for Interpreting Binary Adsorption Isotherms from Concentration Pulse Chromatography Data. *Adsorption* **2000**, *6*, 293–309.

27. Harlick, P.J.E.; Tezel, F.H. An experimental adsorbent screening study for CO_2 removal from N_2. *Microporous and Mesoporous Materials* **2004**, 76, 71-79.

28. Ojo, A. F.; Fitch, R.F.; Bülow, M. Removal of Carbon Dioxide from Gas Streams. US Patent 5,531,808, 1996.

29. Bestfather, C.; Tezel, H.F. Upgrading Landfill Gas by Adsorption: Adsorbent Selection and Equilibrium Data For the Bulk Separation of Carbon Dioxide and Methane. *Article to be submitted for publication in Environmental Science & Technology*, **2009**.

30. Ackley, W.M. Multilayer Adsorbent Beds for PSA gas Separation. US Patent 6,152,991, 2000.

31. USEPA - United States Environmental Protection Agency; Landfill Gas Emissions Model (LandGEM) Version 3.02 User's Guide, Document # EPA-600/R-05/047, May 2005; www.epa.gov/ttn/catc/dir1/landgem-v302-guide.pdf, accessed November 2008.

32. Triebe, R.W.; Tezel, F. H. *Gas Separation and Purification Technology* **1995**, *9*, 223-230.

33. Ruthven, D.M.; Kumar, R. An Experimental Study of Single-Component and Binary Adsorption Equilibria by a Chromatographic Method. *Industrial Engineering Chemical Fundamentals* **1980**, *19*, 27-32.

34. Harlick, P.J.E.; Tezel, F.H. CO_2–N_2 and CO_2–CH_4 Binary Adsorption Isotherms with H-ZSM-5: The Importance of Experimental Data Regression with the Concentration Pulse Method. *Canadian Journal of Chemical Engineering*, **2001**, 79, 236–245.

35. Yang, R.T.; *Gas Separation by Adsorption Processes*; Imperial College Press: New York, 1986.

36. Ruthven, D.M.; *Principles of Adsorption and Adsorption Processes*; Wiley: New York, 1984.

37. Langmuir, I. Journal of the American Chemical Society 1918, 40, 1361-1403.

38. Delhotal, C.; de la Chesnaye, F.; Gardiner, A.; Bates, J.; Sankovski, A., Estimating potential reductions of methane and nitrous oxide emissions from waste, energy and industry. In: de la Chesnaye F.C. & Weyant, J. (eds): *The Energy Journal*, Special Issue: Multi-Greenhouse Gas Mitigation and Climate Policy, **2006**.

39. Golden, T. Air Products and Chemicals, Inc. Various personal communications 2006-2008.

40. Cooper, D.C, Alley, F.C., *Air Pollution Control 3rd addition: A Design Approach*; Waveland Press, Inc:. Long Grove, Illinois, 2002.

41. Keller, J.; Staudt, R. *Springer* **2005**, 1-420.

42. Ruthven, D.M.; Loughlin, K.F.; Holborow, K.A. Multicomponent sorption equilibrium in molecular sieve zeolites. *Chemical Engineering Science* **1973**, 28, 701-709.

43. Cavenati, S.; Grande, C.A.; Rodrigues, A.E. *J. of Chem. Eng. Data* **2004**, *49*, 1095-1101.

44. Cavenati, S.; Grande, C.A.; Rodrigues, A.E. Upgrade of Methane from Landfill Gas by Pressure Swing Adsorption. *Energy and Fuels* **2005a**, *19*, 2545-2555.

Chapter IV: Conclusions & Recommendations

General Conclusions

Chapter II

The equilibrium adsorption properties of three zeolites (NaLSX, NaY and CaX) were measured as screening parameters for the bulk separation of CO_2 and CH_4. All of the adsorbents showed high selectivity for CO_2 at low partial pressures due to the high potential of CO_2 relative to CH_4. The equilibrium isotherms exhibited high capacity for CO_2 and low capacity for CH_4.

NaLSX was studied in more detail because it has the highest cation density of all the zeolites studied and limited data is available for this adsorbent behaviour at pressures above atmospheric. Therefore measurements of its isothermal capacity from 40-150 °C up to 4 atm and the limiting heat of adsorption and Henry's Law constant were determined. NaLSX exhibited the highest capacity for CO_2 even at elevated temperatures due to its low Si/Al ratio and high density of cations. However the high potential for CO_2 adsorption also showed it to have a higher limiting heat of adsorption.

The ideal selectivity for NaLSX-CO_2 was shown to range from very favourable (up to 400 with ratio of Henry's Law Constants) to slightly favourable (5-20 with AWC selectivity). The large difference in these selectivities indicates the significant effect bed heating has on a bulk separation. VPSA bed temperature changes were in the magnitude of 70 to 140 °C based on adiabatic process for a pressure ratio of 80.

The zeolite equilibrium isotherms were used to evaluate expected working capacity and adiabatic working capacity for various VPSA operating conditions. NaLSX was shown to have the highest CO_2 working capacity for a bulk separation of LFG. The adiabatic working capacity was much smaller in comparison due to the heating effects that occur in a VPSA. As such NaX and NaY showed the highest AWC for the conditions selected although their selectivity increases with bed temperature. This suggests that the VPSA could be operated at higher temperatures effectively for the bulk separation of CO_2/CH_4 if the operation remains thermally stable.

In conclusion NaLSX, NaX and NaY show applicability for the bulk separation of CO_2/CH_4. All the zeolites studied have selectivity for CO_2 adsorption at low partial pressures due to the quadrupole moment. This bulk separation is sensitive to heating and it should be an important consideration in designing the separation process. Additionally all of the zeolites used are sensitive to water and NMOC adsorption therefore the pre-treatment of the landfill gas is an important step before the bulk separation. The result of a VPSA application to upgrade LFG will reduce GHG emissions, as well as produce high purity carbon dioxide and methane products.

Chapter III

The CO_2/CH_4 equilibrium adsorption behaviour on NaLSX is highly selective for CO_2 with high capacities. A LFG separation factor of 40 is observed at the LFG composition and the experimental conditions of this study. The binary isotherms exhibit capacity that is comparable to CECA 13X zeolite adsorbents at temperatures below 150 °C.

Increasing the total pressure increased the CO_2 capacity and selectivity was maintained above 20. The CPC technique for binary measurement was adapted relatively simply to measure binary equilibrium at pressures above atmospheric. These conditions reflect the actual PSA operating which are significantly different from results based on pure isotherms and extended Langmuir model.

Based on the present study conditions LFG upgrading by adsorption is not as cost effective as are other LFG utilization technologies. Future increases in NG prices up to $20/mmBTU would make LFG upgrading profitable for landfills greater than 4 Mt for the conditions studied. The energy put into separating LFG is greater than that recovered. Therefore government incentives are required to encourage the utilization of this renewable biogas as an alternative fuel source.

Recommendations

1. Zeolites are known to have macropore and micropore resistance to mass transfer which can control the VPSA process. The equilibrium adsorption behaviour indicates process selectivity but it does not take into account the kinetics. Therefore measurements of CH_4 and CO_2 diffusion into the adsorbents presented in this studied should be quantified with a gravimetric or zero length column system (Brandani, 2002). After which a detailed process model would provide a method for optimising the VPSA temperature and pressure conditions.

2. The CPC limiting heat of adsorption (ΔH_o) requires validation with a more sensitive piece of equipment like an adsorption calorimeter to measure the limiting heat of adsorption. The high adsorption potential at low partial pressures is an advantage of NaLSX although it is challenging to quantify precisely.

3. The economic analysis of upgrading landfill gas can be expanded to include more scenarios. Currently the bulk separation via PSA is used to determine the breakeven costs of such a process. The pre-treatment of the landfill gas and final pre-purification or compression of the product is not considered. Nor is the by-product CO_2, sequestered or compressed. The full scenario will always be very limited in its application because the economics are highly dependant upon the location of the LFG utilization site. Also the costs of LFG upgrading in developing countries may be more accessible if local technologies and materials are utilized. The standard of living benefits of renewable energy projects in isolated communities in developing countries can also have an impact on global GHG emissions.

4. The LFG pre-treatment system removes the trace gases and water from the gas stream prior to the CO_2/CH_4 bulk separation. This system is not trivial because it is essential to remove all the gas components that are more polar than CO_2 and CH_4. Otherwise they will be irreversibly adsorbed to the zeolite bed in the VPSA. In addition the removal of particulates and siloxanes is essential if the gas is to be combusted in a turbine engine or directed into a NG pipeline. Further research is required to characterize these trace components and ensure a robust pre-treatment is capable of protecting the upgrading processes downstream of the raw landfill gas.

Appendices

The following Appendicies are included in the thesis to compliment the work in the two papers.

Appendix A includes all the data from the isotherm measurements. In addition there is an uncertainty analysis on volumetric isotherms. The TD Toth fits to all of the isotherms not shown in Chapter II are provided as well as the isosteric Heat of adsorption calculations for CO_2 and CH_4 on NaLSX.

Appendix B includes the thermodynamic consistency test for the binary results presented. The method of calculating the binary isotherm from the effective slope measurements is clarified. In addition the capital costs and operational costs for the economic analysis are also described in detail.

Appendix C provides a brief description on the structure of zeolite adsorbents.

Appendix D describes the operation of the constant volume system used to measure pure gas isotherms.

Appendix E describes the operation of the Gas Chromatograph (GC) for the measurement of the Henry's Law constants for pure gases. The manual also describes the method for measurement of the mixture gas effective adsorption slope in the GC.

Appendix A – Supplementary Information for Chapter II:

Upgrading Landfill Gas by Adsorption:

Adsorbent Selection and Equilibrium Data

For the Bulk Separation of

Carbon Dioxide and Methane

A.1 Constant Volume System Isotherm Method

The adsorption isotherms were determined with a volumetric gas adsorption apparatus. This system is equipped with Swagelock® valves and two mks *Baratron*® pressure transducers that were employed for their respective low and high pressure ranges. The first pressure transducer, a *1000 Torr mks Baratron® Capacitance Manometer*, is applied to the lower pressure range of up to 120 kPa with an uncertainty of ± 0.001 kPa. The second pressure transducer, a *250 psia mks Baratron® Pressure Transducer*, is applied in the range of pressures above 120 kPa with an uncertainty of ± 0.08 kPa. The volume of the interconnecting tubing (V_i) and manifold (V_d) are displayed in Table A.1 for the volumetric system used in the following experiments.

The free space (V_s) or "dead volume" is the volume of the sample cell that is not occupied by the adsorbent. The dead volume is estimated after initial adsorbent regeneration and before the isotherm measurements are taken. The dead space is measured by the expansion of Helium (He) gas into the sample cell (with adsorbent) at the same temperature as the isotherm. It is assumed that the volume available to the He atoms is the same as that for the CH_4 and CO_2 gas molecules. Also, He adsorption and swelling of the adsorbent is considered negligible. The dead volume is calculated for each isotherm and is estimated with an uncertainty of ± 0.3 ml.

Table A.1 - Volume of manifold with both pressure transducers open (V_{d1}), with only 250 psia pressure transducer open (V_{d2}), and interconnecting tubing (V_i).

V_{d1} (ml)	V_{d2} (ml)	V_i (ml)
53.97	39.42	6.70

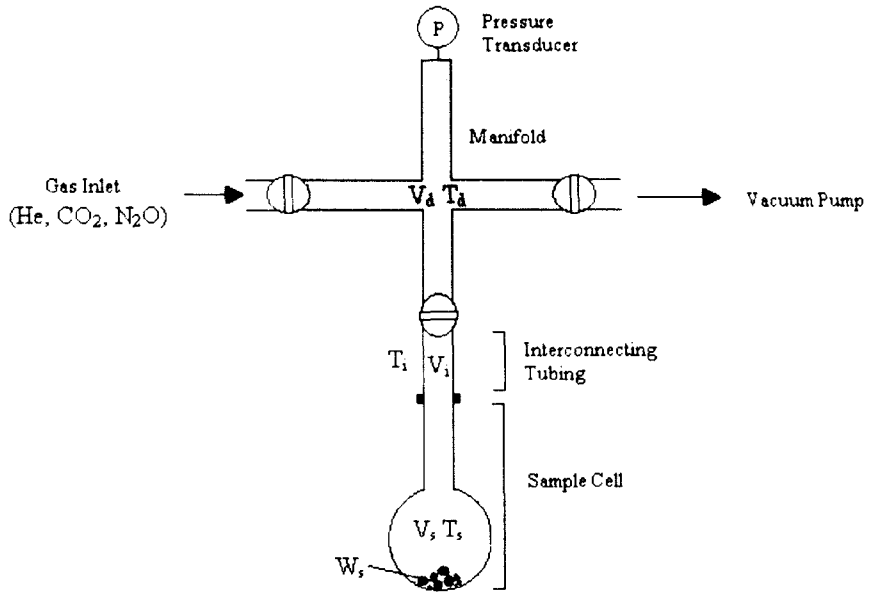

Figure A.1 - Schematic of volumetric system with manifold, interconnecting tubing, and free space in sample cell.

The operation of the volumetric apparatus is based upon the gas laws. In the pressure range for the experiments presented in this report, the ideal gas law is considered applicable (below critical pressures of CO_2 and CH_4). In this system a known quantity of pure gas is admitted into a sample cell volume that contains the adsorbent at a constant temperature. As adsorption takes place the sample cell pressure decreases (over a period of 1 to 15 hrs). Once the system has reached equilibrium, the volume adsorbed can be calculated from the difference between the pressure and the amount of gas required to fill the free space in the sample cell.

The operation of the volumetric system follows an isotherm construction based upon a point-by-point measurement of the pressure change in the gas. The pressure of the gas is increased incrementally for each measurement of the equilibrium.

The following equations illustrate the determination of the number of moles of adsorbed gas (n_a) per adsorbent weight by estimation of the volume of gas adsorbed (V_a).

$$\frac{n_a}{W_s} = \frac{V_a P_R}{W_s T_R} = \frac{1}{W_s}\left[\frac{P_1 V_d}{T_{d1}} - \frac{P_2 V_d}{T_{d2}} - P_2\left(\frac{V_s}{T_{s2}} + \frac{V_i}{T_{i2}}\right) + P_c\left(\frac{V_s}{T_{sc}} + \frac{V_i}{T_{ic}}\right)\right] \qquad (1)$$

Where n_a is the number of moles of gas adsorbed (m-mol)

V_a is the volume of gas adsorbed (ml)

W_s is the weight of the outgassed sample (g)

P_R is the pressure of the adsorbed gas at standard conditions (760 mmHg)

P_1 is the pressure in the manifold before introduction into the sample cell (mmHg)

P_2 is the pressure of the expanded gas into the sample cell and manifold (mmHg)

P_e is the equilibrium pressure in the sample cell (previous equilibrium pressure in mmHg)

V_d is the volume of the manifold (ml)

V_s is the volume of the free space in the sample cell (ml)

V_i is the volume of the interconnecting tubing (ml)

T_R is the temperature of the adsorbed gas at standard conditions (273.15 K)

T_d is the temperature of the manifold (K)

T_s is the temperature of the adsorbent sample (K)

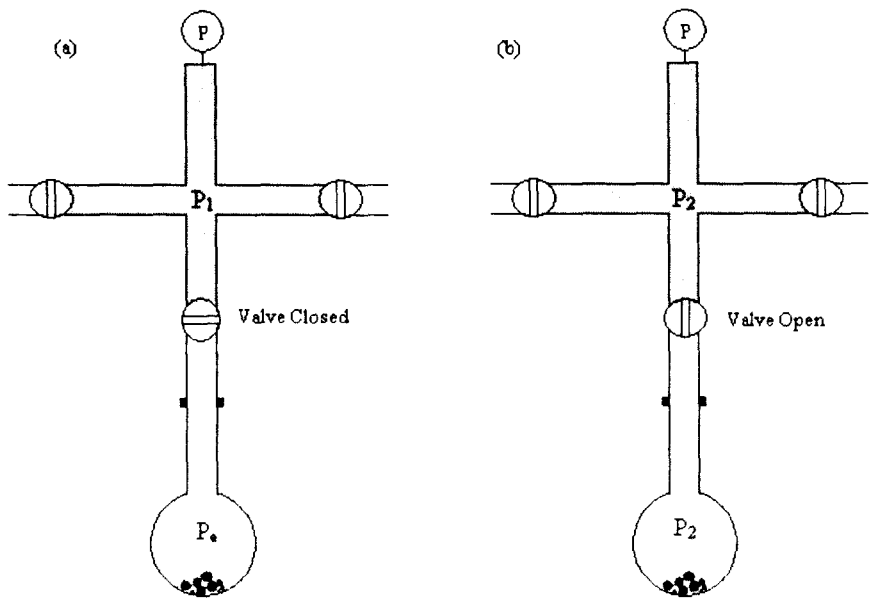

Figure A.2 - (a) System with high pressure pure gas in manifold (P1) and sample cell at previous equilibrium pressure (Pe). (b) System at final equilibrium pressure (P2) after expansion.

CO_2 Isotherm Raw Data measured with Volumetric System

NALSX Isotherms

10-Jul	20-Jul		
Na LSX CO2 40°C			40.6
P (atm)	n (mmol/g)	T (K)	
0.0067	0.000	314.05	
0.0077	0.604	313.75	
0.0124	1.509	313.85	
0.0528	2.576	314.45	
0.3258	4.066	311.85	
1.3729	5.042	314.05	
2.7147	5.493	314.85	
3.6444	5.737	313.45	

06-Feb	20-Feb		
Na LSX CO2 70°C			70.8
P (atm)	n (mmol/g)	T (K)	
0.007	0.000	343.65	
0.037	0.996	345.95	
0.122	1.873	341.95	
0.241	2.667	344.75	
0.371	3.338	343.65	
0.584	3.823	343.65	
0.979	3.922	345.95	
1.781	4.407	341.95	
2.270	4.805	344.75	
2.870	4.632	343.65	
3.478	4.805	343.65	

16-Aug	23-Aug		
Na LSX CO2 100°C			100.0
P (atm)	n (mmol/g)	T (K)	
0.0067	0.000	373.25	
0.0431	0.823	373.65	
0.1234	1.603	373.55	
0.2619	2.197	372.85	
0.4497	2.656	372.05	
0.6502	2.983	373.05	
1.1495	3.309	375.45	
1.6838	3.669	372.85	
2.8483	4.093	373.95	
3.4943	4.315	371.15	

29-Apr	20-May CB		
Na LSX CO2 150°C			149.0
P (atm)	n (mmol/g)	T (K)	
0.007	0.000	421.45	
0.101	0.565	421.05	
0.240	1.055	422.45	
0.426	1.463	423.35	
0.885	1.917	421.95	
1.410	2.357	421.35	
2.341	2.728	422.45	
3.001	2.993	422.35	
3.497	3.184	422.35	
3.962	3.335	422.85	
4.210	3.480	421.85	

NAY CO2 Isotherms

17-Jun	30-Jun		
NaY CO2 40°C			40.8
P (atm)	n (mmol/g)	T (K)	
0.005	0.000	314.45	
0.034	0.633	314.15	
0.125	1.516	314.05	
0.255	2.379	313.65	
0.549	3.209	313.55	
1.036	3.958	313.45	
1.276	4.176	314.15	
1.422	4.435	313.95	
1.961	4.736	313.95	
2.588	4.913	313.65	

16-Jun	02-Jul		
NaY CO2 100°C			101.0
P (atm)	n (mmol/g)	T (K)	
0.007	0.000	374.35	
0.203	0.564	373.95	
0.397	1.011	372.85	
0.541	1.415	374.65	
0.722	1.665	373.75	
1.242	2.123	373.45	
1.676	2.505	372.55	
2.148	3.007	375.65	
2.916	3.452	376.35	

Cax CO2 Isotherms

18-Apr	28-Apr		
Ca X CO2 40°C			39.8
P (atm)	n (mmol/g)	T (K)	
0.01	0.00	312.35	
0.01	0.18	313.15	
0.01	0.71	312.55	
0.04	1.61	312.5	
0.14	2.74	312.85	
0.53	3.54	313.3	
1.36	4.27	312.7	
2.59	4.62	314.2	
3.61	4.81	313.5	

20-May	06-Jun		
Ca X CO2 100°C			99.4
P (atm)	n (mmol/g)	T (K)	
0.01	0.00	372.45	
0.26	1.36	372.45	
0.69	2.11	372.65	
1.19	2.69	372.6	
1.57	3.05	373.25	
2.00	3.26	372.9	
2.41	3.51	370.8	
3.10	3.71	373.4	
3.40	3.82	372.7	

Desorption Isotherm Data

03-Apr	29-Apr		
Na LSX CO2 27°C			27.6
P (atm)	n (mmol/g)	T (K)	
0.0053	0	300.75	
0.0180	0.49828413	301.15	
0.0486	0.997176826	300.85	
0.1119	1.528093607	302.25	
0.1683	2.067549804	302.75	
0.2643	2.95938282	301.45	
0.4943	3.70094069	301.35	
0.8176	4.27026782	300.85	
1.0832	4.459060448	301.95	
1.4146	4.643374571	301.15	
1.6898	4.841824144	299.95	
2.1902	4.985432132	299.55	
2.5878	5.095559447	298.55	
3.0232	5.158275675	299.35	
3.3612	5.197276742	299.85	
3.4944	5.249493962	299.25	

24-Apr	17-Jun		
Na LSX CO2 40°C			40.9
P (atm)	n (mmol/g)	T (K)	
0.007	0.000	315.85	
0.029	2.107	313.85	
0.219	3.755	314.35	
0.704	4.548	314.55	
1.910	5.015	314.75	
3.450	5.386	312.95	
4.399	5.536	313.45	
0.007	0.000	313.45	
0.035	1.955	313.65	
0.261	3.514	313.45	
0.762	4.157	314.05	
1.923	4.575	314.05	
3.433	4.943	314.05	
4.421	5.100	314.05	

30-Nov	31-Jan CB desorption isotherm		
Na LSX CO2 40°C			40.6
P (atm)	n (mmol/g)	T (K)	
0.007	0.000	313.95	
0.046	2.624	313.35	
0.052	2.714	313.65	
0.059	2.819	313.25	
0.069	2.938	313.65	
0.079	3.081	312.95	
0.098	3.243	313.45	
0.125	3.446	313.55	
0.169	3.701	313.55	
0.280	4.020	313.85	
0.354	4.188	314.15	
0.483	4.389	314.05	
0.690	4.597	314.25	
1.144	4.870	314.15	
1.672	5.081	312.95	
2.462	5.220	314.95	
2.836	5.331	313.65	
3.522	5.403	313.65	

Isotherm Repeats for NaLSX JCR

25-Sep	08-Oct		
Na LSX CO2 70°C (1)			71.6
P (atm)	n (mmol/g)	T (K)	
7.8688E-05	0.000	344.25	
0.00745458	0.424	348.85	
0.01325607	0.903	344.35	
0.02485904	1.371	343.85	
0.04806499	1.775	343.85	
0.10766208	2.286	345.05	
0.21765628	2.869	344.35	
0.47330003	3.498	345.05	
0.90334483	4.032	344.25	
1.16223829	4.184	344.95	
1.4644612	4.331	344.55	
1.88367363	4.448	345.15	
2.32021784	4.501	344.25	
2.78709266	4.521	344.25	
3.19547273	4.451	344.25	

13-Mar	01-Apr		
Na LSX CO2 70°C (2)			71.1
P (atm)	n (mmol/g)	T (K)	
0.0072	0.000	344.65	
0.0782	0.790	343.05	
0.0959	1.662	344.85	
0.1787	2.421	343.55	
0.3291	3.114	343.55	
0.5679	3.538	345.55	
1.3586	4.020	343.35	
2.3898	4.323	346.65	
2.9372	4.661	342.05	
3.6483	4.730	345.05	

03-Apr	23-Apr		
Na LSX CO2 70°C (3)			70.6
P (atm)	n (mmol/g)	T (K)	
0.0070	0.000	343.45	
0.0248	0.603	343.35	
0.0724	1.245	343.45	
0.1673	1.832	344.55	
0.2862	2.342	344.65	
0.4217	2.739	344.75	
0.7666	3.232	343.35	
1.2697	3.767	343.95	
2.1023	4.138	344.45	
2.7701	4.419	342.95	
3.1679	4.643	342.85	

CH_4 Isotherm Raw Data measured with Volumetric System

CH4 Isotherms on NALSX

24-Jul	10-Aug CB	
Na LSX CH_4 40°C		**40.5**
P (atm)	n (mmol/g)	T (K)
0.007	0.000	314.15
0.346	0.165	314.05
0.661	0.330	310.05
0.923	0.490	313.15
1.275	0.545	313.45
1.693	0.685	313.75
2.148	0.816	314.85
2.980	1.061	314.55
3.605	1.198	315.05

13-Nov	26-Nov CB	
Na LSX CH_4 70°C		**70.1**
P (atm)	n (mmol/g)	T (K)
0.007	0.000	344.75
0.320	0.100	343.25
0.699	0.223	342.15
1.015	0.421	344.35
1.437	0.477	343.75
2.265	0.575	343.15
2.854	0.706	342.25
3.209	0.772	342.55

29-Aug	14-Sep CB	
Na LSX CH_4 100°C		**100.7**
P (atm)	n (mmol/g)	T (K)
0.007	0.000	373.45
0.294	0.058	372.25
0.645	0.128	372.95
0.958	0.245	373.85
1.305	0.284	376.15
1.683	0.361	373.75
2.281	0.465	375.95
2.990	0.589	372.35
3.405	0.695	373.35
3.712	0.746	373.95

CAX Isotherm on CH4

13-Mar	31-Mar CB	
Ca X CH_4 40°C		**40.6**
P (atm)	n (mmol/g)	T (K)
9.22E-05	0	314.35
0.330228	0.310622	313.95
0.543301	0.52017	312.85
0.903521	0.695581	312.35
1.28009	0.835645	313.85
1.498042	0.908852	313.65
1.700607	1.033982	313.85
2.18048	1.162969	314.65
2.519533	1.274879	313.55
2.882417	1.333828	315.45
2.984242	1.407442	312.95

NALSX Isotherm on CH4 (repeats, higher temperature)

30-Jan	13-Feb CB	
Na LSX CH_4 40°C (2)		**40.6**
P (atm)	n (mmol/g)	T (K)
0.000103	0	313.25
0.395099	0.178206	313.35
0.945186	0.448726	313.65
1.62153	0.732921	312.85
1.893423	0.817932	314.55
2.216227	0.925296	314.75
2.621358	1.085965	313.85
2.995074	1.186924	313.75
3.294047	1.264637	313.65

29-Apr	15-May CB	
Na LSX CH_4 150°C		**148.8**
P (atm)	n (mmol/g)	T (K)
0.005	0.000	420.95
1.263	0.136	421.85
1.837	0.255	422.55
2.317	0.297	422.15
2.821	0.359	422.45
3.175	0.399	421.85
3.389	0.430	422.15

NALSX N2 Isotherm

05-Jan	21-Jan CB	
Na LSX N_2 40°C		**40.8**
P (atm)	n (mmol/g)	T (K)
8.41E-05	0	313.65
0.273268	0.123316	314.75
0.74899	0.271127	313.95
1.074401	0.353452	313.45
1.441713	0.443949	313.15
1.530539	0.504627	314.05
1.954084	0.606369	314.25
2.36788	0.693801	314.35
2.943079	0.801585	313.55
3.407787	0.913377	313.45
4.04798	1.024612	314.65

CO_2 & CH_4 Isotherm Data obtained from Literature

NaX CO_2 and CH_4 @ 40, 70 & 100 °C

Mulgundmath, V.P., Tezel, F.H., Saatcioglu, T., Golden, T.C. *The Canadian Journal of Chemical Engineering*, Article in press Jan 2009

Na X CO2 40°C

P (atm)	n (mmol/g)	T (K)
0.007211	0.000000	314.65
0.007697	0.169204	313.15
0.010443	0.589740	313.05
0.033297	1.430609	312.85
0.139102	2.437121	313.55
1.077823	3.620312	313.15
2.499448	3.974887	313.55
3.817589	4.222350	312.95

Na X CH_4 40°C

P (atm)	n (mmol/g)	T (K)
0.008	0.000	314.65
0.108	0.045	313.15
0.659	0.279	313.05
1.875	0.473	312.85
3.480	1.003	313.55

Na X CO2 70°C

P (atm)	n (mmol/g)	T (K)
0.000000	0.007369	344.65
0.018556	0.652378	343.15
0.088642	1.740216	343.05
0.265573	2.338178	342.85
0.497909	2.997284	343.55
1.200823	3.205644	343.15
1.895787	3.468547	343.55
2.350539	3.625655	342.95
3.005722	3.822468	342.95

Na X CO2 100°C

P (atm)	n (mmol/g)	T (K)
0.007592	0.000000	373.45
0.017027	0.152685	372.65
0.049028	0.502906	372.15
0.143544	1.125508	370.55
0.422795	1.925603	371.55
1.203722	2.715102	370.35
2.460347	3.404462	370.95

Na X CH_4 100°C

P (atm)	n (mmol/g)	T (K)
0.008	0.000	373.45
0.153	0.032	372.65
0.863	0.108	372.15
1.568	0.129	370.55
2.576	0.236	371.55
3.439	0.351	370.35
4.334	0.443	370.95

Silicalite CO_2 and CH_4 @ 40, 70 & 100 °C

Li, P.; Tezel, F.H. *Journal of Colloid and Interface Science* **2007**, *313*, 12-17

Silicalite CO_2 40°C

P (atm)	q (m-mole)
0.003706	0
0.013356	0.090469
0.058729	0.222026
0.149227	0.382957
0.285961	0.566213
0.476292	0.778697
0.755045	0.999896
1.11156	1.215982
1.612672	1.441223
2.338198	1.633033
3.306522	1.795086
4.574078	1.936034

Silicalite CH_4 40°C

P (atm)	q (m-mole)
0.006971	0
0.089979	0.052329
0.241395	0.13343
0.448401	0.232096
0.711541	0.341767
1.035425	0.459231
1.389324	0.573838
1.835869	0.695673
2.388611	0.814674
3.046636	0.93795
3.839075	1.05832
4.791538	1.183427

Silicalite CO_2 70°C

P (atm)	q (m-mole)
0.007512	0
0.026319	0.07276
0.100964	0.18904
0.194431	0.299965
0.330059	0.443027
0.53533	0.596665
0.812784	0.767254
1.193208	0.955156
1.697427	1.163757
2.410881	1.36335
3.372528	1.547837
4.64537	1.742991

Silicalite CH_4 70°C

P (atm)	q (m-mole)
0.006946	0
0.103896	0.034816
0.268302	0.089432
0.482526	0.157594
0.751876	0.233887
1.075434	0.321125
1.445065	0.40975
1.874131	0.520297
2.454125	0.635812
3.073268	0.736578
3.926716	0.878008
4.847583	1.002447

Silicalite CO_2 100°C

P (atm)	q (m-mole)
0.003544	0
0.034871	0.059235
0.109714	0.130248
0.22126	0.21064
0.376999	0.299776
0.588279	0.40008
0.866015	0.522269
1.254233	0.656477
1.751684	0.82796
2.43863	1.024916
3.390799	1.223506
4.650351	1.444769

Silicalite CH_4 100°C

P (atm)	q (m-mole)
0.006855	0
0.112925	0.026526
0.282655	0.068381
0.501179	0.120971
0.772819	0.182361
1.098753	0.252857
1.477306	0.329939
1.934421	0.4114
2.475558	0.514193
3.123091	0.630762
3.927696	0.753543
4.890211	0.892456

NaY CH_4 @ 40 & 70 °C

Talu, O.; Zhang, S.; Hayhurst, D.T. *Journal of Physical Chemistry* **1993**, 97, 12894-

Na Y CH_4 40°C

P (atm)	n (mmol/g)
1.09	0.28
2.37	0.556
4.39	0.951
7.20	1.429
9.99	1.778
14.12	2.2
18.20	2.514
21.40	2.734
25.14	2.926
28.46	3.066

Na Y CH_4 70°C

P (atm)	n (mmol/g)
1.834	0.226
3.931	0.420
7.026	0.696
10.699	1.006
12.242	1.285
14.347	1.546
21.950	1.780
25.83568	1.993
29.11424	2.184

A.2 Henry Constant Determined from Isotherm

The Henry's law constant (K) is determined from the slope of the isotherm at zero coverage. This slope can be estimated from the Langmuir isotherm model parameters.

$$q = \frac{q_{\infty} bP}{1 + bP} \tag{2}$$

Where q is the amount adsorbed (mol/lg)

q_{∞} is the saturation capacity (mol/kg)

b is the affinity constant (atm^{-1})

P is the pressure (atm)

The Langmuir isotherm model parameters are fit with a least squares minimization technique. The two parameter estimates of q_{∞} and b are used to determine the slope of the isotherm at zero coverage.

$$K = \lim_{P \to 0} \frac{dq}{dP} = q_{\infty} b \tag{3}$$

Where K is the dimensional Henry's Law constant (mol/kg atm). The following figure illustrates the fit of the Langmuir to the NaLSX isotherm on CH_4 and CO_2 at 150 °C.

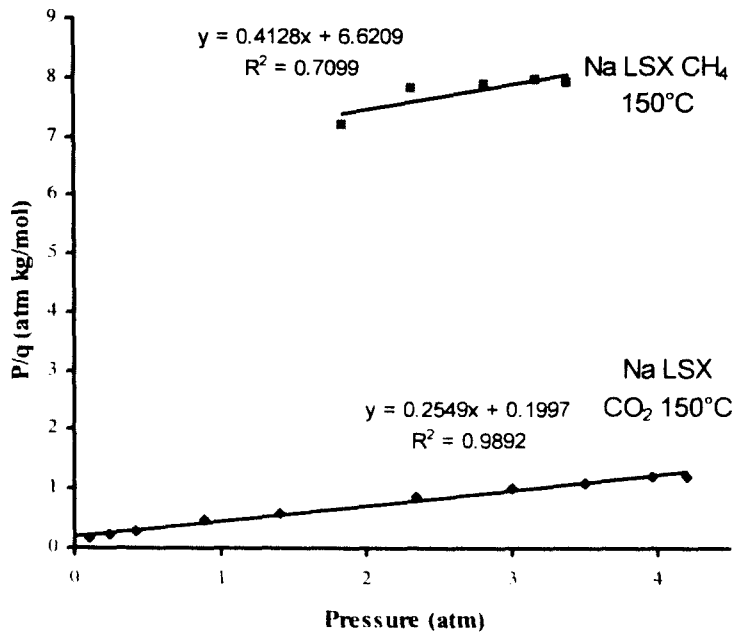

Figure A.3 - Langmuir fit NaLSX 150°C

The dimensionless Henry's Law constant (K_P) is determined from the isotherm temperature (T), and the adsorbent particle density, ρ_{ads} (excluding macropore and micropore volume).

$$K = K_P RT\rho_{ads} \tag{4}$$

The adsorbent particle density was measured with non-adsorbing He gas at room temperature in the CVS system. This density excluded the void space in the particle assuming that the adsorbate gas has access to the same pores in the zeolite structure as He.

A.3 CVS Isotherm Uncertainty

The constant volume method has a degree of uncertainty associated with its measurements. For example, sources of error include: pressure measurement, volume estimation, temperature variation, weight measurement, and gas purity. These measurement errors in the amount adsorbed have been quantified by error propagation for CO_2 and CH_4 isotherms. The uncertainty based on instrument precision is 0.4 to 1% error in amount adsorbed for the experimental range in this study. This is well below acceptable levels but the error accumulates due to the cumulative method of CVS isotherm construction. To minimize the cumulative errors as few isotherm data points as possible (8 to 10) were taken (Keller and Staudt, 2005).

The uncertainty in the CVS Langmuir isotherm model was determined by repeating the following experiments: NaLSX-CO_2 70 °C (3 isotherms) and NaLSX-CH_4 40 °C (2 isotherms). The isotherms were fit to the Langmuir isotherm model (1) and the 95% Joint Confidence Region of the parameters q_s and b were evaluated. Figure A.4 shows the extreme upper and lower confidence regions for the CO_2 and CH_4 Langmuir isotherm model.

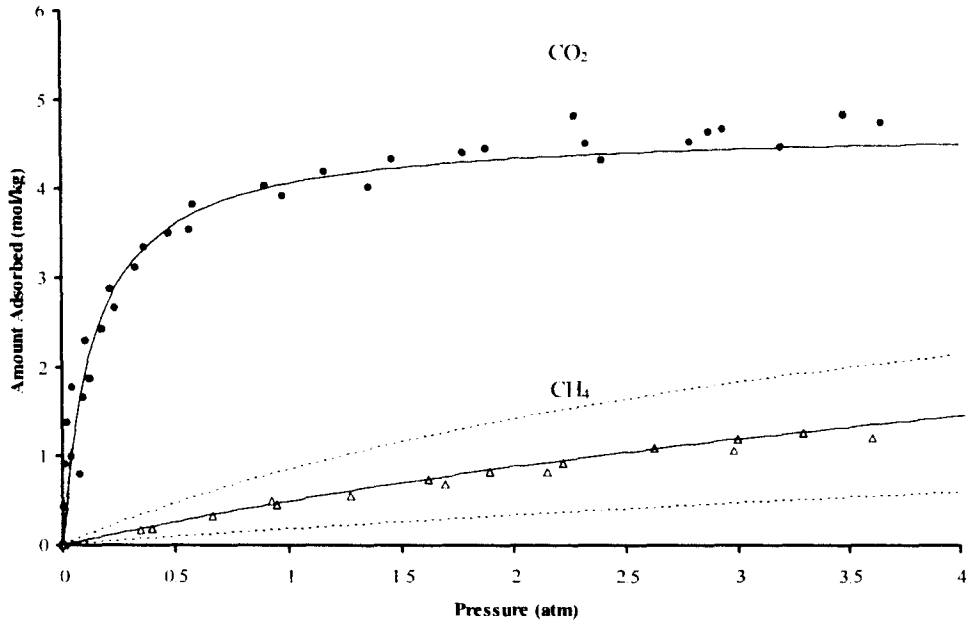

Figure A.4 – NaLSX isotherm Uncertainty (95% CI for two repeats of CH_4 isotherm at 40°C with different CVS CO_2 95% CI for 3 isotherms 70 ° C with different CVS for one isotherm).

The shape of the CO_2 isotherm results in a confidence interval that does not capture variability at pressures below 0.1 atm and then remains relatively constant at ± 8% capacity. CH_4 adsorption capacity has uncertainty in the range ± 20% that increases with partial pressure. Similar studies with acetonitrile adsorption on FAS adsorbent have found uncertainties between gravimetric and volumetric isotherms as large as 13.4 % (Kuznetsov, Movera, and Rakhmanova, 1999). The CH_4 isotherm has greater uncertainty than CO_2 that increases with pressure. This behaviour is due to the lower number of data points (increases confidence interval) and the greater number of parameter combinations that can describe the linear isotherm shape.

There is random error around the Langmuir model for both CO_2 and CH_4 due to measurement errors although the data appear to follow the trend. The confidence interval of the Langmuir model is greater than the error introduced with measurement uncertainty. Therefore the uncertainty in the CVS is relatively small and isotherm replication is accurate within reason.

A.4 Joint Confidence Region

The Langmuir Isotherm model is a nonlinear model.

$$\frac{q}{q_{\infty}} = \frac{bP}{1+bP} \tag{5}$$

Therefore, the estimation of the parameter uncertainty is determined from the joint confidence interval. The maximum likely hood estimate is determined by minimizing the sum of squared residuals (SSR) that is:

$$SSR = \sum \left(q_{data} - q_{langmuir}(q_{\infty}, b)\right)^2 \tag{6}$$

Assuming that the errors are normally distributed the joint confidence contours are found by trial and error with the following equation:

$$SSR^* \leq SSR\left[1 + \frac{p}{n-p} f_{p,n-p,\alpha}\right] \tag{7}$$

Where SSR is the value obtained from the maximum likely hood estimate in (6) above.

SSR^* is the sum square residual determined by manipulating the parameters to resolve (7) above.

p is the number of parameters in the model (2 for Langmuir)

n is the number of data (isotherm data points)

$f_{p,n-p,\alpha}$ is the f-statistic associated with the number of parameters and degrees of freedom.

For the NaLSX CO_2 70°C Isotherms, there are 36 data points (n). The joint confidence region (JCR) and maximum likelihood estimate are shown in the figure below.

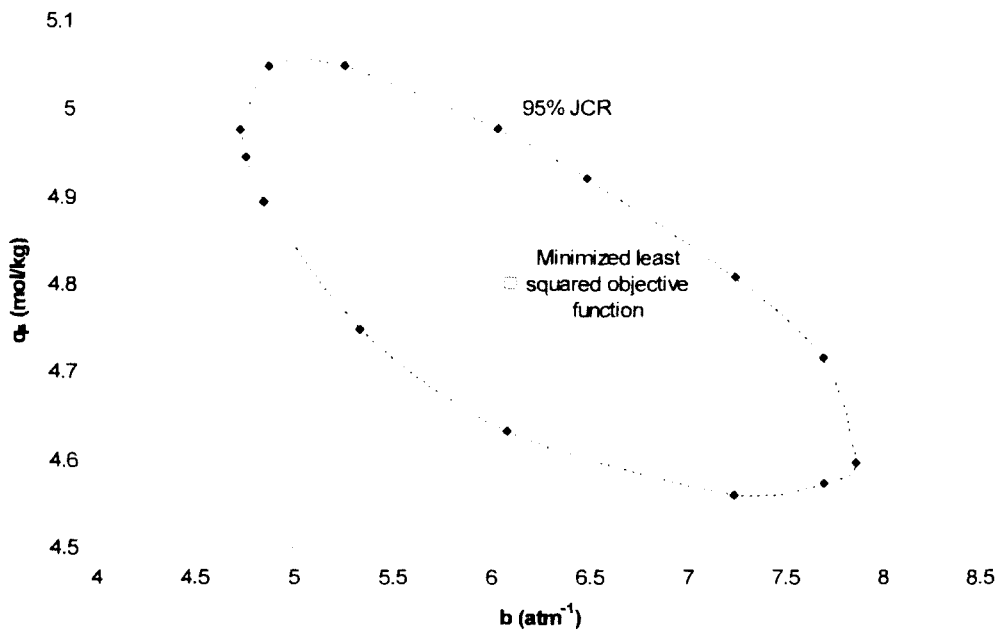

Figure A.5 - CO_2 NaLSX 70 °C Isotherm Joint Confidence region for Langmuir Isotherm model.

The following table summarizes the Langmuir isotherm parameter estimated and the 95% confidence interval ($\alpha = 0.025$).

Table A.5 - Langmuir CO_2 isotherm parameter confidence interval.

	MAX	Minimum SSR	MIN
q_s (mol/kg)	5.048	4.800	4.560
b (atm^{-1})	7.865	6.109	4.753
SSR	3.198	2.681	3.198

For the NaLSX CH_4 40°C Isotherms, there are 18 data points (n). The joint confidence region (JCR) and maximum likelihood estimate are shown in the figure below.

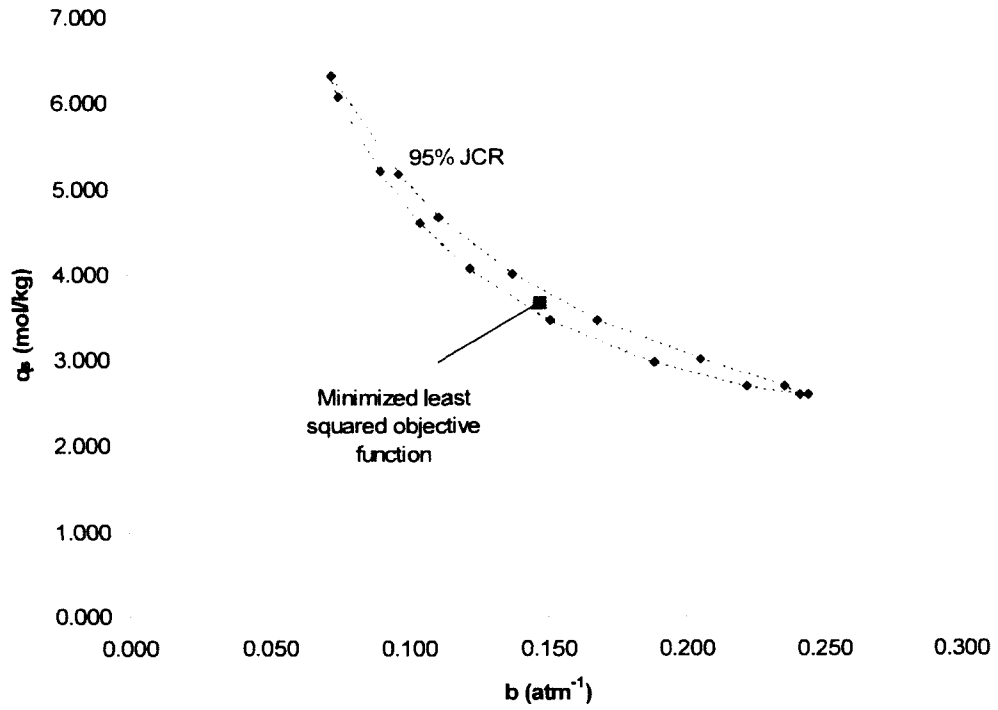

Figure A.6 - CH_4 NaLSX 40 °C Isotherm Joint Confidence region for Langmuir Isotherm model.

The following table summarizes the Langmuir isotherm parameter estimated and the 95% confidence interval ($\alpha = 0.025$).

Table A.6 - Langmuir CH_4 isotherm parameter confidence interval.

	MAX	Minimum SSR	MIN
q_s (mol/kg)	6.312	3.658	2.599
b (atm^{-1})	0.245	0.148	0.073
SSR	0.050	0.034	0.050

The JCR for the CH_4 isotherm is larger than that of CO_2 because it is linear in shape (more parameter combinations that can describe this behaviour) and it has less data points.

A.5 TD Toth Isotherm Fits

The following isotherms for CO_2 and CH_4 data were measured in the same laboratory by other researchers. The isotherms on NaX at 40, 70, and 100 °C were measured by Mulgundmath and Tezel, (2009). The isotherms on silicalite at 40, 70, and 100 °C were measured by Li and Tezel, (2008). The CH_4 isotherms on NaY of Talu, Zhang, and Hayhirst, (1993) were not measured in the same UO laboratory. All of these isotherms were included in the analysis to complete a thorough adsorbent screening. They were fit to the TD Toth isotherm model with the intention of determining their AWC for the bulk separation of LFG in a VPSA cycle.

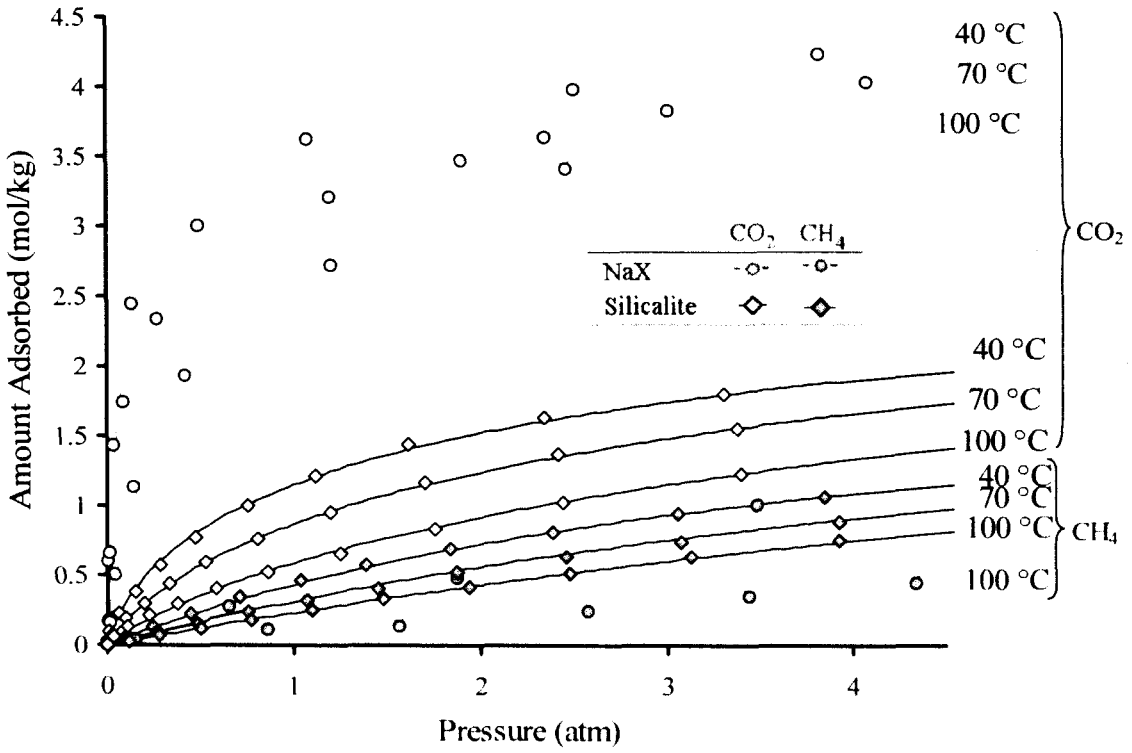

Figure A.7 – CO_2 & CH_4 NaX (Munglumath and Tezel, 2008) and silicalite (Li and Tezel, 2007) isotherms fit with TD Toth isotherm equation.

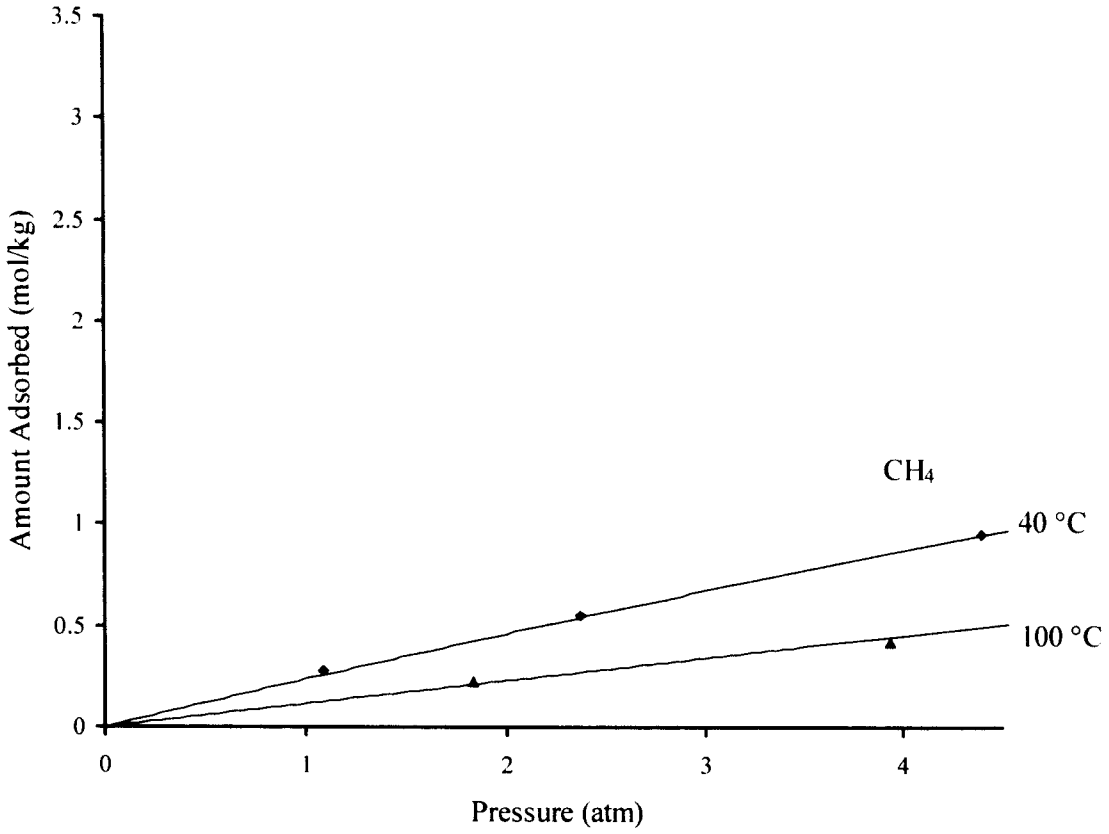

Figure A.8 - CH_4 isotherms on NaY of Talu, Zhang, and Hayhirst, (1993) fit to the TD Toth Isotherm model

A.6 CPC Raw Data

The Concentration Pulse Chromatographic (CPC) technique was use to measure the Henry's Law constant for CO_2 and CH_4 on NaLSX at various temperatures and 1 atm. The first moment (μ) of a pulse passed through the adsorbent column was measured several times at each temperature.

$$\mu = \frac{\int_0^\infty c(t-\mu_1)dt}{\int_0^\infty c dt} \tag{8}$$

$$\mu = \frac{L}{v}\left[1+\left(\frac{1-\varepsilon}{\varepsilon}\right)K\right] \tag{9}$$

The raw data for every injection is not presented here because it would be too lengthy. Instead the average Henry's Law constant is presented with the 95% confidence interval (based on the students-t distribution).

Table A.7 - Chromotographic method for NaLSX

Adsorbent	Adsorbate	Temperature (°C)	Dimensional Henry Constant (mol/kg atm)	95% Confidence Interval (mol/kg atm)	Reference
NaLSX	CO2	200	1.81	0.68	UO laboratory
NaLSX	CO2	150	4.13	0.14	UO laboratory
NaLSX	CO2	100	15.02	0.42	UO laboratory
NaLSX	CO2	70	50.5	-	Langmuir Fit
NaLSX	CO2	40	94.8	-	Langmuir Fit
NaLSX	CH4	150	0.038	0.017	UO laboratory
NaLSX	CH4	100	0.072	0.004	UO laboratory
NaLSX	CH4	70	0.115	0.009	UO laboratory
NaLSX	CH4	40	0.233	0.016	UO laboratory

The 95% Confidence interval is determined for a series of values as follows:

$$95\%CI = \overline{X} + t_{0.025,df}\frac{s}{\sqrt{n}} \tag{10}$$

Where CI is the 95% Confidence interval
X is the average value
$t_{0.025,df}$ is the students-t distribution for two sided test
df is the number of degrees of freedom

n is the number of values in the series

The limiting Heat of Adsorption (ΔH_0) was also determined from these values from a line of best fit.

$$\frac{d \ln K_P}{dT} = \frac{\Delta H_0}{RT^2} \tag{11}$$

The Limiting Heat of adsorption is provided below with the 95% confidence interval for the measurements.

Table A.8 - Limiting Heat of Adsorption

	Adsorbate -ΔH (kJ/mol)	
Adsorbent	CO2	CH4
NaLSX	**27.9**	**18.37**
+/- 95% CI	**5.21**	**0.03**

All of the above results are discussed in Chapter II of this thesis. The confidence interval is determined from a line of best fit on the van't Hoff plot.

A.7 Isosteric Heat of Adsorption (ΔH)

The isosteric heat of adsorption (ΔH) is the change in heat of adsorption due to interactions of the surface and adsorbed molecules. It is a function of the amount adsorbed (q) and can be evaluated from the differences in isotherm equilibrium pressure (Ruthven, 1984).

$$\ln p = const - \frac{\Delta H}{RT} \tag{12}$$

A plot of ln p vs $1/T$ with lines of constant coverage from the isotherm equilibrium data can be regressed and the slope provides an estimate of the isosteric heat of adsorption. Similarly to the limiting Heat of adsorption, the uncertainty of the isosteric heat of adsorption is determined from the slope of a best fit line of constant coverage for the CVS isotherm data.

The isosteric Heat of adsorption is determined by using equation (7) using the CO_2 and CH_4 isotherms. The data is presented in Figure A.9 for CO_2 is from coverage greater than 1 mol/kg.

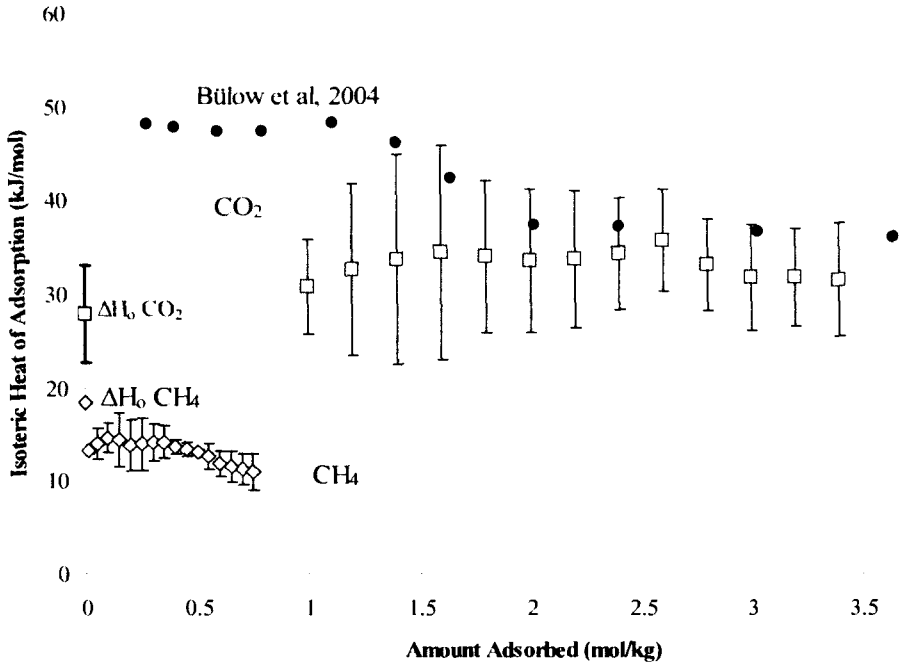

Figure A.9 – NaLSX CO_2 (squares) and CH_4 (diamonds) isosteric heat of adsorption with limiting heat of adsorption from Table II - 8. CPC data (empty symbols) compared with Bülow et al, 2004 (solid circles) for CO_2.

The isosteric heat of adsorption for CO_2 on NaLSX remains relatively constant around 30 kJ/mol for amounts adsorbed above 1 mol/kg. The relatively constant value indicates a homogeneous adsorption sites at higher coverage. These values show agreement with the limiting heat of adsorption as calculated with the CPC (27.9 kJ/mol). The trend of isosteric heat of adsorption does not decrease as observed on NaLSX by Bülow et al (2004) and NaY by Ghoufi et al (2009). There is some agreement with the data of Bülow et al (2004) for the region of higher coverage (1.5-3.5 mol/kg). The lower region of coverage could not be measured with the CVS to a great degree of accuracy at low pressures. It is likely that NaLSX exhibits heterogeneous surface interactions with CO_2 at these regions as shown by the decreasing trend observed by Bülow et al (2004).

The isosteric heat of adsorption for CH_4 decreases as the amount adsorbed increases suggesting some heterogeneity in the adsorption sites. It was possible to determine the heat of adsorption at low coverage because the relatively constant slope of the CH_4 equilibrium isotherm. The limiting heat of adsorption measured with the CPC is 5 kJ/mol higher than the isosteric method. This is expected for CH_4 because the CPC is more sensitive than the CVS isotherm isostere calculations as shown by the confidence intervals. No data was available for comparison of CH_4-NaLSX results.

A.8 Isobar Plots for NaX, NaY, CaX, Silicalite

The following Isobar plots are provided to support the adiabatic working capacity analysis presented in Chapter II.

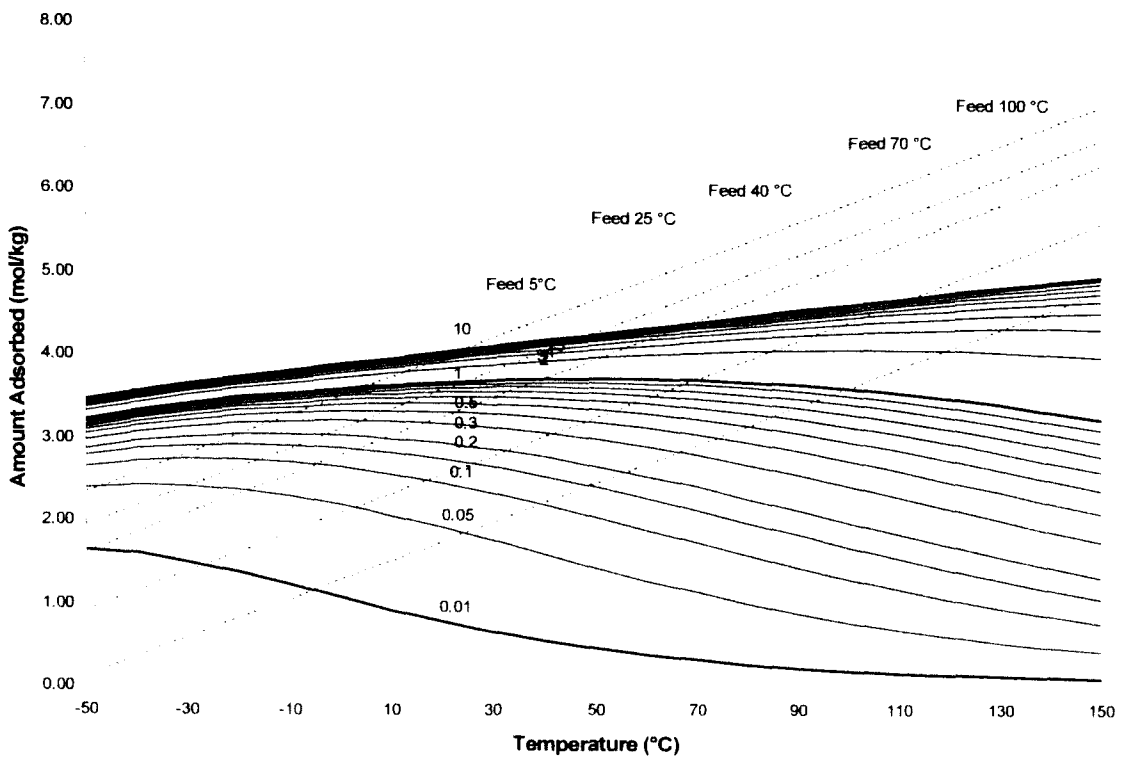

Figure A.10 - Isobar plot of CO_2 adsorption equilibrium on NaX with operating lines for various LFG feed temperatures.

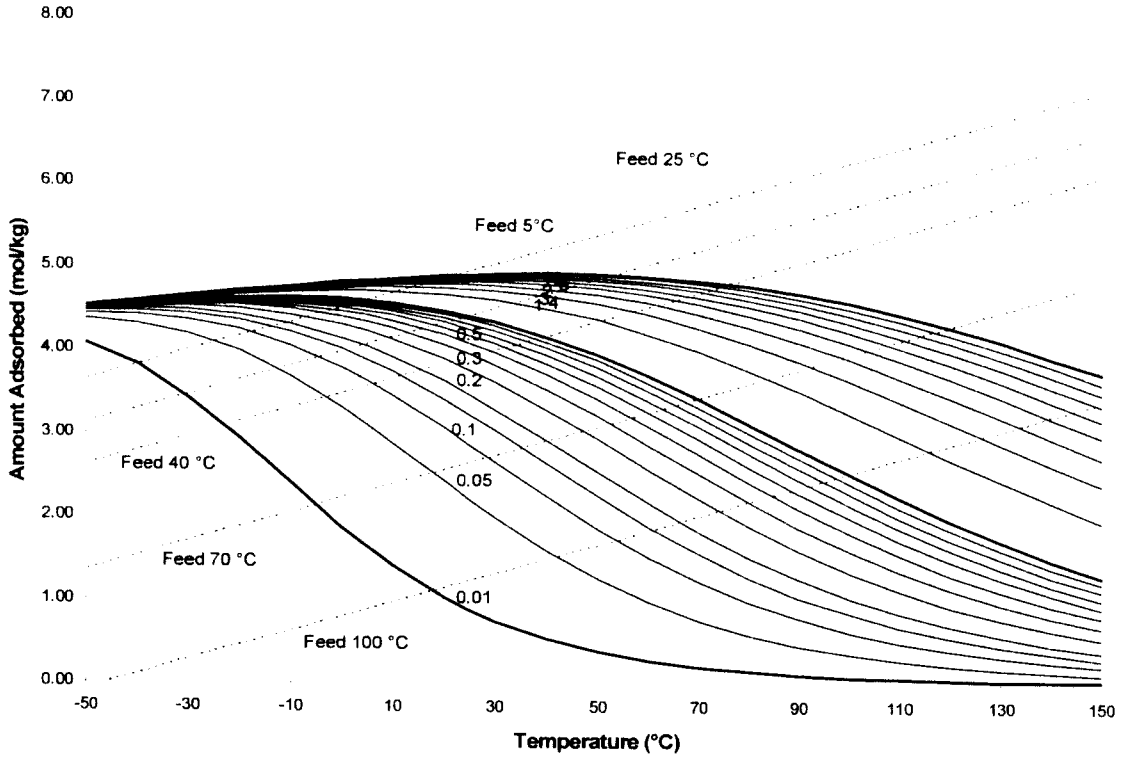

Figure A.11 - Isobar plot of CO_2 adsorption equilibrium on CaX with operating lines for various LFG feed temperatures.

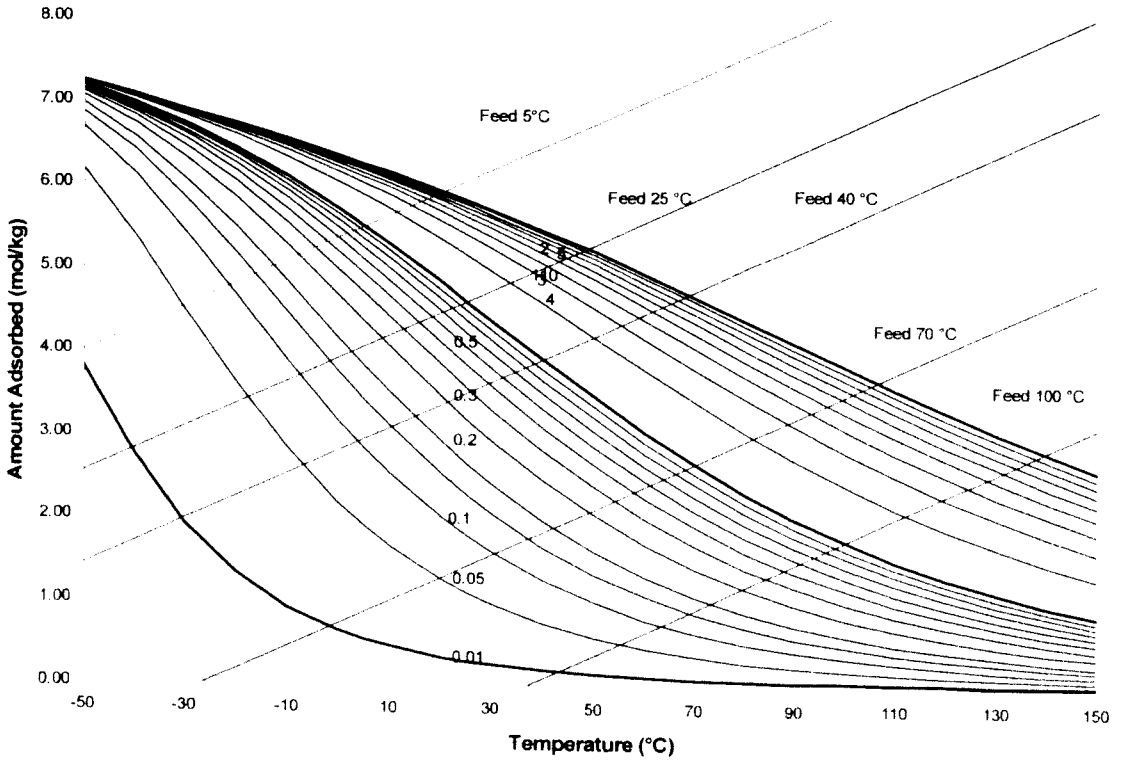

Figure A.12 - Isobar plot of CO_2 adsorption equilibrium on NaY with operating lines for various LFG feed temperatures.

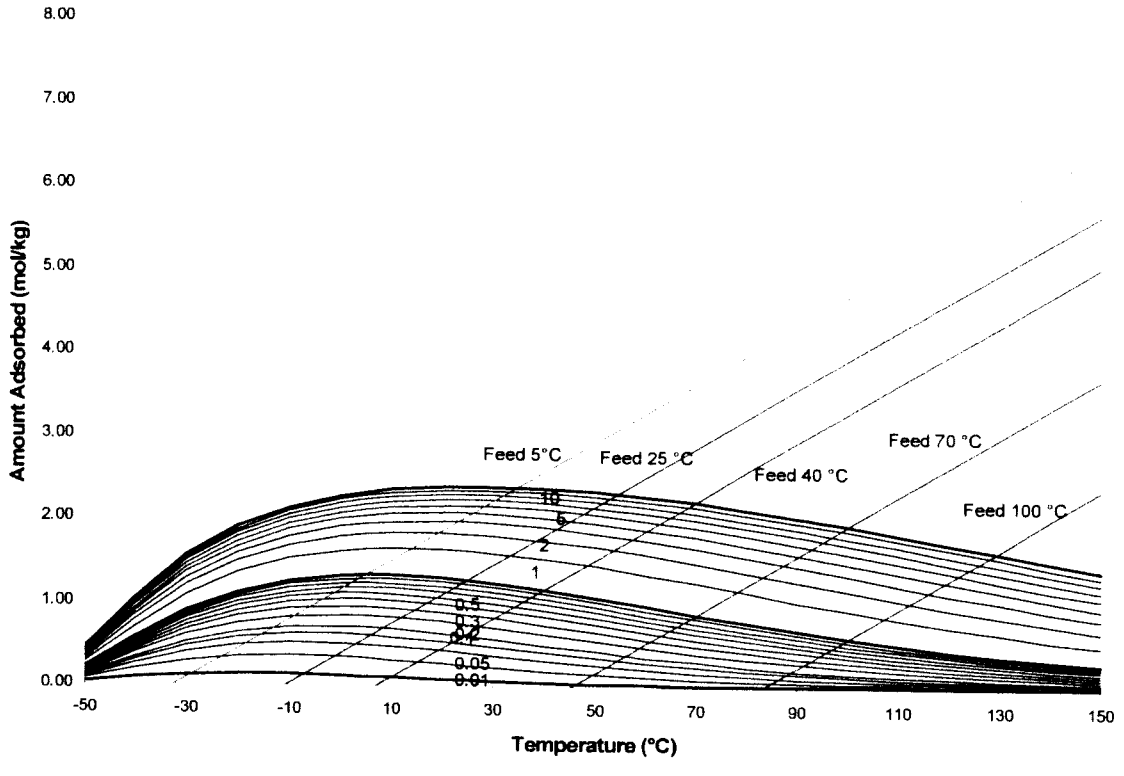

Figure A.13 - Isobar plot of CO_2 adsorption equilibrium on Silicalite with operating lines for various LFG feed temperatures.

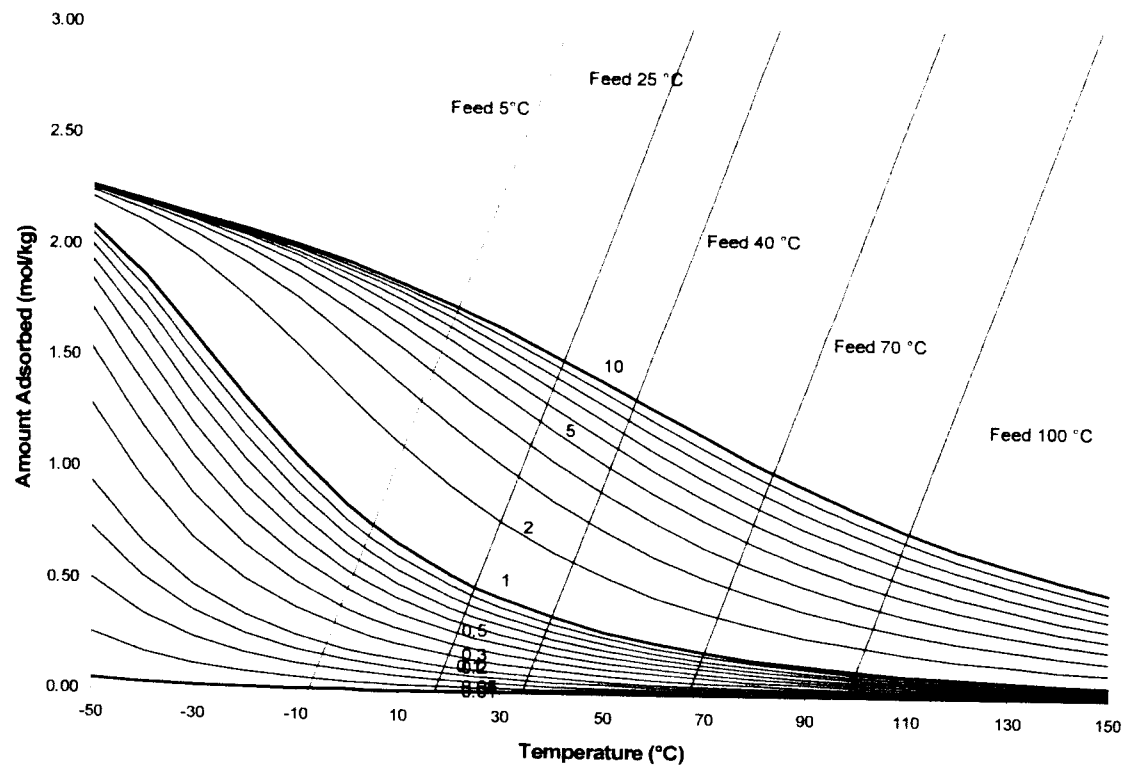

Figure A.14 - Isobar plot of CH_4 adsorption equilibrium on NaX with operating lines for various LFG feed temperatures.

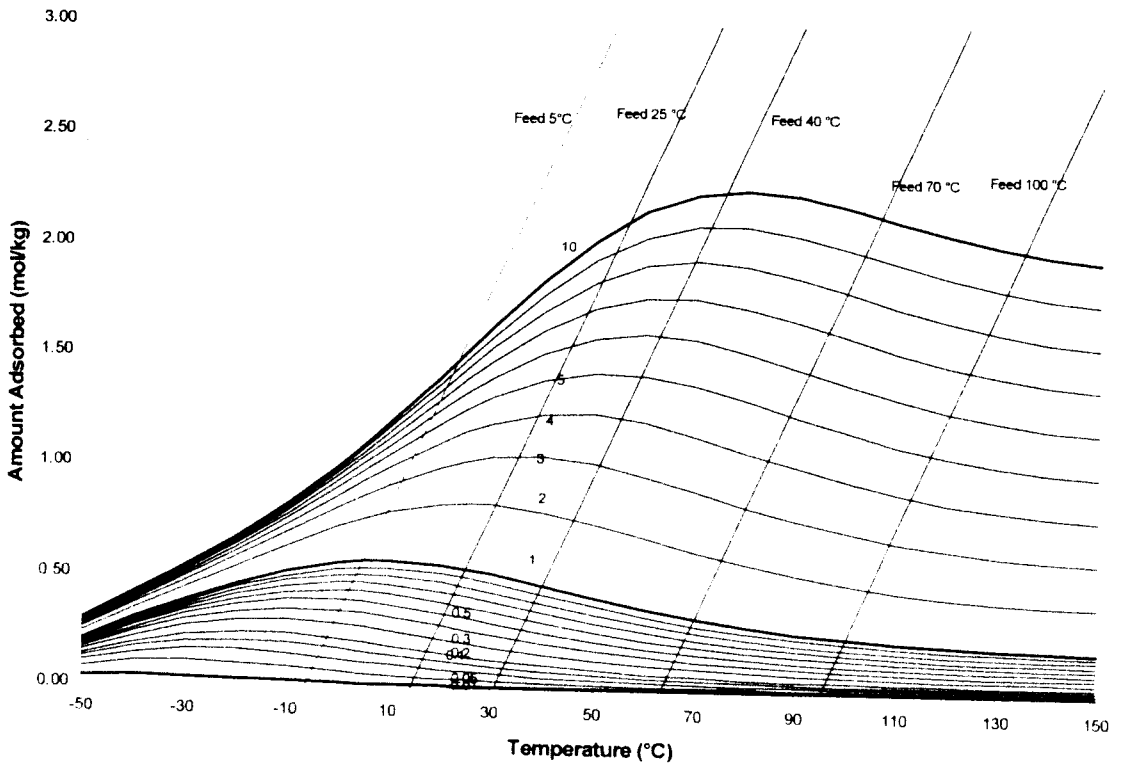

Figure A.15 - Isobar plot of CH_4 adsorption equilibrium on NaLSX with operating lines for various LFG feed temperatures.

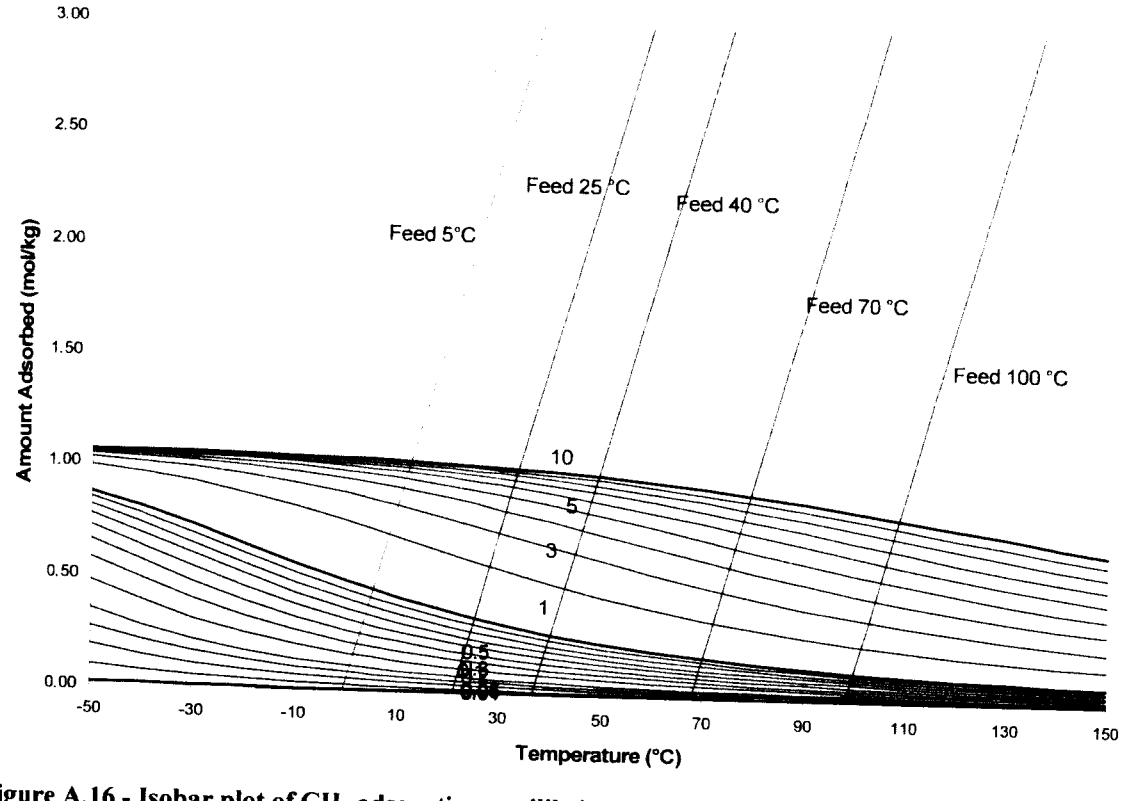

Figure A.16 - Isobar plot of CH_4 adsorption equilibrium on Silicalite with operating lines for various LFG feed temperatures.

Appendix B - Supplementary Information for Chapter III:

Upgrading Landfill Gas by Adsorption:

Economic Analysis and

Binary Adsorption Behaviour of

Carbon Dioxide and Methane on NaLSX

B.1 Thermodynamic Consistency Test (TCT)

The quality of the binary equilibrium isotherm is verified with the thermodynamic consistency test (TCT). The Thermodynamic Consistency Test described by Rao and Sircar (1999) is used to evaluate the reliability between pure component data and binary systems at fixed temperatures and pressures. The basis of the comparison is the non-isothermal Gibbsian surface excess model (Sircar, 1985). Chromatographic measurements of CO_2/CH_4 on silicalite by Li and Tezel (2007) exhibit thermodynamic consistency.

Method

The CO_2/CH_4 – NaLSX system presented is compared to the pure component equilibrium with the thermodynamic consistency integral and differential test.

The goal of the consistency test is to validate multicomponent equilibrium data for extrapolation.

The Integral TCT compares the pure and binary equilibrium surface potentials with the following equation (Rao and Sircar, 1999):

$$\frac{\varphi_2^*(P)-\varphi_1^*(P)}{RT}=\int_0^1\frac{\left(n_1^m y_2-n_2^m y_1\right)}{y_1 y_2}dy_1 \tag{13}$$

Where $y_1 + y_2 = 1$ are the mole fractions

T is the system temperature (constant and measured in K)

P is the system Pressure (constant and measured in atm)

n_i^m is the amount adsorbed of species i in the binary isotherm (mol/kg constant P and T)

Φ_i^* is the surface excess and is determined from the pure isotherm data as follows:

$$\frac{\phi_i^*(P)}{RT}=-\int_0^P\frac{n_i^{m*}}{P}dP \tag{14}$$

Where n_i^{m*} is the amount of adsorbed of species i for the pure isotherm (mol/kg constant T). For calculation simplicity, the integral of the isotherm is estimated from the Langmuir Isotherm Equation.

$$\theta = \frac{n_i^{m*}}{n_{si}} = \frac{B_i P}{1 + B_i P} \tag{15}$$

Where n_{si} is the saturation capacity and B_i is the equilibrium constant for species i at a constant temperature. The integral of the Langmuir equation is given by:

$$-\int_0^{P} \frac{n_1^{m*}}{P} dP = -n_{si} \ln(1 + B_i P) \tag{16}$$

The integral on the right hand side of equation (4) is evaluated from the binary equilibrium data. The binary data are presented as a function of the mole fraction because they were measured with the HT-CPM.

The Differential TCT compares the pure and binary surface potentials with differentials and is considered more rigorous than the TCT integral test (Rao and Sircar, 1999). The differential surface potential is evaluated individually for methane and carbon dioxide with the following equations.

$$n_2^{m*}(P,T) = n^m(P,T,y_1) - P\frac{\delta}{\delta P}\left\{\int_0^{y_1}\left[\frac{\left(n_1^m y_2 - n_2^m y_1\right)}{y_1 y_2}\right]_{P,T} dy_1\right\}_{T,y_1} \tag{17}$$

$$n_1^{m*}(P,T) = n^m(P,T,y_1) + P\frac{\delta}{\delta P}\left\{\int_{y_1}^{1}\left[\frac{\left(n_1^m y_2 - n_2^m y_1\right)}{y_1 y_2}\right]_{P,T} dy_1\right\}_{T,y_1} \tag{18}$$

Where

$$n^m = \sum_i n_i^m \tag{19}$$

The LHS of equation (5) and (6) is taken from the pure component isotherms. The RHS of both equations is the difference between the total amount adsorbed (at a fixed pressure, temperature and composition) and the pressure multiplied by the differential in area with respect to pressure (at the same conditions). Equation (5) differs from (6) only in that the integral direction is reversed.

Integral Results

The integral TCT requires the pure isotherms be compared with that under the binary isotherms. A plot of n/P was utilized to determine the area under the pure isotherm n/P

curve (according to equation (4)). Figure B.1 illustrates the area under the n/P curve and the Langmuir model that is used to calculate the area between experimental data.

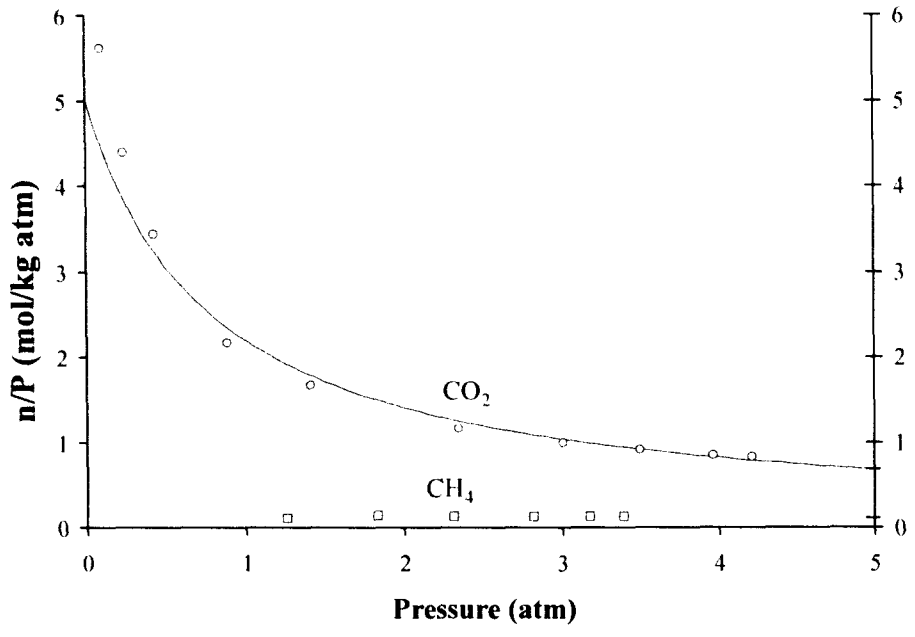

Figure B.1 - Area under the curve CO_2 and CH_4 on NaLSX at 150 °C

The integral test results are presented in the Table B.1 with the LHS and the RHS of equation (4) presented as well as the difference between the two:

Table B.1 - Integral Thermodynamic Consistency of CO_2/CH_4 on NaLSX at 150 °C and total pressure of 1 and 3.3 atm.

Pressure (atm)	area CO_2 (mol/kg)	area CH_4 (mol/kg)	LHS (pure) (mol/kg)	RHS (binary) (mol/kg)	% Difference (mol/kg)
1	-3.23	-0.15	3.08	0.74	76%
3.27	-6.45	-0.45	6.00	1.36	77%

There is a large discrepancy between the binary isotherm integral TCT for CO_2/CH_4 on NaLSX at 150 °C. The difference arises from the pure isotherm potentials (LHS) which are relatively large in comparison to the binary isotherm integral (RHS). There is a significant difference because the CO_2 affinity for adsorption is much greater than that of CH_4. When one species is adsorbed more appreciably then the other the LHS of equation (4) becomes much larger than the RHS. The pure isotherm data are much greater than that of the binary equilibrium and the discrepancy increases with increasing pressure. It is suggested by Rao and Sircar (1999) that inconsistencies of up to 10% are

acceptable in the integral test. The large discrepancy exhibited in this study may likely be caused by the non-ideality of the CO_2/CH_4 system where CO_2 is adsorbed much more preferentially over CH_4.

Differential Results

The CO_2/CH_4 equilibrium data at 150 °C is presented for a total pressure of 1 atm and 3.27 atm (± 0.11). These two pressures allow for the differential thermodynamic consistency test to be evaluated for the NaLSX system at a constant temperature and at regular mole fraction intervals. The differential test results are presented for methane and carbon dioxide in Table B.2 andB.3, respectively.

Table B.2 - Differential Thermodynamic Consistency Test for CH_4 on NaLSX at 150 °C, 1 and 3.3 atm.

Pressure (atm)	Mole Fraction (Y_{CO2})	Total amount adsorbed n_m (mol/kg)	Area under Integral (mol/kg)	Change in Area with Pressure (mol/kg atm)	LHS (mol/kg)	RHS (mol/kg)	% Difference
1.0	0.2	0.19	0.02	0.03	0.14	0.17	15%
1.0	0.4	0.42	0.08	0.07	0.14	0.35	59%
1.0	0.6	0.81	0.20	0.13	0.14	0.68	79%
1.0	0.8	1.37	0.41	0.19	0.14	1.18	88%
3.3	0.2	0.69	0.08	0.03	0.41	0.60	32%
3.3	0.4	1.04	0.24	0.07	0.41	0.80	49%
3.3	0.6	1.56	0.49	0.13	0.41	1.14	64%
3.3	0.8	2.28	0.85	0.19	0.41	1.64	75%

Table B.3 - Differential Thermodynamic Consistency Test for CO_2 on NaLSX at 150 °C, 1 and 3.3 atm.

Pressure (atm)	Mole Fraction (Y_{CO2})	Total amount adsorbed n_m (mol/kg)	Area under Integral (mol/kg)	Change in Area with Pressure (mol/kg atm)	LHS (mol/kg)	RHS (mol/kg)	% Difference
1.0	0.2	0.19	0.72	0.24	2.20	0.44	80%
1.0	0.4	0.42	0.66	0.20	2.20	0.62	72%
1.0	0.6	0.81	0.55	0.14	2.20	0.95	57%
1.0	0.8	1.37	0.34	0.08	2.20	1.45	34%
3.3	0.2	0.69	1.27	0.24	3.16	1.49	53%
3.3	0.4	1.04	1.11	0.20	3.16	1.69	47%
3.3	0.6	1.56	0.87	0.14	3.16	2.03	36%
3.3	0.8	2.28	0.51	0.08	3.16	2.53	20%

The Differential TCT highlights significant discrepancies in the binary and pure equilibrium surface potentials of methane and carbon dioxide. Similarly to the Integral TCT the inconsistency is due to the selectivity of NaLSX for CO_2 in the binary mixture. The binary isotherm does not have comparable CO_2 uptake to the pure component CO_2 isotherms. The RHS only becomes comparable when the mole fraction is almost entirely CO_2 due to the linear binary isotherm shape. The methane binary isotherm capacity is magnitudes lower than the pure isotherm. Therefore consistency only occurs at high methane and carbon dioxide fractions. The linear isotherm of NaLSX for CO_2/CH_4 results in thermodynamic consistency for mixtures of mainly CO_2 and mainly CH_4.

CO_2/CH_4 equilibria on NaLSX at 150 °C, 1 and 3.3 atm do not exhibit thermodynamic consistency. The methane isotherm capacity is minor compared to CO_2 and therefore its contribution to the TCT (for pure components) is significantly less. This imbalance results in the large discrepancy between the pure and binary surface excess comparison. It is shown that the binary Langmuir system is thermodynamically consistent when the saturation adsorption capacities of all components in the mixture are equivalent (Rao and Sircar, 1999). If the Extended Langmuir isotherm model is used for this binary equilibrium, it also fails the Integral TCT (differences above 75%). The binary systems studied here have large differences in saturation capacity which suggests difficulty in determining thermodynamic consistency for non-ideal mixtures.

B.2 Propagation of Measurement Errors in the CPC measurements

The propagation of measurement errors is determined for the Henry's Law constant (K_P) in. The uncertainty of each measurement in the CPC technique contributes to the effective slope calculation. For example, the length of the column (10.5 ± 0.05), the estimation of the void fraction (0.421 ± 0.005), the flow rate of the carrier gas (15.00 ± 0.07 cm^3/min), the change in temperature (150.0 ± 0.1°C), and the density of the adsorbent particles (2.23 ± 0.05 g/cm^3).

$$K = \frac{\varepsilon}{1-\varepsilon}\left(\frac{\mu\nu}{L} - 1\right)$$

$$\Delta K = \left[\frac{K}{\varepsilon(1-\varepsilon)}\right]\Delta\varepsilon + \left[\left(\frac{\varepsilon}{1-\varepsilon}\right)\frac{\nu}{L}\right]\Delta\mu + \left[\left(\frac{\varepsilon}{1-\varepsilon}\right)\frac{\mu}{L}\right]\Delta\nu + \left[\left(\frac{\varepsilon}{1-\varepsilon}\right)\frac{\mu\nu}{L^2}\right]\Delta L \qquad \text{(20 A and B)}$$

The sum of all these errors, propagated to the effective slope (K_p) is less than 4%. The most significant contributors were the void fraction and adsorbent density estimation. The largest contributor to uncertainty in the Henry's Law constant was the first moment variability.

The pressure drop over the column was negligible for the column flowrate, thermal conditions, and adsorbent particle size used in these experiments. The Ergun equation was utilized to estimate the pressure drop across the column at the conditions of 30 cm^3/min, 150 °C for a CH_4 and CO_2 mixture. The maximum value of 0.001 to 0.0005 atm was calculated and no change in pressure was observed when the sample was injected into the system. Pressure drop contributions were negligible and are not considered in the variability of the first moment.

The variability associated with the first moment calculation resulted in 6 to 1% of the uncertainty in the effective slope. This is greater than the measurement uncertainty (less than 4%). The total uncertainty of K_p varied with composition and remained below 10% such that the significant difference in effective slope measurements was observable between compositions.

B.3 "Fitting" Binary Isotherm

The data measured with the CPC technique is presented below for the CO_2/CH_4 on NaLSX at 150 °C, 1.0 and 3.3 atm total pressure.

Table B.4 - Effective Slope CPC measurements for NaLSX at 150 °C, 3.3 atm

Adsorbate	Date	YCO2	Tc (°C)	column flow (cc/min)	bubble flow (cc/min)	Ptotal (atm)	first moment (s)	K	K' (mol/kg atm)
CH4	18-Jun	0.05	150	14.77	33.0	3.17	278.3	99.4	1.37
CH4	26-Jun	0.07	150	19.86	44.0	3.15	103.0	49.1	0.69
CH4	8-Jul	0.11	150	12.74	30.3	3.40	140.3	42.8	0.56
CH4	5-Jun	0.15	150	14.80	31.1	3.01	135.0	47.9	0.59
CH4	10-Jul	0.25	150	13.51	30.0	3.19	79.6	25.5	0.35
CH4	2-Jul	0.36	150	12.82	30.9	3.40	52.5	15.7	0.20
CH4	11-Jun	0.50	150	14.50	34.5	3.38	43.3	14.6	0.19
CH4	13-Jun	0.70	150	13.75	33.8	3.48	26.2	8.0	0.10
CH4	4-Jul	0.87	150	11.40	26.4	3.33	23.0	5.7	0.07
CH4	22-May	1.00	150	13.76	31.5	3.21	21.1	6.3	0.08
Adsorbate	Date	YCO2	Tc (°C)	column flow (cc/min)	bubble flow (cc/min)	Ptotal (atm)	first moment (s)	K	K' (mmol/g atm)
CO2	22-May	0.00	150	13.69	31.3	3.22	938.0	311.9	4.10
CO2	18-Jun	0.05	150	14.95	33.4	3.17	253.0	90.7	1.17
CO2	26-Jun	0.07	150	20.03	44.4	3.15	99.2	47.0	0.61
CO2	8-Jul	0.11	150	12.49	29.7	3.40	132.5	37.5	0.48
CO2	5-Jun	0.15	150	14.80	31.1	3.01	102.8	36.3	0.46
CO2	10-Jul	0.25	150	13.69	30.3	3.19	67.9	22.1	0.29
CO2	2-Jul	0.36	150	12.76	30.8	3.40	44.8	13.0	0.17
CO2	11-Jun	0.50	150	14.07	33.5	3.38	34.0	11.0	0.14
CO2	13-Jun	0.70	150	13.75	33.8	3.48	21.5	6.3	0.08
CO2	4-Jul	0.87	150	11.17	25.8	3.33	16.8	3.8	0.05

The injections are performed for CO_2 and CH_4 and the average is shown below. At the endpoints (Y = 1 and Y = 0), only one species is injected because the carrier gas is not a mixture. The average effective slope, its 95% confidence interval and the pressure is provided in the table below.

Table B.5 - Average Effective slope for NaLSX CO_2/CH_4 at 3.27 atm (+/- 0.11), 150 °C

Y_{CO2}	K' (mol/kg atm)	95% CI	P (atm)
0.00	**4.099**	**0.429**	**3.20**
0.05	1.273	0.153	3.17
0.07	0.646	0.067	3.15
0.11	0.522	0.056	3.40
0.15	0.524	0.103	3.01
0.25	0.317	0.045	3.19
0.36	0.186	0.025	3.40
0.50	0.163	0.028	3.38
0.70	0.093	0.028	3.48
0.87	0.061	0.017	3.33
1.00	**0.079**	**0.018**	**3.23**

The binary isotherm is determined from the data in the table above. The steps to the solution are provided below:

1. The effective slope is "fit" using MS Excel non-linear solver to the equation (4) in Chapter III.

$$K_{I'} = A_1 + A_2 y_1 + A_3 y_1^2 + A_4 \ln\left(\left|y_1 + \lambda\right|\right) \tag{21}$$

The solver is allowed to change the Ai parameters to minimize the SSR and the value for λ is fixed.

Table B.6 – Effect of changing lambda on SSR.

A1	A2	A3	A4	λ	SSR
-3.9655	8.052255	-4.11436	-1.73165	0.01	0.242615
-2.86314	5.748004	-2.88853	-1.30614	0.005	0.148674
-2.87443	5.76397	-2.88853	-1.30614	0.004827	0.147176
-1.92307	3.722955	-1.77384	-0.96737	0.002	0.10635
-1.50456	2.804384	-1.25815	-0.82254	0.0011	0.101431
-1.44782	2.679103	-1.18739	-0.80315	0.001	0.101486
-1.29019	2.33016	-0.98981	-0.74955	0.00075	0.102573
-0.5674	0.715387	-0.06718	-0.50802	0.0001	0.125518
-0.14817	-0.22993	0.477707	-0.37007	0.00001	0.152396
0.251083	-1.13445	1.001342	-0.23943	1E-07	0.187035
0.361296	-1.38478	1.146598	-0.20346	1E-08	0.19813
-0.57	0.722658	-0.07217	-0.5083	-0.0001	0.125122
-1.11691	1.954596	-0.78183	-0.68711	-0.0005	0.104277
-1.32214	2.416542	-1.04783	-0.75383	-0.00075	0.100868
-1.44514	2.69339	-1.20725	-0.79369	-0.00093	0.10005
-1.49099	2.7964	-1.26643	-0.80851	-0.00099	0.099987
-1.49435	2.804125	-1.27101	-0.8096	-0.001	0.099988
-1.50077	2.818584	-1.27935	-0.81168	-0.00101	0.099992
-1.52618	2.87577	-1.31228	-0.81989	-0.00105	0.100031
-1.55732	2.945852	-1.35264	-0.82994	-0.0011	0.100136
-1.78687	3.462477	-1.6502	-0.90383	-0.0015	0.102899
-3.2884	6.836575	-3.59238	-1.37746	-0.005	0.228426
-5.01671	10.64652	-5.74973	-1.90833	-0.01	0.798296
5.114092	-12.901	8.260296	0.865432	-0.1	2.891574

The following figure shows the results.

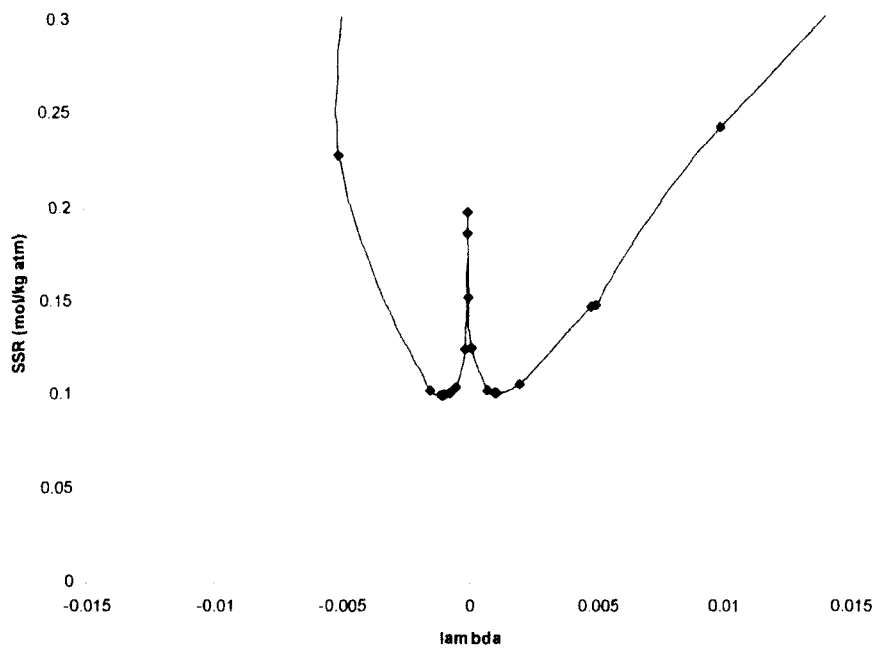

Figure B.2 - SSR vs λ using equation (4)

It is evident from the table and figure above that there is a local minimum for very small values of lambda and there is a reflection in the y axis. The reflection is due to the absolute value in the logarithmic term of equation (4). The λ value is then constrained to the minimum range of 0.0001 to 0.01 for future minimization techniques. This is done because the polynomial is highly dependant upon the value of lambda and if it is allowed to vary a solution is next to impossible to achieve.

2. The second step is to fit the experimental data to equation (8) in Chapter III with the range of λ fixed. The solution is reached when the SSR is minimized by changing the values for the parameters B_i and C_i and applying the constraints of equations (9) to (11) are satisfied.

Table B.7 - Constraints for NaLSX 3.3 atm 150 °C

Pure Isotherm Capacity		
Q(CO2)	3.164	mol/kg
Q(CH4)	0.397	mol/kg
Henry's Constant		
Kp(CO2)	4.099	mol/kg atm
Kp(CH4)	0.079	mol/kg atm

The application of the constraints and limiting the range of λ significantly reduces the number of solutions to the objective function. This method also reduces the time to find the solution for non-ideal mixtures such as CO_2/CH_4.

B.4 Economic Analysis

LANDGEM

LandGem is an EPA model that is commonly used to predict the amount of LFG produced from a municipal solid waste landfill. It is based on a first order decomposition rate equation with parameters that have been determined empirically from numerous landfills in the US. The model is based on the following equation (USEPA, 2005):

$$Q_t = WL_o k e^{-k(t-t_i)} \tag{22}$$

Where Q_t is the volume of biogas at time t (m^3/yr)

L_o is the potential production of methane capacity (m^3/tonnes of waste)

W are the waste receipts (tonnes)

k is the biogas generation decay parameter (yr^{-1})

t is the time since the beginning of landfilling (yr)

t_i is the period during which there is no biogas generation (yr)

The waste receipts (based on landfill shortfall accumulation) and parameters above are the only inputs used in the model to predict the landfill gas emissions. The active lifetime of the landfill is estimated at 25 years having a variable design capacity depending on the desired LFG flow rate. Default conventional landfill parameters were selected to model the LFG production. That is a biogas generation decay parameter of 0.05 (yr^{-1}), CH_4 production capacity of 170 m^3/tonne of waste and LFG with a 50% CH_4 content.

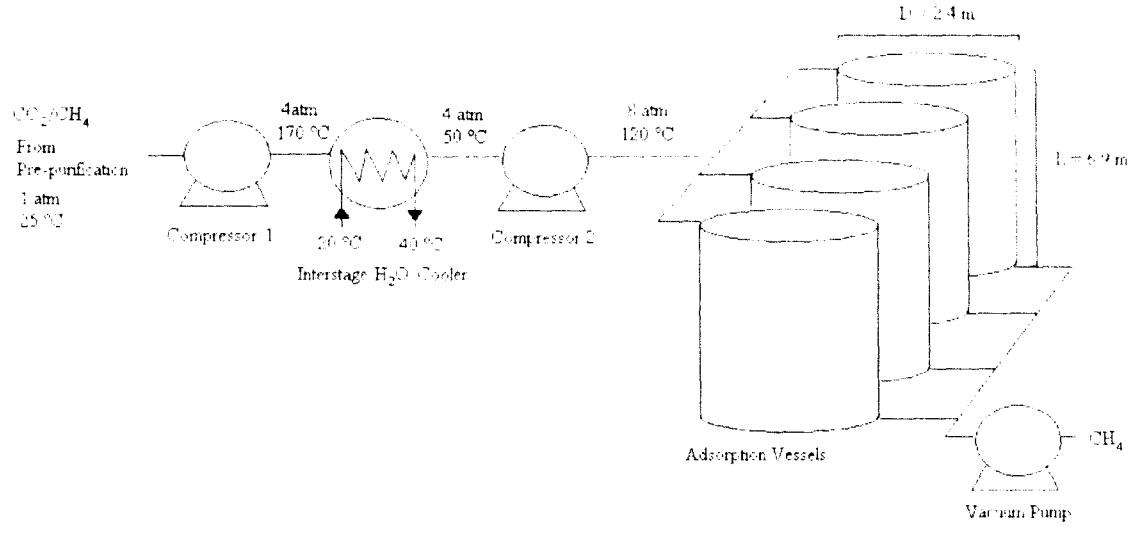

Figure B.3 - LFG VPSA bulk separation process

Capital costs

The schematic of the VPSA separation process is illustrated in Figure B.3. The capital costs for this system were determined based on the input flow rate and scaled according according to equipment heuristics. The inlet gas passes through two compression stages and one interstage cooler with water at 20 °C available for cooling. The adsorbent capacity was calculated from the adiabatic working capacity (2.5 mol CO_2/kg NaLSX) at an average feed temperature of 120 °C. The adsorbent price of NaLSX ($6.60 CAD/kg) was used to determine the total adsorber and adsorbent cost. The ratio of the total adsorption system cost (includes valves, piping, instrumentation, etc.) to the adsorbent cost (R_c) was related as a function of the volumetric flowrate into the column for carbon bed adsorbers (Cooper and Alley, 2002).

$$R_c = 6.98Q^{0.133} \tag{23}$$

Where the flowrate Q (ft^3/min) is corrected with conversion factor for the mass fraction CO_2 adsorbed/biogas feed to that of a typical carbon bed adsorber. The cost heuristic equation above is for carbon bed trace pentane removal from air. This type of system has a much lower loading with respect to throughput than a bulk separation. Therefore the flowrate was corrected by multiplying a ratio of the mass loading/feed volume throughput. This changed the size of the adsorber vessel required for a bulk separation to approximate a representative total cost to adsorber vessel and adsorbent

cost. A two stage compressor was selected to elevate the feed pressure from 1 to 8 atm in combination with a stainless steel (304) shell and tube water heat exchanger for interstage cooling. The vacuum pump was sized for adsorbent regeneration from 1 to 0.1 atm for an adsorption cycle time of 30 minutes.

The purchased equipment cost was then multiplied by three factors from Keller (2007) to account for the delivery costs (18%), direct installation costs (44%) and indirect installation costs (31%).

Operational Costs

The operational costs are based on 24 hr operation for 350 days/year for labour ($22.60 CAD/hr), supervision (15% of the labour) and maintenance (5% of the total installed cost). The utilities include electricity ($0.06/kWh) and cooling water ($0.02/1000 L). The power demand is determined from the compressor and vacuum pump horsepower with an adiabatic efficiency of 80% with the following equation for isentropic gas compression:

$$H_P = \left(\frac{n}{n-1}\right) z_1 \frac{R}{MW} T_1 \left[\left(\frac{P_2}{P_1}\right)^{(n-1)/n} - 1\right] \tag{24}$$

And the temperature change in the gas is determined for an adiabatic compression with the following equation:

$$T_2 = T_1 \left\{1 + \frac{1}{\varepsilon_a}\left[\left(\frac{P_2}{P_1}\right)^{(n-1)/n} - 1\right]\right\} \tag{25}$$

Finally, the power demand of the compressor is determined from the mass flow rate (M) of the gas and the electric motor efficiency:

$$Power\ \ demand = \frac{H_P W}{\varepsilon_a \varepsilon_m} \tag{26}$$

Where n is the equal to the specific heat of the gas (50/50 mixture of CO_2 and CH_4 1.307)

T_1 is the temperature of the gas before compression (K)

P_1 is the pressure of the gas before compression (atm)

P_2 is the temperature of the gas after compression (atm)

R is the ideal gas constant (8.314 J/mol K)

MW is the volume average molecular weight of LFG (50/50 CO_2 and CH_4 30.03 g/mol)

z_1 is the correction for non-ideal gas behaviour (assumed 1.0 for this pressure and temperature range)

T_2 is the temperature of the gas after compression (K)

ε_a is the adiabatic compression efficiency (80% is selected for centrifugal pumps)

H_P is the polytropic head indicating the energy required for compression (J/g)

W is the mass flowrate of the gas (kg/s)

ε_m is the motor efficiency (91% assumed for an electric motor).

The cooling water rate is controlled such that the compressed gas enters the second stage of compression (4 to 8 atm) at 50 °C. The flow rate of cooling water was determined for a simple adiabatic tube and shell heat exchanger which was sized as follows:

$$\begin{aligned} Q_H &= Q_C \\ WC_p(T_2 - T_1) &= wc_p(t_2 - t_1) \\ Q_H &= UA\Delta T_{LM} \\ T_{LM} &= \frac{\left[(T_2 - t_2) - (T_1 - t_1)\right]}{\ln\left[(T_2 - t_2)/(T_1 - t_1)\right]} \end{aligned} \tag{27}$$

Where Q_H is the thermal energy transferred from the hot gas (kJ)

Q_C is the thermal energy transferred to the cooling water (kJ)

W and C_P are the gas mass flow rate (kg/s) and heat capacity (1.25 kJ/kg K), respectively

w and c_p are the water mass flow rate (kg/s) and heat capacity (4.17 kJ/kg K), respectively

T_1 and T_2 are the gas inlet and outlet temperature (K), respectively

t_1 and t_2 are the water inlet and outlet temperature (K), respectively

U is the heat exchanger coefficient for a shell and tube with compressed gas on the inside and water on the outside (199 W/m^2 K)

A is the tube area (m^2) for a 1 inch outer diameter steel tube with a variable length such that the liquid velocity was maintained between 1 and 3 (m/s).

ΔT_{LM} is the log-mean temperature difference for the heat liquid and gas (K).

The exhaust gas enters the adsorbent column at a temperature of approximately 120 °C. The number of adsorbers and flow rate of cooling water is provided in the table below for various landfill sizes:

Table B.8. - Scaling of adsorbers and cooling water for Landfill size

LFG input (m^3/hr)	# of adsorber vessels (160 m^3 each)	Cooling water flow rate (L/min)
50	1	1.8
100	2	3.6
250	3	9.0
500	4	18
750	6	27
1000	8	36
1500	12	54
2000	16	72

The LFG input in the table above assumes only 50% of the LFG generated actually enters the upgrading process. Adsorbent bed replacement is also considered every 8 years and the cost is distributed over the 15 year project lifetime at an interest rate of 7%.

The capital and operational costs for the 9.4 Mt landfill case in the are distributed as illustrated in Figure B.4.

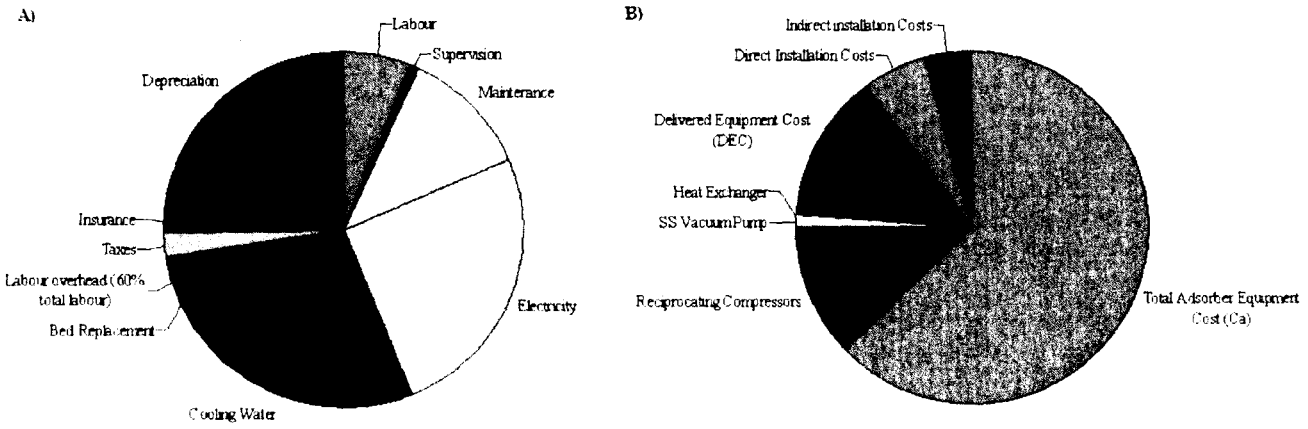

Figure B.4 - Economic Operational (A) and Capital (B) Costs for a 9.4 Mt landfill processing 2000 m^3/hr LFG with 16 adsorbers filled with NaLSX.

It can be seen that the operational costs ($2.1 million/year) are largely made up of electricity and cooling water. By selecting an adsorbent that has high adsorbent capacity at elevated temperatures, the operational costs can be decreased significantly. The capital costs ($7.2 million) are can be distributed over the 15 year project lifetime and are made up main of the adsorber and adsorber equipment cost (63%).

Appendix C:

Zeolite Structure and Cations

Zeolites are crystalline aluminosilicates and are composed of SiO_4 and AlO_4. tetrahedra that build larger Beta-cages and repeating sodalite cages. They contain cations that can be exchanged to modify the selectivity for components in gas mixtures. The cations distribute themselves within this framework to balance the overall charge and minimize the system free energy (Yang, 2003).

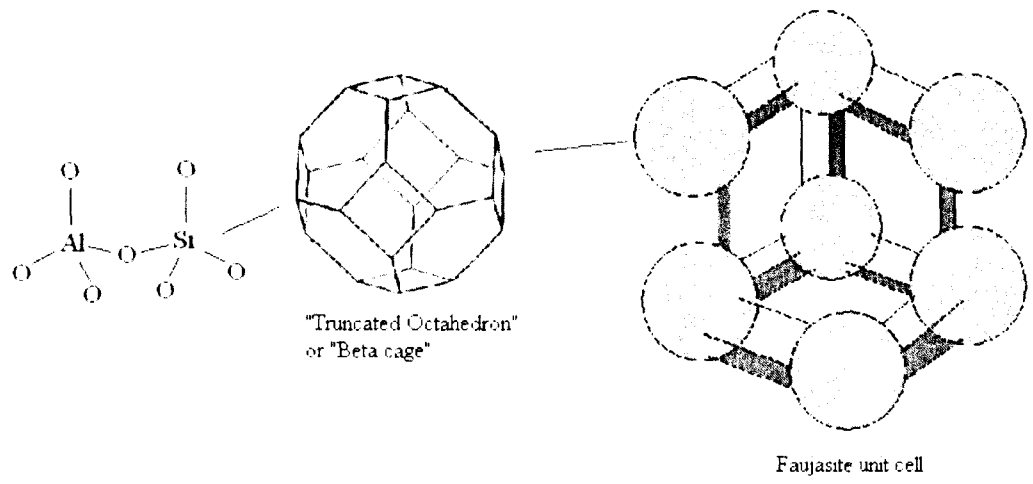

Figure C.1 - Zeolite SiO_4 and AlO_4 sodalite cages & Faujasite unit cell (IZA, 2008)

The 12 ring oxygen apertures allow the movement of gas molecules through (like CO_2 and CH_4) the structure to interact with the cations within the framework. There exist several adsorption sites within a zeolite supercage located around the cations. The adsorbent SiO_4 to AlO_4 (Si/Al) ratio determines the number of ions within the zeolite framework to balance the overall charge. X and Y type zeolites have the same crystalline structure (Figure C.1 above) and a Si/Al ratio in the range of 1.0-1.5 and 1.5-3.0 respectively (Yang, 2003). For example NaX (Si/Al = 1.28) contains up to 84 Na^+ cations (Ruthven, 1984). X type zeolites can contain cations at all possible sites within the faujasite cell whereas Y zeolites cannot and all sites are not necessarily accessible to the adsorbate gases (Walton, Abney and LeVan, 2006). NaX is currently used to commercially remove CO_2 from air before cryogenic separation of O_2 and N_2 (Yang, 2003). Cation type and Si/Al ratio are customized to optimize a PSA separation like LFG.

Bulk separations are most widely explored in the air separation industry. LiLSX has been shown to be the best commercial O_2/N_2 adsorbent available although NaX is also used for the equilibrium separation (Yang, 2003). The adsorptive properties of zeolites are modified by changing the Si/Al ratio and exchanging cations. The type of cation changes the electric field and the available pore volume in the crystalline aluminosilicates structure (Walton et al, 2006). For example, the Na^+ cations within the LSX zeolite for smaller, Li^+ cations.

Table C.1 - Cation properties (Yang, 2003)

	Ionic Radius (Å)	Polarizability (10^{-24} cm^3)
Li^+	0.68	0.029
Na^+	0.97	0.180
Ca^{2+}	0.99	0.471

The abundance of Na^+ cations in X zeolites leads to a high affinity for CO_2 adsorption and a significant physical interaction. A strong interaction suggests a high heat of adsorption or even chemical adsorption.

Appendix D:

Constant Volume System Manual and Checklist

Various Authors in

University of Ottawa Adsorption Lab

Step by step: How to do an isotherm

1. Weight the adsorbent

    a. Choose the appropriate container for the sample, based on the pressure that will be used. The figure below show the shape of the appropriate container for isotherm performed at pressure above 3 atm.

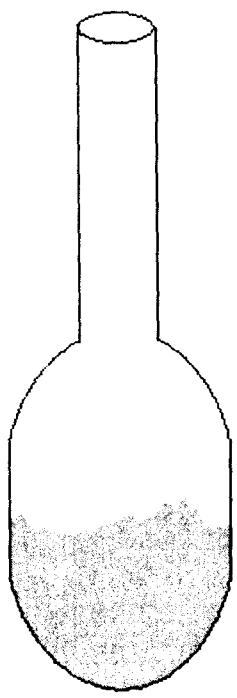

Figure D.1 - Container for isotherm at high pressure

    b. Using the balance, weight between 2 and 3 grams of adsorbent and put it in the container. Use the provided funnel to make sure that all the adsorbent weighed is in the container. One method is as follows: weight the empty container, fill it with the adsorbent (approximately half of it) and weight the container again with the adsorbent. When powder is used as adsorbent, it is very difficult to put all what is weight in the container; therefore the proposed procedure should be followed. When the container is weighted with the powder in it, make sure that there is no powder stick on the outside of the container.

    c. Put a blue cap on the container until you installed it in the unit. This will avoid moisture adsorption and prevent particulates from entering the container as well as any loss of the adsorbent.

2. Regenerate the adsorbent

   a. Installed the sample cell with the adsorbent in the volumetric brown unit (see the following diagram).

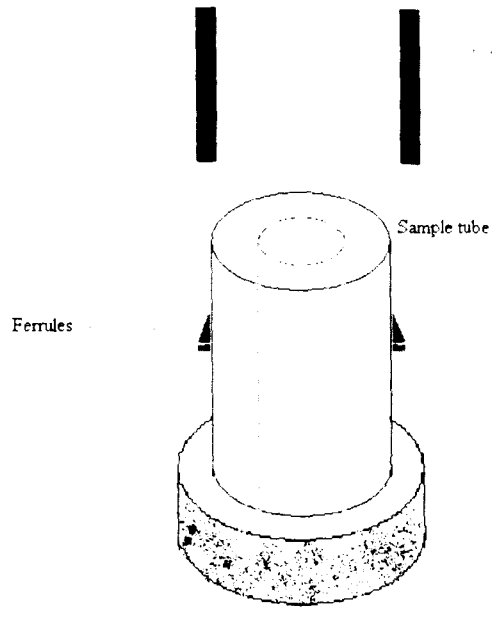

Figure D.2 - Sample cell installation

   b. Scotch tape the probe of the thermometer on the sample container. Put glass wool around the top of the sample cell to isolate it.

   c. Make sure all valves are in the appropriate position. Open the sample valve, the vacuum valve, the low pressure isolating valve and the high pressure transducer isolating valve.

   d. Under vacuum, increase the temperature to the desired regeneration temperature (above 300°C). The simplest way is to increase the voltage at a mark below the desired temperature and when steady state is reached (approximately 1h to go from 25°C to 300°C), increase it by little step to the final temperature. Even if some temperatures are indicated corresponding to certain voltages, they are not necessarily accurate. It is easier to start low and increase the temperature. The scotch tape will likely burn and smell, it has to be replaced after the regeneration.

e. When the desired temperature is reached, wait for regeneration to complete (usually 8h to 10h). Leave the vacuum valve open during the entire process.

f. At the end of the regeneration, decrease the thermal jacket voltage to zero and let the sample cool to desired isotherm temperature. Remove the mineral wool will help the temperature to decrease, but be careful to not touch the sample container (which is at 350°C). When the sample is at room temperature, scotch tape the probe of the thermometer on the container.

3. Measure the dead volume of the sample

The dead volume is the volume in the interconnecting tubing, and the sample cell (minus the volume of the adsorbent).

a. Under vacuum, increase the temperature to the desired isotherm temperature. For each point keep a record of: the temperature of the sample (yellow digital thermometer read-out), the temperature of the manifold (mercury thermometer in the unit), and the pressure from the three pressure transducers (from the computer, with LabView) must be noted.

b. Note pressure and temperature data when sample and vacuum valves are open, and the desired temperature is reached and is at steady-state.

c. Close the vacuum and sample valves and allow Helium to enter the manifold. Wait for the system to reach equilibrium. Take pressure and temperature data.

d. Open the sample valve. Wait for the system to reach equilibrium. Take pressure and temperature data.

e. This measurement (b, c, d) should be done at two different pressures: low (with lower pressure transducers in operation) and high (with hlow pressure transducers isolated from the sample and manifold; above 1 atm) for an accurate dead volume measurement.

4. Realise an isotherm

- Before taking the first point of the isotherm, take pressure and temperature data when sample and vacuum valves are open.

- For points of the isotherm: Close the vacuum and sample valves and put the desired gas in the manifold (at the desired pressure). Wait for the system to reach equilibrium. Take pressure and temperature data.

- Open the sample valve. Wait for the system to reach equilibrium (equilibrium times vary). Take pressure and temperature data.

- Repeat the steps b and c, until the isotherm is at the higher desired pressure. If the pressure is higher than 1000 torr, close the low pressure isolating valve. This section can be vacuumed using the low pressure vacuum valve.

- The number of isotherm points that need to be taken vary for the given adsorbent-adsorbate system, temperature, and pressure range. Ideally there should be no more than 8 isotherm points because errors in volume and pressure measurements can propagate significantly.

5. Regenerate the sample

   a. When the last point is taken, open the vacuum valve, with the sample valve open.

   b. Follow the same procedure explained in section 2 to regenerate the sample.

   c. When the regeneration is finished, and the sample is at room temperature, remove it from the unit, put a blue cap on and weight the sample.

6. Reweigh the sample

   a. The last step is to weight the sample again. All adsorbent weights should be of outgased adsorbent (i.e. with nothing adsorbed to it). The initial weight is called the "wet weight", after regeneration the "dry weight" is determined.

   b. Weight the regenerated adsorbent sample in a metal tray.

   c. The empty container weight should be used to determine the dry weight if the adsorbent is in powder form (i.e. it is too hard to get all the adsorbent powder out so weigh the regenerated sample by differences). Therefore weigh the adsorbent cell with the regenerated adsorbent in it.

Volumetric system checklist

1. Gas cylinders
    - Check the lines for leaks with soap and water or by vacuuming lines.

2. Sample Precautions
    - If the adsorbent is a powder. use a dust mask when handling and ensure seal frit (SS filter) is inserted in between sample tube and manifold. This filter protects the system from adsorbent particles.

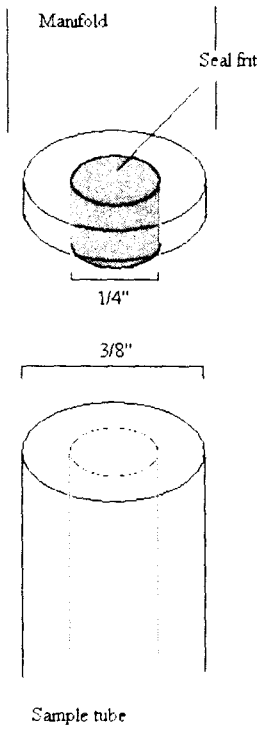

Figure D.3 - Particulate Filter Installation

3. Connecting Sample Cell
    - Ensure ferrules are in the correct position

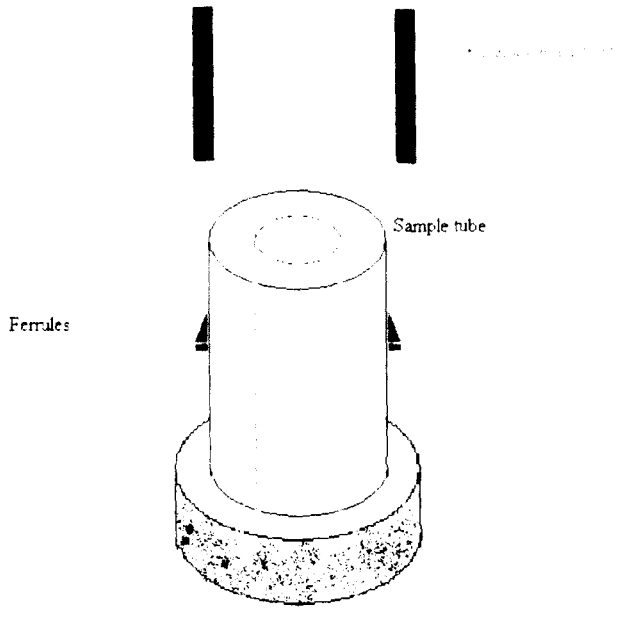

Figure D.4 - Connecting Sample Cell

- Do not over-tighten hand screw (esp. do not use pliers only to be tightened by hand)
- Ensure sample cell does not leak (in dead volume estimate)

4. General System Operation

    - Try to take an equilibrium point at a similar time to minimize variations in data due to voltage and room temperature affects (Each equilibrium time may exceed 48 hours for some samples especially CO_2).

5. Pressure Safety

    Blue system:
    - Ensure automated valve voltage is set to 0.75 (for 250 psi pressure transducer 0.75 is equivalent to 1000 torr)

    Brown system:
    - Once the pressure in the manifold exceeds 1000 torr (XX Voltage reading on 160 psi pressure transducer) isolate 40 and 1000 torr pressure

transducers from sample cell and 160 psi pressure transducer. The valve isolating the high pressure transducer (160 psi) should be open in order to take pressure measurement.

- Make sure that valves for input gas are closed when opening the vacuum valve.
- Always close the vacuum valve before installing or removing the sample container.
- The reference side evacuation valve should be always open (to compensate for system leaks).

Both Systems:

- The schematic diagrams for both the Blue and the Brown units can be found on the respective units along with a recent copy of the calibration done for all the pressure transducers.
- To calibrate all the pressure transducers within a unit, use the calibrated pressure transducer which is always kept in Dr. Tezel's office.
- Glass sample tubes are guaranteed only to 5 atm (absolute) therefore any pressure above this limit requires a metal container to catch shards (if sample tube breaks).

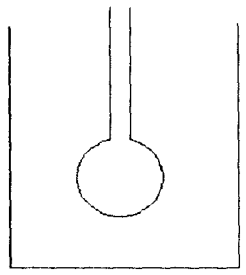

Figure D.5 - Pressure Safety

6. System Shutdown
    - Ensure all valves are in closed position, vacuum pump and thermal jacket turned off.

7. Cleaning Glass Sample tube
    - Sample tubes are cleaned with small amount of soap in water followed by drying in the oven (overnight at around 150 °C).

- If tube is very dirty a small amount of nitric acid can be used to clean followed by above instructions. ***when using nitric acid done gloves, lab coat, and safety glasses***

8. Safety Equipment
    - When using dry ice use work gloves, lab coat, and safety goggles.

9. Manual
    - There is also a manual with theory of operation and calculation details kept on the unit.

Data point for dead volume

- Take pressure and temperature data when sample and vacuum valves are open.
- Close the vacuum and sample valves and put Helium in the manifold. Wait for the system to reach equilibrium. Take pressure and temperature data.
- Open the sample valve. Wait for the system to reach equilibrium. Take pressure and temperature data.

This measurement should be done at least two different pressures; low and high for accurate measurement.

Data point for isotherm

- Before taking the first point of the isotherm, take pressure and temperature data when sample and vacuum valves are open. For points of the isotherm: Close the vacuum and sample valves and put the desired gas in the manifold (at the desired pressure).
- Wait for the system to reach equilibrium. Take pressure and temperature data.
- Open the sample valve. Wait for the system to reach equilibrium (equilibrium times vary). Take pressure and temperature data.

IMPORTANT NOTE: You should be instructed on how to use the Volumetric system by someone who is well versed in its operation. This checklist and User guide is only a reference and should not be used without direction or supervision. If you are not comfortable with the operation of the volumetric unit PLEASE ask questions. This is a very expensive piece of equipment and can be damaged easily.

Appendix E – Operational Manual for the Gas Chromatograph

GAS CHROMATOGRAPHY USING BINARY ISOTHERMS

"HOW TO USE THE GC 3300"

By

Various students in the Adsorption Lab at
University of Ottawa

Submitted

To

Dr. Handan Tezel

INTRODUCTION

The purpose of this report is to provide a user friendly guide for those who wish to use the GC 3300. It is also important to note that this document is written based on the assumption that the user is familiar with the concept of gas chromatography and adsorbent packing for the GC Column. Hence, this manual will only provide the user with the basic procedures for operating the equipment including calibrating, regenerating and running the system. An illustration is shown below of the GC 3300 in figure 1.

Figure 1.

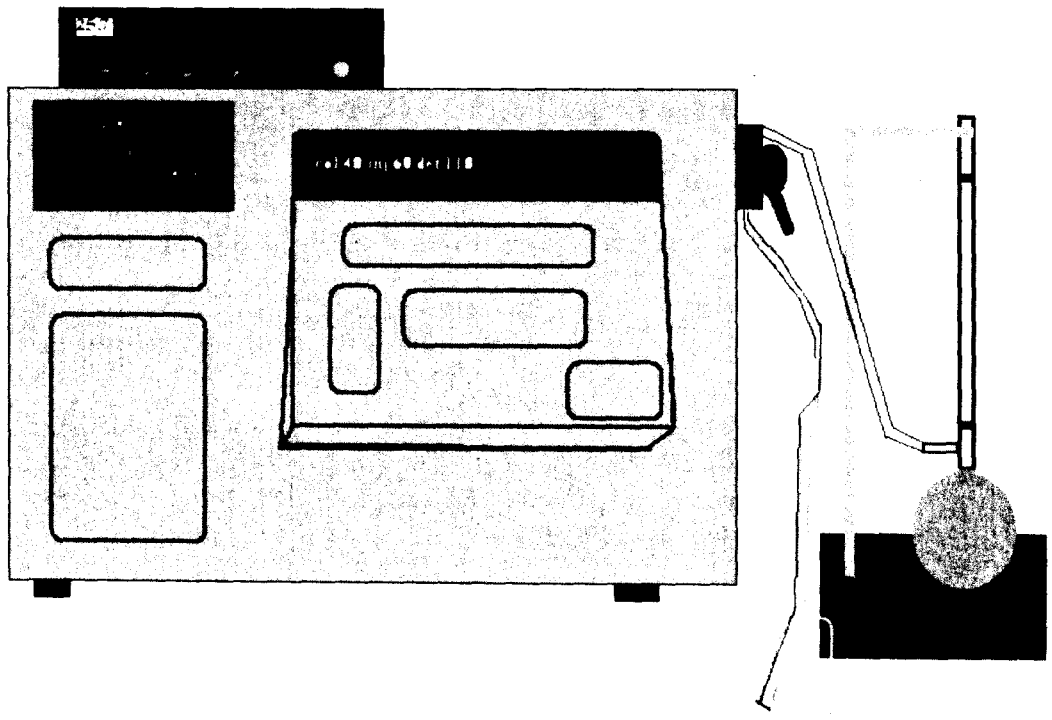

CALIBRATION

HOW DO WE CALIBRATE THE SYSTEM?

Before commencing any GC experiment, it is essential to calibrate the system for each individual carrier gas. In a binary system we have two carrier gases, Carrier A and Carrier B. These are labelled on the mass flow controllers (MCF's) accordingly. The Channel Controller (the black box on top of the GC) has 4 channels which are connected to four different MFCS. The one's we are interested in are channels number TWO and number FOUR. By using the switch on the right of the Channel Controller we can adjust which MFC we would like to control.

***In our case, Channel 2 is for Carrier Gas B (CO_2) and Channel 4 is for Carrier Gas A (CH_4).**

When calibrating it is important to remember that we calibrate each Carrier Gas individually. Thus, if we are calibrating Carrier A then we must make sure that Carrier B is set to ZERO on channel 2 or the valve is closed on our Carrier B gas cylinder.

Once the user has made sure that Carrier B is set to a flow rate of ZERO, then they are ready to calibrate Carrier Gas A.

For our calibration processes, we will be using a Bubble Meter illustrated below.

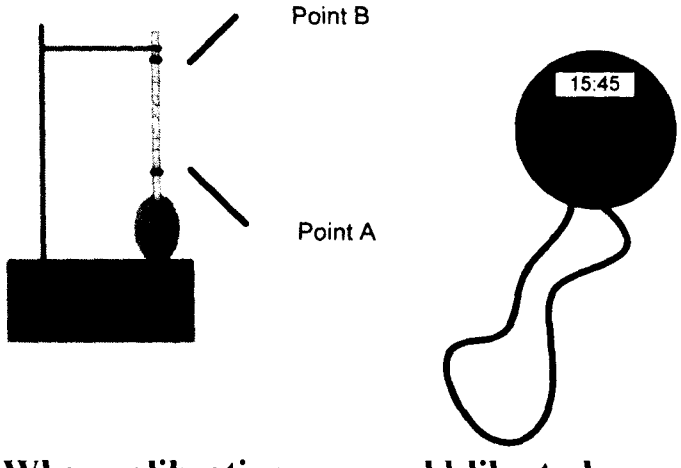

When calibrating we would like to have our highest indicator value set to a value that will give a 16 cc/min flow rate on the bubble meter. What this means, is that the time required for a bubble to travel from point A to point B (16 mL or 16 cubic centimetres) should take approximately 16 seconds on our stop watch. It is also important to note that when the user is doing this process, the choice of bubbles should be ones that are NOT foamy and ones that are clear. Bubbles can be obtained by squeezing the rubber band at the bottom of the 16 mL cylinder shown in the illustration.

HOW DO WE KNOW WHAT VALUE TO SET THE INDICATOR?

The only way is through trial and error. First set the indicator to an arbitrary value, say 50.0, then proceed to take some time measurements using the bubble meter with the stop watch.

* **If the time taken for a bubble to travel 16 mL is HIGHER than 16 seconds, SET A HIGHER FLOW RATE until you get your time to be approximately 16 seconds.**

* **If the time taken for a bubble to travel is LESS than 16 seconds, SET A LOWER FLOW RATE until you get your time to be approximately 16 seconds.**

Once you have an indicator value which gives you a 16 cc/min flow rate on the bubble meter, divide the indicator value by 10 so as to obtain 10 additional indicator values.

Then take time trials with the indicator value that was set to obtain 16 cc/min as your highest value. In other words if an indicator value of 50.0 was needed to record a 16 cc/min flow rate, then you should have 10 additional points decreasing by 5, so your next value would be 45.0 and then 40.0 and etc. until you reach 5.0 as your last value.

***It is recommended that the user takes several time trials for each indicator value (e.g. 4).**

***IMPORTANT WHEN SETTING AN INDICATOR VALUE THE USER MUST WAIT FOR THE PROCESS TO STEADY!!!**

HOW DO WE KNOW WHEN THE PROCESS IS STEADY?

In order to know when the process is steady, we use the computer software LabView. This can be done by running the program (press the white arrow on the top left corner), Scaling the X-axis (time) to about 600-1000 times greater than the start of the line and the y-axis (voltage) to about 3.0 higher and lower then the line and wait until the line straightens out. This is shown in *figure 3*.

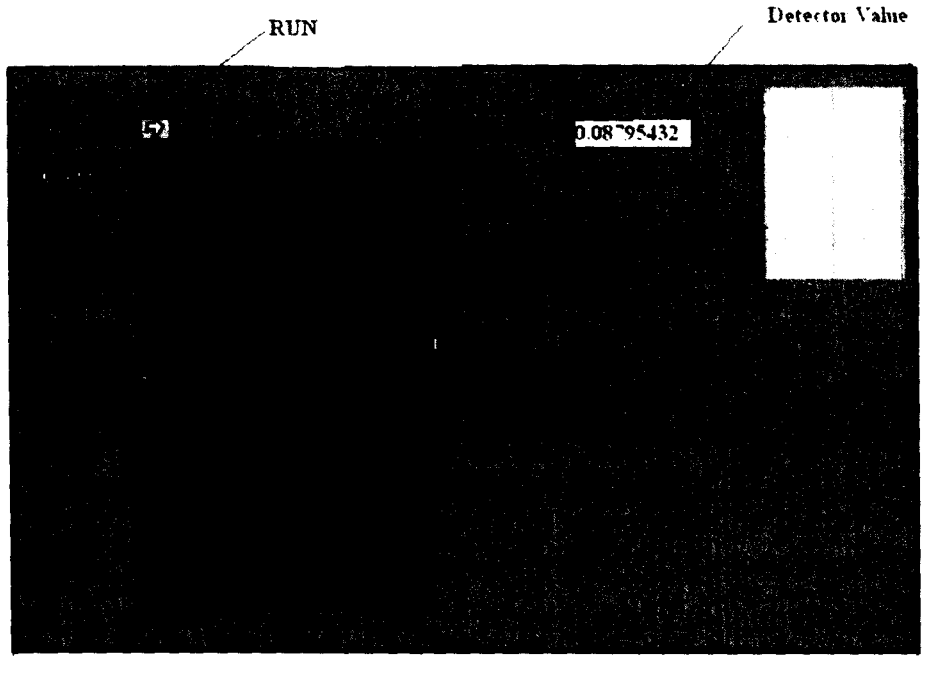

Once the calibration is done for Carrier Gas A, set the channel reading to 0.0 and then proceed to repeat all of the steps for calibrating Carrier Gas B.

REGENERATION

HOW DO WE REGENERATE THE SYSTEM?

***IMPORTANT: WE REGENRATE USING HELIUM AND WITH THE COLUMN TEMPERATURE SET TO 300 DEGREES.**

***DURING REGENRATION, HELIUM SHOULD BE THE ONLY CARRIER GAS RUNNING THROUGH THE SYSTEM.**

HOW CAN WE SWITCH THE CARRIER GAS TO HELIUM WITHOUT FEAR OF DAMAGING THE DETECTOR?

In order to do this, the user can have one carrier gas running, let's say Carbon dioxide as our Carrier B Gas set to any arbitrary flow rate and switch the Carrier Gas A with the Helium. Then the user can open the

valve for the helium gas cylinder and set a fairly high flow rate (ex. 65.0) then turn off the Carrier Gas B and using the build/modify key on the machine raise the column temperature to 300 degrees.

***IMPORTANT: MAKE SURE THAT HELIUM IS THE ONLY CARRIER GAS RUNNING BEFORE RAISING THE TEMPERATURE AND ALSO MAKE SURE THAT IF ANY OTHER CARRIERS ARE CONNECTED THAT THEY ARE SET TO 0.0 OR HAVE THEIR VALVE CLOSED!!!**

CHECK TO MAKE SURE THE HELIUM IS RUNNING THROUGH THE SYSTEM BY USING THE BUBBLE METER!!

The system should be allowed to regenerate for 24 hours.

After 24 hours, the user can bring down the column temperature to the desired value and then switch the helium to the desired Carrier Gas using the same method that was used to connect the helium before regenerating.

***ALSO: DO NOT BE ALARMED IF THE INJECTOR AND DETECTOR TEMPERATURE INCREASE A FAIR AMOUNT, THIS IS NORMAL.**

RUNNING EXPERIMENTS

Once the regeneration has been completed and the temperature has been set to the desired value, the user is now ready to commence the experiments.

The first experiment that is usually run is the pure carrier gas (ex. Pure CARRIER GAS A) with an injection of the Sample Gas (ex. Sample Gas B). The sample gases are the same as the carriers but only used for a short sample injection. For instance if the binary experiment one is doing is nitrogen and carbon dioxide, they will have four gas cylinders to work with, one nitrogen cylinder as the carrier gas and one as the sample gas, as well as one carbon dioxide cylinder as the other carrier gas and one as other the sample gas.

For each different gas compositions/indicator values one must do TWO sample injections, one with sample gas A and another with sample gas B.

***HERE IS A STEP BY STEP PROCEDURE TO FOLLOW:**

1. **Use the bubble meter to make sure there is gas running through the GC machine. This can be done by squeezing the rubber band and if there are liquid lines flowing up the cylinder then everything is ok.**

2. **Check the CARRIER GAS CYLINDERS, make sure the valves are completely open, the regulators are set to 40 PSI and use soap water to spray on the connection tubing at the valve to make sure there are NO LEAKS.**

3. **Make sure the INDICATOR VALUES are set accordingly to the desired compositions. REMEMBER: Channel 2 is for CARRIER B and Channel 4 is for Carrier A.**

4. **Open *Labview* and run the program at the desired SCAN RATE (ex. 1 point per second or 10 points per second). Use the stopwatch to make sure that the scan rate is correct (computers are not always reliable!!).**
5. **Make sure the set indicator values/flow rates are in steady-state using the method discussed in the calibration section. In other words, make sure that the VOLTAGE READINGS are not FLUCTUATING SIGNIFICANTLY.**

6. **If the Voltage Readings are fluctuating significantly, PUSH metal lining on the CONNNECTION holding the injector a few times until it improves.**

7. **Connect the desired SAMPLE GAS and just like the Carrier Gases, check for leaks and so on.**

8. **Turn on the sample gas and use the side tubing from the GC and submerge it in a beaker of water to see that there is gas flowing from the sample.**

9. **Adjust the flow rate using only the valve of the sample gas cylinder (open the valve very little) so that there is a LOW flow rate coming from the sample gas.**

10. **Before injecting check that the column, injector and detector temperatures are correct.**

11. **Using your left hand grip the injector so that your hand is in a "thumbs down" postion (not too tightly) and using the stop watch in your right hand. Turn the injector switch up (counterclockwise) in one swift motion and time your injection, usually about 6 seconds. Once this is done turn the injector switch back down (clockwise) again in one swift motion.**

12. **Wait for your CURVE and make sure the base line on the Labview program comes back to the initial range.**

<u>*SEE FIGURE 4.</u>

Figure 4.

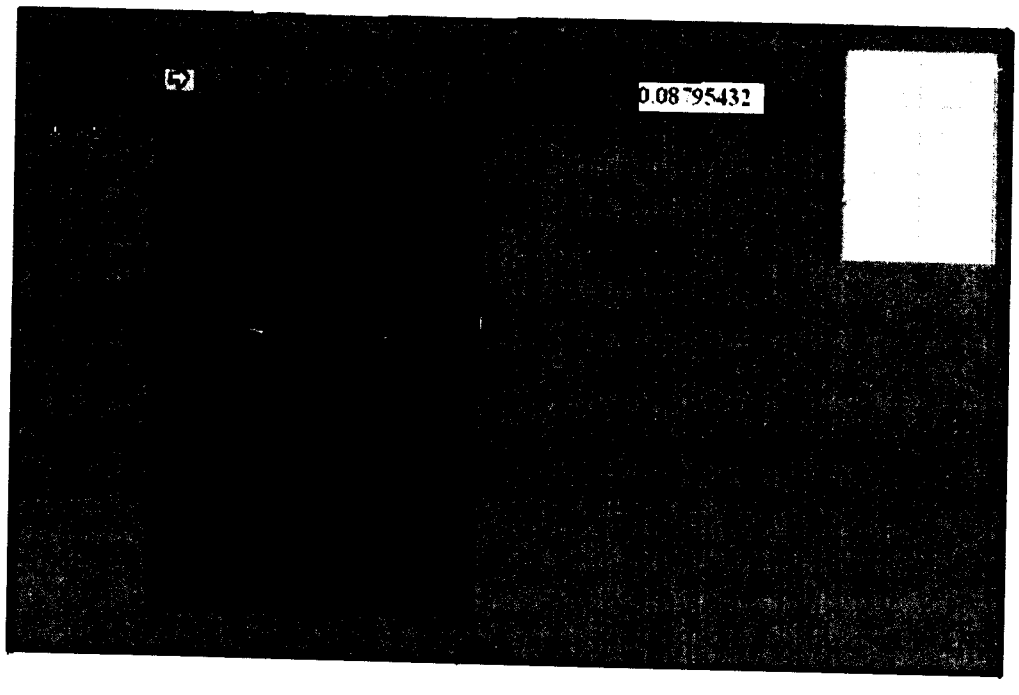

THIS IS A COMMON CO2-N2 OR CO2-CH4 BINARY SYSTEM WITH CO2 SAMPLE INJECTION.

COMMON ERRORS AND PROBLEMS ENCOUNTERED

This section is strictly intended to aid the user with general information on problems that arise quite frequently.

1. **The first and foremost hardship the user will encounter is when switching the GC system on using the switch on the left hand side on the back of the machine. When turning the system on, immediately there will a FAULT MESSAGE saying either POWER FAILURE/WARM START or LOST CARRIER GAS or TCD FILAMENT TEMP LIMITED**

Solution:

***PRESS THE RESET BUTTON ON THE MACHINE**

2. **Often the connection to the detector will not be excellent. Hence sometimes the voltage values on the computer screen seem to fluctuate even though you know for a fact that the system is at steady-state.**

Solution:

***PUSH ON THE METAL PIECE ON THE SMALL BLACK COMPARTMENT HOLDING THE INJECTOR ABOUT 20 TIMES.**

3. **Often when changing a carrier gas for example when we would like to regenerate and switch one carrier to helium, the machine sometimes displays a fault message indicating a LOST CARRIER GAS even though by checking with the bubble meter we know that there is a carrier running through the system.**

Solution:

***AGAIN PUSH THE RESET BUTTON ON THE MACHINE.**

4. **Often when doing the first injection using a pure carrier gas with the other set to 0, so for example 100% Nitrogen carrier and Carbon Dioxide sample the curve takes about 2 days to be completed and over 70 000 second readings on the computer. However excel only allows a maximum of 65000 points.**

Solution:

***SET THE SCAN RATE ON THE COMPUTER SOFTWARE TO 1 POINT PER 10 SECONDS.**

5. **Almost always when we start approaching the high CO2 concentrations, so towards the final few curves the data readings or data processing values may not be completely on par with the data one would expect to see. These injections are more difficult and must be done very carefully if the user would like accurate results.**

Solution:

THESE CURVES DO NOT TAKE VERY LONG AND SEVERAL INJECTIONS CAN BE MADE AND THE BEST RESULTS CAN BE USED. ALSO, THE USER SHOULD DECREASE THE INJECTION TIME OF THEIR SAMPLE GAS TO APPROXIMATELY 2-3 SECONDS OR MAYBE EVEN LESS DEPENDING ON THEIR CURVES.

6. **When dealing with CO2-N2 binary experiments the user will find that towards the higher CO2 concentrations mentioned in problem 5 that the N2 sample injections from approximately 85%-100% CO2 concentrations reach a maximum voltage value and instead of observing a curve the user observes what appears to be a rectangular curve with the peak turning into a straight line and then decreasing to the baseline value. This is illustrated on the next page in figure 5.**

Figure 5.

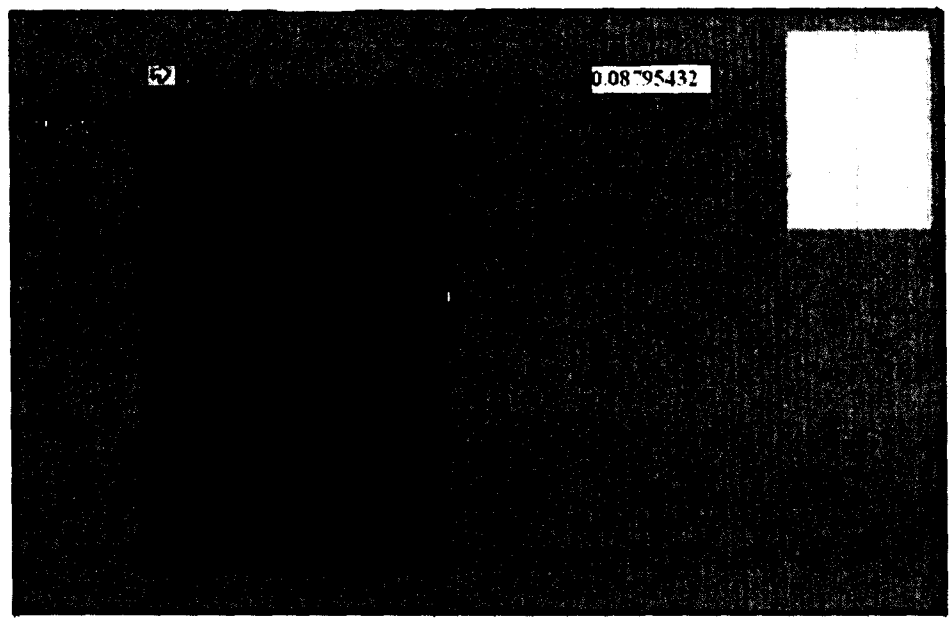

Solution:

***WHEN DOING THE N2 INJECTION KEEP THE INJECTOR UP (OPENED) AND PUSH ON THE METAL CONNECTION PIECE ABOUT 20 TIMES THEN TURN IT BACK DOWN. DO THIS UNTIL THE BASELINE VALUES AFTER THE CURVE ARE VERY CLOSE TO THE BASELINE VALUES BEFORE THE CURVE.**

7. FINAL PROBLEM

The user may find a lack of information or perhaps an overwhelming amount of information at first. This may result in slower progress and many mistakes to be made.

Soltuion:

***ASK FOR HELP AND PROPER TRAINING, YOU ARE DEALING WITH AN EXPENSIVE PIECE OF EQUIPEMENT AND IT IS YOUR RIGHT TO BE SUPERVISED AND TRAINED.**